THE CAUSES AND CONSEQUENCES OF PARTICLE SIZE CHANGE IN FLUVIAL SYSTEMS

Kimberly Louise Litwin Miller

A DISSERTATION

in

Earth and Environmental Science

Presented to the Faculties of the University of Pennsylvania

in

Partial Fulfillment of the Requirements for the

Degree of Doctor of Philosophy

2014

Supervisor of Dissertation

Douglas J. Jerolmack
Associate Professor, Earth and Environmental Science

Graduate Group Chairperson

Douglas J. Jerolmack
Associate Professor, Earth and Environmental Science

Dissertation Committee

Jane K. Willenbring, Assistant Professor, Earth and Environmental Science

David Goldsby, Associate Professor, Earth and Environmental Science

Gábor Domokos (external), Professor, Budapest University of Technology and Economics

THE CAUSES AND CONSEQUENCES OF PARTICLE SIZE CHANGE IN FLUVIAL SYSTEMS

Dedicated to MFM

ACKNOWLEDGEMENTS

"At times our own light goes out and is rekindled by a spark from another person. Each of us has cause to think with deep gratitude of those who have lighted the flame within us."
Albert Schweitzer

Along my lengthly journey toward achieving my doctorate, my flame has been lit by so many people; without these people, I would be in the dark. Although I do not have the time or the space to acknowledge everyone who has helped me on my way, I would like to thank a few people that I am eternally grateful for.

First and foremost, I would like to thank my advisor and mentor, Doug Jerolmack. His guidance and support over the past 4 years has made me into the scientist that I am today. There is no one I would rather have as my academic father-figure and role-model. He is the hardest working person I have ever had the pleasure of knowing and his passion for science and exploring new concepts is contagious. I feel truly honored to have had this opportunity to do such innovative and exciting science with such an enthusiastic person.

I am greatly indebted to the members of my committee for taking the time away from their own research to provide me with direction and insight into my projects. Their encouragement and feedback has made this dissertation truly great. I would like to thank Jane Willenbring for her advice throughout my course of my doctorate. She always pushed me to look at my research through a different lens. I would also like to thank David Goldsby for his continued interest in my research. Even before he officially started at Penn, he still has made time to sit down with me and provide feedback and insight into my research projects. I would like to give a special thanks to Gabor Domokos, my external committee member, whose mathematical genius and rigor has made the research more scientifically sound and strong.

I would also like to acknowledge the entire faculty and staff of the department of Earth

and Environmental Science for providing a supportive environment to learn and foster my scientific skills. I would like to especially thank Art Johnson for his support and friendship through my time at Penn. I would also like to thank Ben Horton for his advice and support during my PhD. I am grateful for Ed Doheny with his enthusiasm and interest in my research. Ed is overflowing with knowledge about rock mechanics and has given me new ways to view my research. I would also like to thank Steve Phipps; he not only showed true interest in my research, but also, while TAing for him, taught me about the joys and pains of developing a course from scratch. Finally, I would like to thank Alain Plante. His leadership through both the Luquillo CZO for my research in Puerto Rico and undergraduate advising for TAing has provided so much support and assistance. And although Fred Scatena is no longer with us, I would like to acknowledge him for the time and energy he put towards my research. I was fortunate to have the opportunity to do field work with him in Puerto Rico and to TA for him for one semester during my time at Penn. His excitement and dedication to science was truly admirable and I hope that I can be the same with my work.

I would be nowhere without the daily aid of the administrative staff at Penn. First, I need to thank Joan for everything she does for the graduate students. If there is ever a question, she has the answer. She has gone to battle for me countless times and I am so grateful for her. I would also like to thank Arlene Mand for keeping the department running smoothly. I also would like to thank the crew over at the DRL business office: Rebecca Perry, Jason Seta, and Audrey Mascicchi. Without their help I would never get paid, have supplies, or get reimbursed.

My research would not be complete without the aid of the many field and laboratory assistants. I would like to thank Christinia Dietzen, Claire Masteller, Marcie Occhi, Colin Phillips, and Gerard Salter for their hard work in the Puerto Rico jungle. As well as Steven Hall, Gilles Brocard, and Miguel Leon for their support, guidance, and aid in Puerto Rico. I would also like to thank Jennifer Walker, Carolyn Gombert, and Gerard Salter for their time and assistance in the lab. I would like to thank Leonard Sklar and Brendan Murphy

for their help during our two-week stint at RFS measuring rock strength properties. A special thanks to David Vann for all his guidance in using lab equipment; this department would not run without him. Additionally, I would like to acknowledge Timi Szabo for collaborating on the Puerto Rico research. Our discussions on pebble abrasion are always enlightening. She is one of the most dedicated and smartest people I know.

I have had the great pleasure of being part of an amazing research team at Penn and would like to thank every member of the group. First, I would like to thank my fellow grad students: Meredith Reitz, Raleigh Martin, Colin Phillips, and Dylan Lee. This experience would not have been the same without their lasting friendship, support, and guidance. Next, I would like to thank the pos-docs for sharing their wisdom: Fede Falcini, Morgane Houssais, Carlos Ortiz. And finally, I would like to thank the undergrads in the group who do such amazing science and truly inspiring: Anastasia Piliouras, Claire Masteller, Gerard Salter, Sam Shaw, and Rachel Glade. I feel very privileged to have had the chance to work with all of these amazing people.

I am extremely thankful for the my friends who have brought such joy to my life. For their camaraderie and support over the past four years, I would like to thank my fellow graduate students: Brandon Hedrick, Nicole Khan, Tina Dura, Vanessa Boschi, Maddie Stone, Bing Xu, and Liz Coward. For their friendship I would like to thank my neighbors Mike Keane and Zach Bloom. I would like to thank my oldest and best friend Jason Kopeck for always listening to me. I would like to thank Kaylan Dorsch for showing me true generosity and kindness; I have never met another person like her and I know we will be lifelong friends. Thanks to Todd and Colleen Derby for their friendship and always being 'relaxed as hell'. And thank you to Sean Gallagher for always being available; our friendship has helped me get through the struggles of the last few months.

Finally, I would like to thank my family for everything they have done for me over the years. I thank my parents, Bob, Denise, Liz, and Kathryn, for raising me and teaching me to never give up. Their support throughout my life has made me into the person I am today.

I would like to thank my in-laws, Mary Ann and George Miller, for their love and kindness in taking me into their family. I would also like to thank my siblings Megan, Katie, Mike, and Christine for their faith in me and my work. I would like to give a special thanks to my twin sister, Amanda. She is my best friend and I cannot imagine what my life would be without her. She is always there standing by my side, sticking up for me, and helping me be strong. Finally, I would like to thank my partner and my husband, Matt. He is my rock and his unconditional love has fueled my flame every time it goes out. Thank you so much for putting up with all of my craziness during the last 11 years of our lives but especially for the support over the last four year. He helps me celebrate by highs, and keeps me calm during my stresses. Thank you.

Funding support for my graduate education was provided by the Luquillo Critical Zone Observatory 1 NSF EAR 0722476 and the University of Pennsylvania Benjamin Franklin Fellowship. Travel grants from the Graduate and Professional Student Assembly (GAPSA), the School of Arts and Sciences (SAS), the SAS Student Government (SASgov). Research costs were supported by the Jerolmack Discretionary Fund, the Luquillo Critical Zone Observatory 1 NSF EAR 0722476, and the Luquillo Critical Zone Observatory 2 NSF EAR 1331841.

ABSTRACT

THE CAUSES AND CONSEQUENCES OF PARTICLE SIZE CHANGE IN FLUVIAL SYSTEMS

Kimberly Louise Litwin Miller

Douglas J. Jerolmack

One of the most common features in fluvial environments is the systematic downstream decline in grain size, which is usually attributed to either abrasion - the reduction in sediment size due to attrition of mass - or selective sorting - the size segregation of grains due to their relative transport mobility. Despite the ubiquity of this grain pattern and the extensive research on both of these processes, there remains questions regarding the underlying principles driving abrasion and sorting, as well as the relative contribution of these processes to grain fining. Therefore, a mechanistic understanding of these processes is necessary to observe their direct effect on pattern formation. This dissertation investigates the controls and limits on abrasion and sorting through field studies and laboratory experiments. First, using the well-defined boundary conditions of an alluvial fan, we examine how grain hiding limits gravel sorting by tracking changes in the grain size distribution measured using a novel image-based technique. Further downfan, we compare surface sand fractions measured in the field with those from the lab and show that the gravel-sand sorting profiles are self-similar, suggesting generality in their development. In a second field study, using detailed hand and image-based measurements characterizing size and shape of thousands of grains throughout a watershed, we are able to directly observe the effectiveness of abrasion. We then input these measurements into a simple numerical model to tease apart the contribution of abrasion and sorting to downstream grains size and shape evolution. Finally, we conduct laboratory experiments to isolate the effects of impact energy on abrasion rates and use material properties of the grains to collapse mass loss curves between different lithologies. We measure the grain size distribution of the products of abrasion to show

that they are in agreement with expectations from brittle fracture theory. The results from this work indicate that both sorting and abrasion are effective mechanisms in producing downstream grain size patterns. Because grain size exerts a strong control on channel morphology, understanding the controls on particle size change fosters a more complete picture of the fluvial system.

TABLE OF CONTENTS

LIST OF TABLES

LIST OF ILLUSTRATIONS

CHAPTER 1 : Introduction

Rivers are dynamic natural systems that display a variety of patterns on different spatial scales. On the basin-wide scale, channels maintain a smooth concave longitudinal profile through the interplay of tectonics, climate, erosion, and sediment supply (*Sinha and Parker*, 1996; *Sklar and Dietrich*, 1998). On the reach scale, channel-form can organize into the sinuous curves of a meandering river through flow instabilities caused by sediment transport (*Leopold et al.*, 1957; *Parker*, 1976). As the sediment load increases, the channel will adjust its pattern to the many threads of a braided river (*Leopold et al.*, 1957; *Parker*, 1976). On this same scale, sediment can sort due to local variations in flow conditions to produce a pattern of alternating bars (*Schumm*, 1985; *Colombini et al.*, 1987). On the even smaller channel-bed scale, sand and silt transported as both bedload and suspended load form the intricate bedform patterns of ripples, dunes, and antidunes (*Kennedy*, 1969). All of these patterns observed in fluvial systems share one common concept – the fundamental driving force governing their formation is sediment transport. In turn, for given flow conditions sediment transport is controlled by grain size, determining the modes and rates of transport (*van Rijn*, 1984a,b). Therefore, particle size is perhaps the most important quantity for understanding the form and patterns of river systems.

Sediment itself is observed to systematically reduce in size downstream forming ubiquitous fining patterns. Downstream fining patterns are usually attributed to two dominant processes: abrasion (*Kodama*, 1994a; *Lewin and Brewer*, 2002; *Attal et al.*, 2006) and selective sorting (*Paola et al.*, 1992; *Ferguson et al.*, 1996). Abrasion is the process by which the diminution of grain size is caused by the chipping and wearing away of grains due to energetic collisions (*Wentworth*, 1919; *Kuenen*, 1956; *Sneed and Folk*, 1958; *Parker*, 1991; *Kodama*, 1994a; *Lewin and Brewer*, 2002). Whereas selective sorting is the process by which grain size decreases downstream due to the preferential mobility of smaller grains as larger grains are deposited out of the flow (*Paola et al.*, 1992; *Ferguson et al.*, 1996; *Gasparini et al.*, 1999). Although it is generally agreed that observed downstream fining patterns are

produced in some degree by both abrasion and sorting, there has been considerable debate regarding their relative importance (*Parker*, 1991; *Paola et al.*, 1992; *Kodama*, 1994b; *Ferguson et al.*, 1996; *Attal et al.*, 2006). It has been hypothesized that the difference in the apparent importance of these processes could depend on channel environment, where selective sorting is dominant in aggradational systems since it requires the deposition of sediment (*Shaw and Kellerhals*, 1982; *Dawson*, 1988). Furthermore, lithology has been shown to be a factor determining the proportion of each process to produce grain fining since selective sorting tends to dominate in channels with resistant lithologies because the effects of abrasion are diminished (*Parker*, 1991). However, because of the lack of understanding of the mechanics governing abrasion and sorting, there is no way to quantify how different factors, like channel environment and lithology, will influence their contribution to grain fining. Currently, there is no systematic method to tease apart the effects of abrasion and selective sorting on downstream grain size fining.

Sternberg (1875) was the first to quantitatively explain downstream fining by abrasion and empirically described the diminution of grain size by the exponential function:

$$D = D_0 e^{-\alpha x} \tag{1.1}$$

where D is the grain size at downstream distance x, D_0 is the initial grain size, and α is the diminution coefficient. Although it is known that the amount of abrasion depends on the energy delivered to the grain (*Bitter*, 1963), α values remain the most common way to characterize abrasion rates, despite its lack of mechanistic foundation. However, some progress has been made to link grain kinematics to abrasion. Research investigating the abrasion from windblown sand showed that the volume removed from wooden fence posts scales with the total impact energy of sand grains colliding with the surface (*Anderson*, 1986). Translating this idea to fluvial systems, impacts with the bed and other grains during bedload transport provide the required energy for abrasion. In addition to impact energy, lithology has been shown to exert a strong control on abrasion rates (*Kuenen*, 1956;

Kodama, 1994a; *Lewin and Brewer*, 2002; *Attal and Lave*, 2009). Laboratory simulations of grain-to-grain abrasion in a circular flume produced attrition rates spanning two orders of magnitude depending on lithology (*Attal and Lave*, 2009). Moreover, strength and material properties, like tensile strength and Young's modulus, are known to have a large effect on abrasion rates, but little is known about their exact contribution (*Attal and Lave*, 2009; *Wang et al.*, 2011). In addition, recent research has shown the effects of grain shape on abrasion. A geometric theory derived by *Domokos et al.* (2014) models abrasion as a surface curvature dependent process. This theory is confirmed through experiments looking at the abrasion of initially square pebbles in a rotating drum which showed that protruding areas of the pebble's surface, marked by points high curvature, are quickly worn away first (*Durian et al.*, 2006; *Domokos et al.*, 2014). Although previous work has shown that collision energy, lithology, and grain shape govern abrasion, more work is needed to explicitly quantify their effects so we may observe them in nature.

In a different manner, selective sorting produces grain fining through segregation of grain sizes during transport. *Paola et al.* (1992) conducted flume experiments under constant water discharge where a prograding wedge of gravel exhibited strong sorting patterns, indicating that transport and deposition of poorly sorted or bimodal sediment is all that is required to produce sorting patterns. Furthermore, fieldwork completed by *Ferguson et al.* (1996), tracking sediment size and flux along a river, suggested that grain size fining by selective sorting is caused by the channel maintaining near uniform transport rates as the channel slope decreases downstream. Both of these studies highlight selective transport as an effective process in the creation of downstream fining patterns due to the relative mobility of smaller grains. Although intuitive that smaller grains are easier to transport, this is not always the case for heterogeneous grain size mixtures, where hiding and protruding of grains on the bed can alter their mobility (*Parker*, 1990). For instance, a small grain sitting in a pocket of larger grains will require a higher stress to be transported than that same grain sitting on a bed of similar sized grains. Due to these "hiding effects", a range of grain sizes can be transported under the same flow conditions; this phenomenon is referred to

as equal mobility (*Parker and Klingeman*, 1982; *Wiberg and Smith*, 1987). Equal mobility can obscure the ability of the channel to sort sediment(*Gasparini et al.*, 1999), however, patchiness in bed material, seen in local variations of mean grain size, can suspend its effects causing selective deposition of grains (*Paola and Seal*, 1995). Therefore, the exact interactions between transport and relative grain size in producing sorting patterns is not fully understood.

Regardless of whether abrasion or selective sorting is the cause of downstream fining, grain size patterns have major consequences on channel morphology (*Leopold*, 1992; *Dade and Friend*, 1998). On the basin-wide scale, *Yatsu* (1955) showed that changes in channel slope along 9 rivers in Japan correlated with a change in median grain size. Furthermore, numerical modeling of channel evolution indicates that long profile concavity increases with grain size because of the interdependent relationship between channel gradient and sediment mobility (*Gasparini et al.*, 2004). On the local channel scale, gravel-bedded rivers at equilibrium adjust their channel geometry to transport the median grain size (*Parker*, 1978). Knowing how grain size patterns are formed will shed light on how adjustment timescales between grain size trends, channel geometry, and slope vary so we may better understand the linkages between them.

This dissertation examines several aspects of downstream particle size change: the mutual influence of different grain sizes on sorting patterns, the geometric evolution of pebble shape due to abrasion, the scaling between collisional energy and attrition rates, and the characterization of the products of abrasion. Through field studies and laboratory investigations, this work aims to describe the interplay between grain size and channel morphology by investigating sediment interactions during transport.

Chapter 2 explores grain size patterns produced through sorting processes. From basic sediment transport equations, *Fedele and Paola* (2007) derived Sternberg's Law (eq. (1.1)) resulting from gravel selective sorting. They showed that the mean and standard deviation of the grain size distribution decrease exponentially downstream at the same rate arising in

a constant value of the coefficient of variation, thus suggesting self-similar sorting profiles. However, there is some finite length over which the channel adjusts to this limit of a constant coefficient of variation. In this chapter, we investigate what determines this limit of sorting by tracking the degree of equal mobility of grains. Further downstream, we examine how sand sorts from gravel to form an abrupt feature referred to as the gravel-sand transition, marked by a rapid decrease in median grain size and channel slope. A two-fraction transport model has been proposed to produce this feature due to the effect sand and gravel have on each others relative mobility (*Wilcock and Kenworthy*, 2002). We compare bed surface sand fraction profiles from different field sites and a small-scale laboratory experiment to determine the generality of this sorting feature.

Chapter 3 examines the relative importance of abrasion versus size selective sorting within an entire watershed by quantifying downstream changes in grain size and shape. The geometric theory of abrasion developed by *Domokos et al.* (2014) results in two distinct phases of abrasion. In the first phase, abrasion causes an initially blocky pebble to evolve to the shape of an inscribed ellipsoid, with no change in axis lengths, as the regions of high curvature are worn away. In the second phase, the fully convex ellipsoid evolves to a sphere as axis lengths are reduced. Through the use of several shape descriptors, calculated from both hand measurements and image-based techniques, we seek verification of this two-phase abrasion theory in a natural setting. Then, we determine the contribution of both abrasion and sorting to pebble size and shape evolution by using measured grain data from the field in a numerical model which couples the geometric abrasion theory with basic selective sorting rules.

Chapter 4 investigates the scaling of impact energy on abrasion rates of different lithologies of grains. Previous laboratory experiments on abrasion track mass loss with time in a tumbling mill or circular flume in order to determine diminution coefficients (α) from eq. (1.1) (*Wentworth*, 1919; *Krumbein*, 1941; *Kodama*, 1994a; *Lewin and Brewer*, 2002). However, extrapolating α values from the lab to the field requires the assumption that duration of

experiment is a proxy for distance along a river. This assumption is not always the case, as abrasion can occur while grains are immobile on the bed by collisions of transported grains (*Schumm and Stevens*, 1973; *Brewer et al.*, 1992). Unlike previous experiments, in this chapter, we isolate the impact energy by monitoring the abrasion of well-controlled binary collisions of grains. Furthermore, we measure the strength and material properties of the grains to quantitatively determine their effects on abrasion rates. Finally, we examine the fine particles produced during the abrasion process. Brittle fracture theory states that the daughter products resulting from full fragmentation follows a Weibull distribution (*Brown and Wohletz*, 1995; *Kok*, 2011). Although abrasion of river sediments is at much lower energies than those required for full fragmentation, we hypothesize that brittle fracture theory may apply to abrasion over some limited depth where the collision energy is attenuated. To test this idea, we characterize the grains size distribution of the daughter products of abrasion to see if they display the same functional form expected from brittle fracture theory.

The unifying theme of this dissertation is that grain size is the predominant factor governing channel morphology and therefore a deeper understanding of the mechanisms controlling grain size is necessary. Grain size patterns provide evidence of the interplay between fluid mechanics, granular physics, and material science. By incorporating theories and techniques from these fields, we develop a more complete comprehension of grain size patterns, which elucidates studies of past, present, and future fluvial systems. For example, a mechanistic understanding of grains size will yield insight into past fluvial conditions when these patterns are preserved in the stratigraphic record (*Rice*, 1999). Furthermore, with regards to future river systems, an understanding of the controls on downstream grain size patterns provides guidance for river restoration projects which have implications for stream ecology, such as spawning habitat for fish populations (*Lisle*, 1989; *Kondolf and Wolman*, 1993). Overall, this work provides the framework for starting to view grain size change in a more mechanistic manner.

CHAPTER 2 : Generalized Sorting Profile of Alluvial Fans

Chapter submitted for publication as:

Litwin Miller, K., M. E. Reitz, and D. J. Jerolmack (2014),Generalized sorting profile of alluvial fans, *Geophysical Research Letters* (in review).

Abstract:

Alluvial rivers often exhibit self-similar gravel size distributions and abrupt gravel-sand transitions. Experiments suggest these sorting patterns are established rapidly, but how – and how fast – this convergence occurs in the field is unknown. We examine the establishment of downstream sorting patterns in a km-scale alluvial fan. The sharp transition from canyon to unconfined, channelized fan provides a well-defined boundary condition. The channel changes from deep and entrenched at the fan apex to shallow and depositional over a short distance, exhibiting non-equilibrium behavior. The resulting gravel fining profile is not self-similar; the particle size distribution narrows until approximate equal mobility is achieved. Downfan, the gravel-sand transition appears to exhibit a self-similar form; field and laboratory data collapse when downstream distance is normalized by the location of the transition. Results suggest a generalized sorting profile for alluvial fans as a consequence of the threshold of motion and non-equilibrium channels.

2.1. Introduction and Background

Downstream changes in particle size exert a strong control on sediment transport and alluvial channel geometry. The observed pattern of an exponential decline in downstream particle size is so ubiquitous that it has been elevated to a law (*Sternberg*, 1875; *Rice*, 1999; *Pizzuto*, 1995; *Domokos and Gibbons*, 2013). *Fedele and Paola* (2007) demonstrated that "Sternberg's Law" may arise from size-selective deposition, and revealed an even more remarkable finding. For the case of gravel, a simplification of the transport equations predicts that the standard deviation of the grain size distribution (GSD), σ, decays at a similar exponential rate to the mean, $\bar{D}$; the coefficient of variation $C_v = \sigma/\bar{D}$ thus remains approximately constant (*Fedele and Paola*, 2007). This pattern is borne out in data from natural rivers, and flume experiments of a prograding sediment wedge. The latter suggest that the sorting profile is established early on in river profile evolution, and then essentially "stretches" as the river continues to prograde. As a consequence, sorting profiles at different stages of river evolution are identical when downstream distance (x) is normalized by the length of the gravel reach (L_g), i.e., $x_* = x/L_g$. Determining whether this self-similar sorting profile is as ubiquitous as Sternberg's Law requires substantially more data. A natural question that arises from the *Fedele and Paola* (2007) results is: what determines the limit to sorting in bed load (gravel) streams? A reasonable hypothesis is that size-selective transport narrows the GSD until particles are approximately equally mobile, in terms of their threshold entrainment stress (cf. *Parker and Klingeman*, 1982; *Wiberg and Smith*, 1987), and that the constant C_v is a reflection of this state. This hypothesis has not been tested, and the equilibrium *Fedele and Paola* (2007) theory cannot be used to predict how – or how rapidly – an arbitrarily heterogeneous initial GSD would converge toward a constant value.

Another common grain-size pattern in rivers is the gravel-sand transition. This transition is remarkable for several reasons: (1) it implies that river sediments have a bimodal distribution, regardless of lithology or geologic setting (*Smith and Ferguson*, 1995; *Ferguson*, 2003;

Knighton, 1999); (2) transport conditions change dramatically, from a near-threshold bed load channel in the gravel reach to a suspension-dominated channel in the sandy portion (*Paola et al.*, 1992; *Parker and Cui*, 1998; *Fedele and Paola*, 2007); and (3) the transition takes place over a distance that is small compared to the upstream gravel reach (*Ferguson*, 2003; *Frings*, 2011). Despite the relative abruptness of the gravel-sand transition, it is not infinitesimal; it is marked by a systematic downstream increase in the surface-sand fraction (F_s) from 0 to 1, and a concomitant decrease in slope. There are surprisingly few field data documenting grain size and channel geometry patterns across the gravel-sand transition, and a complete theory is lacking. It has been suggested that the transition is governed partly by the mutual influence of sand and gravel on the threshold entrainment stress of each population (*Wilcock and Kenworthy*, 2002; *Ferguson*, 2003). *Wilcock and Kenworthy* (2002) used laboratory data to demonstrate that an increase in sand fraction causes a decrease in the threshold Shields stress (τ_{*c}) for both gravel and sand; this effect is encapsulated in the empirical formula:

$$\tau_{*cg} = \tau_{*cg1} + (\tau_{*cg0} - \tau_{*cg1}) \exp^{-14F_s} \tag{2.1}$$

where τ_{*cg1} and τ_{*cg0} is the critical Shields stress for gravel with $F_s = 1$ and 0, respectively. The decrease in Shields stress for the sand fraction is greater than that of gravel, causing a segregation of the two size fractions. *Ferguson* (2003) demonstrated that inclusion of this effect in a numerical model for river-profile evolution produced realistic-looking gravel-sand transitions, but model results have not been compared to field data. At present there is no analytic theory for sorting across the gravel-sand transition to complement the self-similar sorting theory for gravel.

Alluvial fans are useful systems to study in order to address the questions raised above. Many fans are strongly depositional and short in length, enhancing the dominance of size-selective deposition and suppressing the confounding effects of abrasion (cf. *Hooke*, 1967; *Blair and McPherson*, 1994; *Parker et al.*, 1998). The apex of an alluvial fan presents

a well-defined upstream boundary condition. Because fans are typically fed by bedrock canyons – which lack deposition – they receive an initially unsorted, heterogeneous GSD. *Stock et al.* (2008) documented rapid deposition and downstream fining, and an associated rapid decrease in channel hydraulic radius, on several alluvial fans. Their observed grain-size trends appear to be qualitatively similar to those seen in much larger rivers, motivating us to quantify these patterns and seek generality. In this study we examine downstream trends in grain size and channel geometry on a kilometer-scale alluvial fan, and make comparisons to previously published meter-scale laboratory experiments. We find that as the channel adjusts from deep and entrenched to shallow and depositional, the gravel fining is not self-similar, and we demonstrate that gravel sorts toward an apparent limit associated with equal mobility. Data suggest that sorting across the gravel-sand transition does indeed exhibit a self-similar form, which should help to guide further theoretical development.

2.2. Methods

The field site for this research is the Dog Canyon alluvial fan (Fig. 2.1a), at Oliver Lee State Park near Alamogordo, New Mexico. Dog Canyon drains the Sacramento Mountain range, which is composed primarily of Pre-Cambrian and Permian limestone and makes up the eastern boundary of the Tularosa Basin (*Herrick*, 1900). At its exit from the mountains the channel crosses a normal fault, which marks the transition to the alluvial fan, and continues as an alluvial channel approximately 12 m wide and 1.2 m deep at the apex of the fan, defined as $x = 0$ km. A secondary channel splits from the main channel at approximately 0.7 km from the fan apex (Fig. 2.1a). Channel substrate is predominantly rounded gravel for the first 1.7 km, and grain size and channel depth decrease systematically over this distance (Fig. 2.1). The fan then transitions over several hundred meters to a sandy bed, at which point alluvial channels become difficult to distinguish. The short distance of the gravel reach precludes abrasion as a contributor to downstream fining patterns, and images confirm that there is no significant shape change for gravels moving down fan. Head-cutting gullies exist in the sandy portion of the fan and have incised up to approximately the beginning of the

gravel-sand transition, ~ 1.7 km from the fan apex. They are distinguishable on the ground by their deep and narrow geometry; their interference with the more subtle alluvial channels at the gravel-sand transition make it impossible to characterize channel geometry on the sand-influenced portion of the fan.

We characterized channel geometry, particle size, and elevation along the fan. The long profile of the main channel of the alluvial fan, as well as the adjacent floodplain (i.e., fan surface), was measured using a Trimble GeoXH differential global positioning system (DGPS) with an associated lateral error of 0.1 m and a vertical error of up to 1 m. The DGPS data were smoothed using a 100 m window moving average; the resulting profile is seen in Fig. 2.1a. The slope (S) above the gravel-sand transition may be approximated as constant and equal to $S = 0.04$, and rapidly decreases over a distance of 900 m to a lower constant value of $S = 0.01$ for the sand-bedded fan (Fig. 2.1a). To allow comparison to sorting models and other river systems, downstream distance is normalized by the length of the gravel reach. We define this length as the distance from the fan apex to the gravel-sand transition, $x_* = x/L_g$, where L_g is determined as the location where channel slope has completed adjustment (i.e., where $S = 0.01$; see Fig. 2.1a) and the gravel fraction is zero. An image-based autocorrelation technique ("Cobble Cam") (*Rubin*, 2004; *Warrick et al.*, 2009) was used to measure the mean grain size ($\bar{D}$) at 34 cross sections of the main channel spaced at intervals of approximately 125 m downstream. This technique also provides a measure of the variation in particle size akin to – but smaller than – the standard deviation, σ (see *Warrick et al.*, 2009). At each cross section, ~ 10 side-by-side images were taken to sample the entire width of the channel; values for $\bar{D}$ and variation from all images were averaged to produce representative values for each cross section. In order to produce estimates for σ at each cross section from images, each variation parameter was multiplied by a constant factor (1.5) that provided the overall best match with values for σ determined from pebble count data (see below). We also measured the surface sand fraction (F_s) of the bed in each image; due to a naturally occurring grain size gap, there was a clear visible distinction between sand (whose particle size could not be determined from

images) and gravel (Fig. 2.1b). Additionally, pebble counts ($n = 100$ grains) (*Wolman*, 1954) were completed at 21 cross sections of the main channel of the alluvial fan, and were used to validate the image method and to examine the full GSD. Finally, channel geometry was measured at 18 locations over the first approximate 1.4 km of the fan from its apex. Locations were selected at approximately constant intervals while preferentially choosing sites with well-defined channel banks. Locations for each cross-section site were recorded using the DGPS, and a laser range-finder with compass attachment was used to survey the channel geometry.

2.3. Sorting and Channel Patterns over the Gravel Reach

Mean grain size (> 2 mm) ($\bar{D}$), measured by both images and pebble counts, shows a distinct downstream fining pattern (Fig. 2.2a). While trends from the two methods generally agree, pebble count data show larger variability. Inspection of the pebble count data reveals that the mean grain size did not converge to a stable value at 100 counts. Since the image analysis method averages over thousands of grains, we believe these results are more reliable. The standard deviation of the grain size (σ) likewise shows a downstream decline for both methods (Fig. 2.2b), with the image technique exhibiting a smoother trend. In contrast to the findings of *Fedele and Paola* (2007), C_v is not a constant value. The coefficient of variation instead declines steadily downstream to $x_* = 0.5$, then begins to fluctuate. In other words, over the first half of the gravel reach, the σ of the GSD decreases faster than the $\bar{D}$, indicating a transient downstream sorting adjustment. Upstream of the location $x_* = 0.5$, sand makes up only a small portion of the substrate ($F_s < 0.1$), while F_s begins to rapidly increase downstream of this location (Fig. 2.3a). We suspect that the gravel sorting pattern becomes disrupted by the presence of sand, because local patchiness of sand and gravel will create strong spatial variations in the threshold of motion (e.g. *Paola and Seal*, 1995). Thus, we interpret the decrease in C_v up to $x_* = 0.5$ as the consequence of size-selective sorting of gravel by bed load transport in the (relative) absence of sand, and the highly variable C_v downstream of this location as reflecting the absence of size-selective

gravel sorting due to the presence of sand.

What physical meaning can be derived from the trend in C_v over the gravel portion of the fan? Our hypothesis is that gravels sort to a limiting GSD that reflects a state of equal mobility. To test this idea, we calculate the ratio of the threshold shear stress of the grain size one standard deviation above the mean ($\tau^c_{\bar{D}+\sigma}$) to that of the grain size one standard deviation below the mean ($\tau^c_{\bar{D}-\sigma}$), using the hiding function from *Wilcock and Crowe* (2003):

$$\frac{\tau_i}{\tau_{50}} = \left(\frac{D_i}{D_{50}}\right)^b \tag{2.2}$$

where

$$b = \frac{0.67}{1 + \exp(1.5 - \frac{D_i}{D_{sm}})} \tag{2.3}$$

and where τ_i and τ_{50} are the critical shear stresses required to transport the i^{th} and 50^{th} percentile grain size D_i and D_{50}, respectively, and D_{sm} is the surface mean grain size. Our image technique only measures the mean, not the median, so we use $\bar{D}$ for both D_{50} and D_{sm}. Pebble count data indicate that the mean and median are typically within 20% of each other. The computed ratio of the threshold stresses, $\bar{D}+\sigma$ to $\bar{D}-\sigma$, decreases towards unity from the apex of the fan to the location $x_* = 0.5$ (Fig. 2.2d). We note that similar results are obtained using threshold stress values computed using the method of *Wiberg and Smith* (1987). These calculations support the notion that gravels on the Dog Canyon fan sort toward a limit of equal mobility, at which point all gravel sizes have comparable entrainment stresses.

2.4. Gravel Sand Transition

As the gravel reaches its sorting limit on Dog Canyon fan, the channel starts to rapidly transition from gravel to sand bedded. The pattern of downstream increase in F_s observed at Dog Canyon (Fig. 2.3a) is similar to the numerical results of *Ferguson* (2003) for model runs that included the *Wilcock and Kenworthy* (2002) two-fraction threshold (eq. (2.1)) [*cf. their Fig. 3*]. We would like to understand whether this gravel-sand transition pattern

is general, and therefore we seek self-similarity in the sand fraction profile. Dog Canyon results are compared to data from two other systems at very different scales. The first is from laboratory experiments of *Reitz and Jerolmack* (2012) with a length scale $L_g \sim 10^{-3}$ km, which featured a bi-modal mixture of granite chips and acrylic sand that scales to a cobble-sand mixture in the field; details of the experiment can be found in *Reitz and Jerolmack* (2012). The second is the Rhine River, with a length scale $L_g \sim 10^2$ km (*Frings*, 2011). For all systems, the gravel-sand transition exhibits a very similar pattern of increasing F_s when distance is normalized by the length of the upstream gravel reach. Downstream changes in F_s appear to follow a sigmoidal curve (Fig. 2.3a). On closer inspection, however, we see that the curve is not symmetric; it may be better approximated as two segments. In the first segment, sand fraction increases slowly and perhaps linearly from $F_s = 0$ at $x_* = 0$ to $F_s \approx 0.2$ at $x_* \approx 0.6$. In the second segment there is a rapid and qualitatively different pattern of increasing F_s toward a value of 1. This proposed separation occurs at a surface sand fraction of 20%, which coincides with the point that a river bed transitions from a gravel-supported to a sand-supported matrix (*Wilcock and Kenworthy*, 2002). As a further test of self-similarity, we plot the length of the gravel-sand transition (as determined from slope changes in river profiles), L_t, against L_g for a large number of rivers using the compilation of (*Ferguson*, 2003) (Fig. 2.3b). The data are best-fit by a power law, which is nearly linear with an exponent of 0.92, implying that L_t is a constant fraction of L_g – approximately 12%. Taken together, the collection of data over different scales indicates that the gravel-sand transition is indeed self-similar.

2.5. Channel Geometry

At its exit from the canyon, the Dog Canyon channel is entrenched relative to the fan surface; the channel at the apex of the fan is relatively deep and narrow. At $x = 550$ m, the channel and fan-surface profiles converge. Over this region, the measured channel depth (h) rapidly decreases and channel geometry shifts from being single-threaded with well-defined banks, to a braided channel with indistinguishable boundaries (Fig. 2.4b). For a self-

formed gravel river at equilibrium, theory predicts that the channel is adjusted such that the Shields stress at bankfull is slightly in excess of the threshold value for the mean grain size (*Parker*, 1978); the average value from field observations is $\tau_* = 1.4\tau_{*c}$ (*Paola et al.*, 1992; *Dade and Friend*, 1998; *Parker and Cui*, 1998; *Parker et al.*, 2007). There is reason to believe, however, that this prediction should not hold on the Dog Canyon fan or alluvial fans generally. In laboratory alluvial fan experiments, *Reitz and Jerolmack* (2012) observed an avulsion (channel switching) cycle of channel cutting, progradation, and backfilling; for most of the avulsion cycle, the channel was entrenched at the fan apex and transitioned downstream to a shallower, depositional form. This pattern is common on alluvial fans, and is what we observe at Dog Canyon. *Reitz and Jerolmack* (2012) proposed that alluvial fan channels are in a perennial state of disequilibrium due to the progradation-avulsion cycle, and that channelization in this setting is a transient phenomenon. To understand controls on transport and channel organization on the Dog Canyon fan, we estimated the bankfull Shields stress profile, $\tau_*(x) = (h(x)S)/(R\bar{D}(x))$, from best-fit equations to downstream trends in h and $\bar{D}$. We compare the calculated bankfull Shields stress with the expected threshold value using the two-fraction threshold eq. (2.1) with a best fit linear relation for F_s over the gravel region of the fan; we computed $\tau_{*cg0} = 0.1082$ by applying the slope correction from (*Mueller et al.*, 2005), and assume a lower value of $\tau_{*cg1} = 0.01$ in accordance with *Wilcock and Kenworthy* (2002) (Fig. 2.4b). Both Shields stress and critical Shields stress decrease exponentially downstream at approximately the same rate, making the ratio almost constant; however, the computed value $\tau_* \approx 6\tau_{*c}$ implies transport that is far above threshold. Moreover, "bankfull" at the entrenched fan apex may not be related to any formative flood, as the transient channel may be incising. Therefore, it is not clear that the estimated Shields stress profile is representative of any actual transport conditions. Based on the entrenched channel head and its transition to a shallow depositional channel downstream, we infer that the Dog Canyon fan is not in equilibrium, and likely exhibits strongly non-uniform transport conditions downstream. It is possible that this transition drives the transient response in grain size sorting along the gravel-dominated portion of the

fan.

2.6. Discussion and Conclusions

Field and laboratory data indicate that sand deposits gradually downstream in a gravel-bed river, until it reaches a critical fraction ($F_s \approx 0.2$) that is sufficient to disrupt the gravel matrix. Three things happen at this point on the Dog Canyon fan: (1) the surface sand fraction increases rapidly; (2) channels quickly decay in depth and disappear; and (3) channel slope begins to decrease. We separate the discussion, therefore, into distinct problems associated with distinct patterns: sorting and channel adjustment in gravel-dominated upstream segment of the fan, and sorting across the gravel-sand transition.

Gravel sorting at Dog Canyon produces a downstream decrease in C_v, in apparent contradiction to the prediction and empirical findings of *Fedele and Paola* (2007). However, this may not be wholly unexpected. Downstream channel geometry indicates non-equilibrium and strongly nonuniform conditions, likely a result of transient channel adjustments due to the cycle of progradation and avulsion. The *Fedele and Paola* (2007) model does not treat mixed gravel-sand transport, it assumes a constant Shields stress, and assumes equilibrium channel conditions. Transient channel dynamics may be causally related to the anomalous gravel-fining trend on Dog Canyon, and this may be a common feature of alluvial fans generally, but more work is needed. It is intriguing that gravel sorting appears to approach a condition of equal mobility (Fig. 2.2d), at which point sand deposition increases rapidly and the gravel sorting pattern is destroyed. There may be a limiting C_v that reflects the limiting hydraulic sensitivity of size-selective entrainment (cf. *Fedele and Paola*, 2007). *Jerolmack et al.* (2011) observed saturation of sorting effects after several kilometers in an aeolian dune field, at the point where the GSD achieved an empirical limit related to modes of grain transport. Future research should explicitly explore and test this idea.

Considering the gravel-sand transition, there is evidence that sorting across the transition follows a self-similar form (Fig. 2.3). The collapse of data from systems spanning 6 orders

of magnitude in spatial scale suggests that the dynamics controlling sand deposition are insensitive to local details of hydraulics, topography and particle size. What is common to all systems is a bimodal GSD, in which the coarse particles deposit first to form a steeper portion of the channel while the finer particles travel in suspension. It appears that the gravel-sand sorting profile emerges rapidly, and then is stretched as rivers lengthen – analogous to proposed self-similar gravel sorting patterns of *Fedele and Paola* (2007). While an analytical model for the gravel-sand transition is currently unavailable, data suggest that there may be a general similarity solution.

Three concepts - size-selective sorting, equal mobility, and transient channel dynamics (*Parker and Klingeman*, 1982; *Wiberg and Smith*, 1987; *Fedele and Paola*, 2007; *Reitz and Jerolmack*, 2012) - have been used to explain the first-order trends in grain size and channel geometry observed on the Dog Canyon fan. Given the generality of these concepts, our conclusions may be critically tested by examining grain-size trends on other alluvial fans.

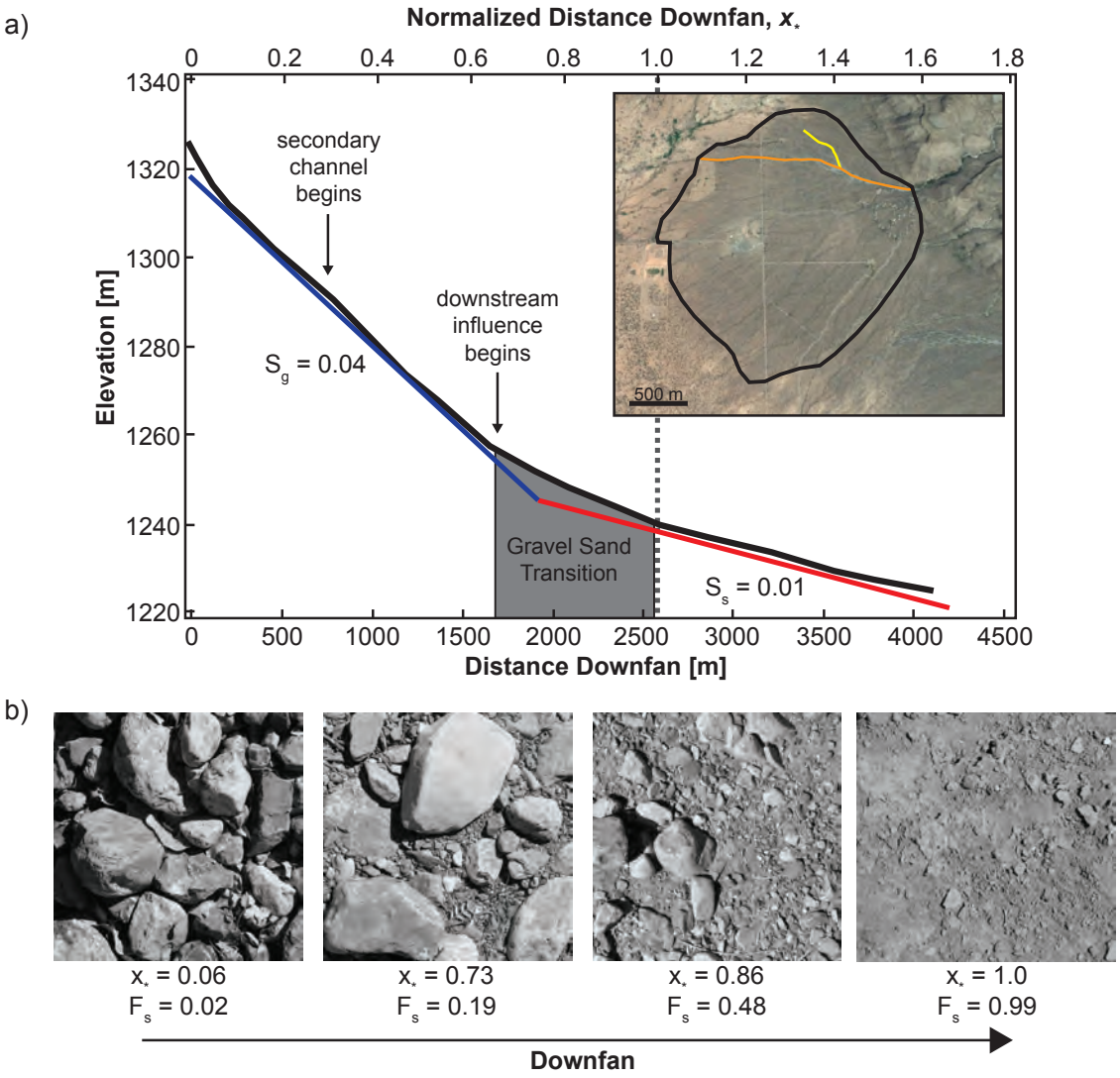

Figure 2.1: Dog Canyon alluvial fan. a) Channel profile from smoothed DGPS data. The upper gravel reach has an approximately constant slope of 0.04 which rapidly decreases to 0.01 after the gravel-sand transition. At $x_* = 0.3$ a secondary channel splits from the main channel. At $x_* = 0.63$ the gravel-sand transition begins and headcutting gullies from downstream start to affect channel geometry. Inset shows aerial image of fan with the entire fan outlined in black, main channel denoted by the orange line, and secondary channel denoted by the yellow line. b) Images of the channel bed illustrating increase in surface sand content.

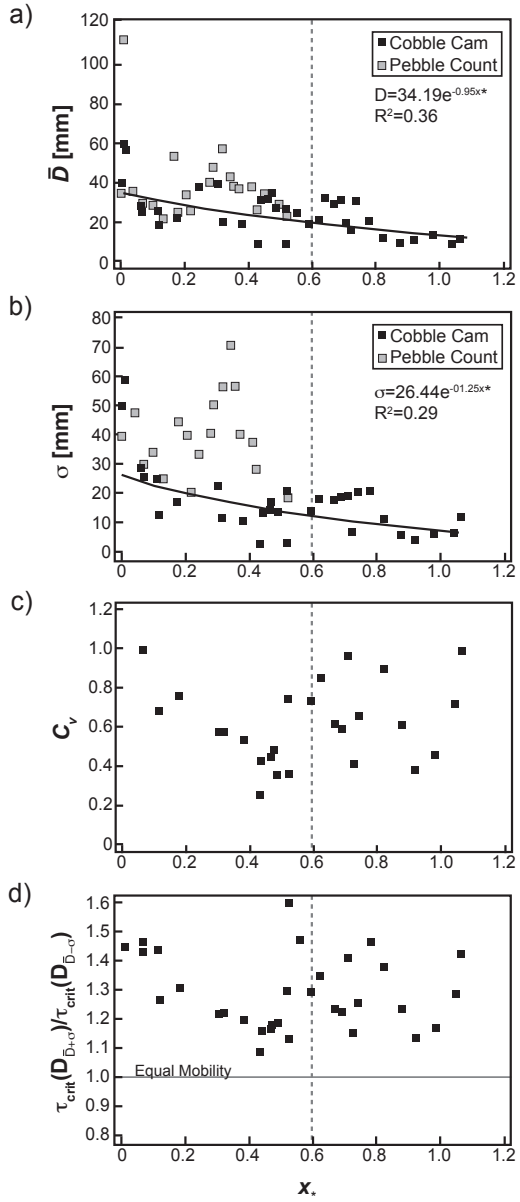

Figure 2.2: Gravel grain-size sorting. Dashed line denotes location where channel bed transitions from gravel to sand matrix. a) Grain size profile from both pebble count and image data shows a decrease downstream. b) Standard deviation of grain size decreases downstream. Exponential fits in (a) and (b) are to image data. c) Coefficient of variation of grain size shows systematic decline in gravel region, and then fluctuates when sand dominates channel. d) Ratio of threshold Shields stress for grain size one standard deviation above and below mean. Plot shows grain size distribution approaches a state of equal mobility.

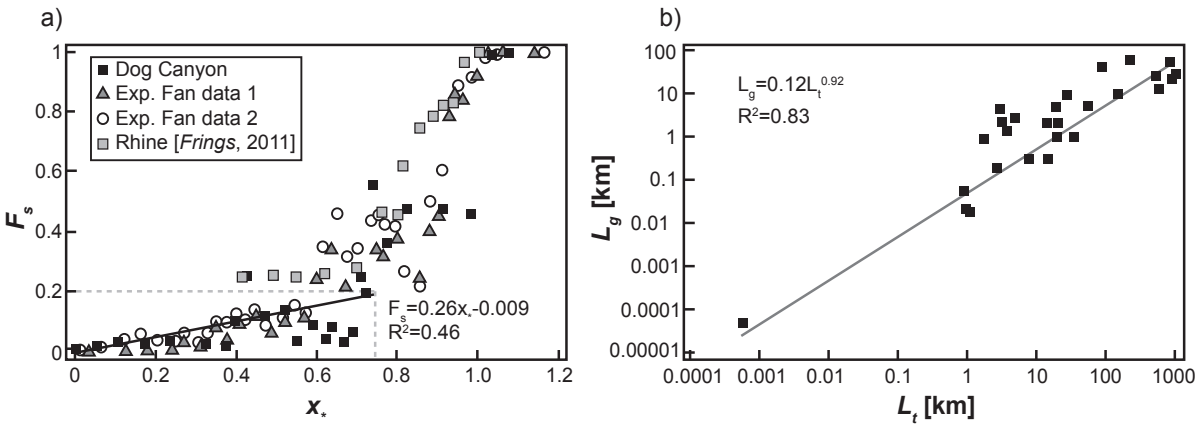

Figure 2.3: Gravel-sand transition. a) Surface sand fraction profile for Dog Canyon alluvial fan, two experimental fans (*Reitz and Jerolmack*, 2012), and the Rhine river (*Frings*, 2011). When sand fraction is plotted versus normalized downstream distance, the curves collapse indicating that the gravel-sand transition is self-similar. b) Compilation of sizes of gravel-sand transitions from data collected by *Ferguson* (2003), Dog Canyon, and fan experiments. The best-fit power law is close to linear (exponent of 0.92) indicating a self-similar "stretching" of the gravel-sand transition.

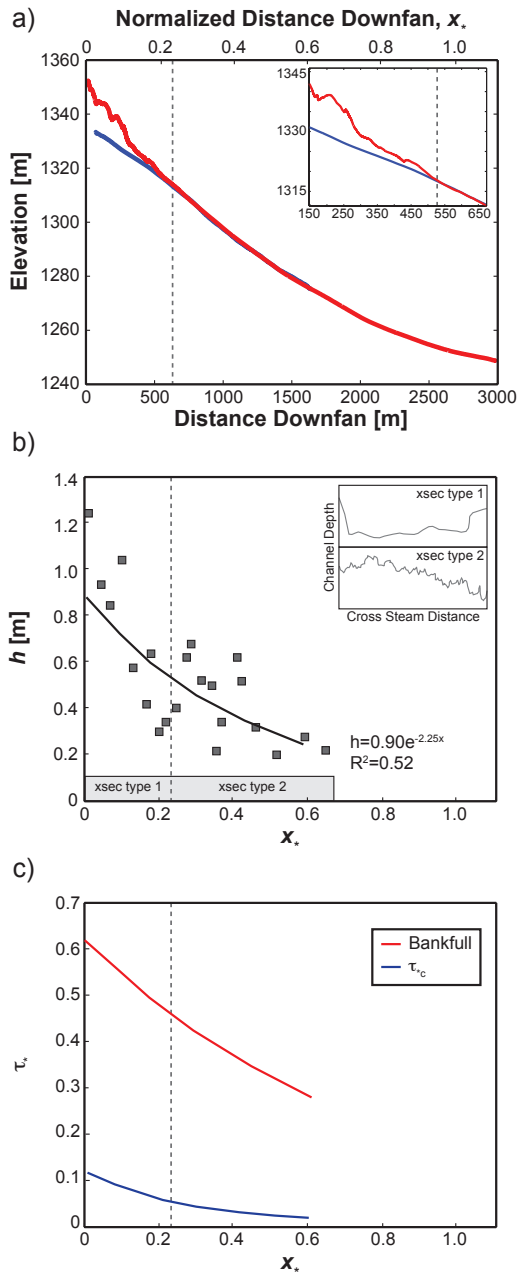

Figure 2.4: Channel geometry. Dashed line denotes location where the channel is no longer entrenched. a) Comparison of fan profile (red) to channel profile (blue) from smoothed DGPS data. Channel is initially entrenched for the first $x = 550$ m. b) Plot of measured average channel depths downstream. Where the channel is not entrenched, the depth is measured as twice the standard deviation of the cross-stream elevation profile. Inset shows the difference in channel geometry in the two regions as the channel transitions from well-defined banks to braided. c) Plot showing estimated bankfull Shields stress (red) and calculated threshold Shields stress.

CHAPTER 3 : Quantifying the Significance of Abrasion and Selective Transport on Downstream Pebble Evolution

Chapter submitted for publication as:

Litwin Miller, K., T. Szabó, D. J. Jerolmack, and G. Domokos (2014), Quantifying the significance of abrasion and selective transport on downstream pebble evolution, *Journal Geophysical Research: Earth Surface* (in review).

Abstract:

It is well known that pebble diameter systematically decreases downstream in rivers. The contribution of abrasion is uncertain, in part because: (1) diameter is insufficient to characterize pebble mass loss due to abrasion; and (2) abrasion rates measured in laboratory experiments cannot be easily extrapolated to the field. A recent geometric theory describes abrasion as a curvature-dependent process that produces a two-phase evolution: in Phase I, initially blocky pebbles round to smooth, convex shapes with little reduction in axis dimensions; then, in Phase II, smooth, convex pebbles slowly reduce their axis dimensions. Here we provide the first confirmation that two-phase abrasion occurs in a natural setting, by examining downstream evolution of shape and size of thousands of pebbles over ~ 10 km in a tropical montane stream. The geometric theory is verified in this river system using a variety of manual and image-based shape parameters, providing a generalizable method for quantifying the significance of abrasion. Phase I occurs over ~ 2 kilometers, in upstream bedrock reaches where abrasion is dominant and sediment storage is limited. In downstream alluvial reaches, where Phase II occurs, we observe the expected exponential decline in pebble diameter. Using a discretized abrasion model (the so called "box equations) with deposition, we deduce that abrasion removes more than 1/3 of the mass of a pebble, but that size-selective sorting dominates downstream changes in pebble diameter. Overall, abrasion is the dominant process in the downstream diminution of pebble mass (but not diameter) in the studied river, with important implications for pebble mobility and the production of fine sediments.

3.1. Introduction

The ubiquitous pattern of rounded river rocks has long been known to result from the smoothing action of abrasion, due to grain-grain collisions during bed load transport (*Wentworth*, 1919; *Kuenen*, 1956; *Sneed and Folk*, 1958; *Parker*, 1991; *Kodama*, 1994a; *Lewin and Brewer*, 2002). The transformation of initially blocky and angular rocks – typical of upstream reaches of rivers – to ellipsoidal pebbles downstream implies that a significant fraction of pebble mass is lost due to abrasion (*Domokos et al.*, 2009; *Szabo et al.*, 2013). The daughter products of abrasion are not infinitesimal; sand and silt produced from pebble collisions may be an important contributor to downstream floodplains, estuaries and beaches, and may help to maintain the observed bimodality of grain size distributions of riverbeds (*Jerolmack and Brzinski*, 2010, and references therein). Although it has long been recognized that shape is an important indicator of the degree of abrasion of a sedimentary particle (so-called "maturity"), surprisingly few studies have quantified the downstream evolution of pebble shape in rivers (*Sneed and Folk*, 1958; *Bradley et al.*, 1972; *Adams*, 1979; *Mikos*, 1995; *Szabo et al.*, 2013).

The most commonly measured quantity in field studies of river rocks is the middle axis length, typically called "diameter", which is used as a proxy descriptor of particle "size" (*Kodama*, 1994b; *Lewin and Brewer*, 2002; *Attal et al.*, 2006). A near-universal trend observed in alluvial rivers, often referred to as "Sternberg's Law" (1875), is that pebble diameter (D) decreases exponentially with distance downstream (x):

$$D(x) = D_0 e^{-\gamma x}, \tag{3.1}$$

where D_0 is initial pebble diameter at the upstream alluvial boundary and γ is an empirically-determined parameter. For decades, researchers have attempted to rationalize this relation (eq. (3.1)) from theory and laboratory experiments (*Krumbein*, 1941; *Adams*, 1978; *Kodama*, 1994a; *Mikos*, 1995; *Lewin and Brewer*, 2002; *Attal and Lave*, 2009). Although

Sternberg originally proposed that this downstream decline in particle diameter was due to abrasion, there is a consensus now that the dominant effect is size-selective transport, in which larger grains are preferentially deposited and smaller particles travel farther downstream (*Paola et al.*, 1992; *Seal and Paola*, 1995; *Paola and Seal*, 1995; *Ferguson et al.*, 1996; *Gasparini et al.*, 1999). In particular, *Fedele and Paola* (2007) derived a simplified theory in which eq. (3.1) arises as a consequence of size-selective sorting. What role, if any then, does abrasion play in the downstream fining of pebbles?

Many researchers have used laboratory experiments to quantify abrasion rate as a result of collisions among pebbles during bed load transport, typically through employing tumbling mills (*Wentworth*, 1919; *Krumbein*, 1941; *Kodama*, 1994a; *Lewin and Brewer*, 2002) or circular flumes (*Lewin and Brewer*, 2002; *Attal et al.*, 2006). Although measured rates vary greatly depending on the type of apparatus employed and also pebble lithology, a unifying conclusion has been that abrasion rates are generally too slow to account for observed fining trends (described by eq. (3.1)) in rivers (*Adams*, 1978; *Hoey and Bluck*, 1999; *Morris and Williams*, 1999). This conclusion is not without objection, however, mainly on two fronts: (1) most experiments do not simulate the high-energy collisions typical of steep mountain streams, and those that do produce results more consistent with expectations from the field (*Kodama*, 1994b; *Lewin and Brewer*, 2002; *Attal and Lave*, 2009); and (2) experiments usually measure mass loss while field studies typically measure changes in diameter, but the two can only be directly compared if the exact shape of the pebbles are known, which they are not (*Kodama*, 1994a; *Lewin and Brewer*, 2002; *Domokos et al.*, 2014). Even if suitable collision energies can be generated in the laboratory, extrapolating these results to the field also requires reliable estimates of the frequency of grain-grain collisions and the transport distances between collisions (*Sklar and Dietrich*, 2004; *Turowski et al.*, 2013). Duration of tumbling mill experiments is used as a proxy for distance in the field, providing only an indirect link to abrasion rate.

A new approach has been undertaken recently, in which a generalized geometric theory

for abrasion (*Firey*, 1974; *Bloore*, 1977) has been adapted to describe the evolution of pebble shape; this process can be visualized by plotting shape descriptors versus volume (*Domokos et al.*, 2014). The model will be described below, but its essence is that abrasion rate at any point on a pebbles surface is a function of the local curvatures. Experiments involving a single initially-cuboid pebble in a tumbler, designed to simulate the idealized conditions assumed in the derivation of the model, showed quantitative agreement with model predictions (*Domokos et al.*, 2014). Results imply that the significance of bed load abrasion in a river may be assessed by examining changes in pebble shape and volume downstream, circumventing the need to extrapolate abrasion rates from the laboratory. A major finding from the geometric theory and its companion experiment was that abrasion of an initially blocky particle occurs in two phases: Phase I, in which the pebble abrades to a convex shape *without any major change in axis dimensions*; after which it proceeds to Phase II, where the convex pebble slowly reduces its axis dimensions.

If two-phase abrasion occurs in rivers, it suggests that most of the mass loss from abrasion goes undetected in field studies because researchers only measure diameter. It is an open question, however, whether the idealized geometric model may be applied to abrasion by bed load in natural field settings. This paper presents the first use of geometric theory to identify two-phase abrasion and its significance in a natural river. First we present the general theoretical framework, which informs our choice of parameters to characterize the size and shape of pebbles. We then introduce a field location in northeast Puerto Rico, where a river was selected that allows us to isolate the contributions of abrasion and size-selective sorting. By examining downstream trends in pebble size and shape over ten kilometers, we test for the qualitative pattern of two-phase abrasion and seek quantitative verification of the geometric model. A simplified abrasion and deposition model is then employed to determine the contribution of abrasion and size-selective sorting to downstream diminution of pebble mass and diameter. Finally, we present a generalized method for determining the contribution of abrasion in other field settings.

3.2. Theory of Pebble Abrasion

3.2.1. Kinetic Energy, Mass Loss, and Sternberg's Law

Numerous theoretical and experimental studies have demonstrated that the magnitude of mass removed from a particle undergoing collision is proportional to the kinetic energy of the impact (*Anderson*, 1986; *Attal and Lave*, 2009; *Domokos and Gibbons*, 2013). Assuming a steady rate of impacts over time, in the continuous limit the rate of mass loss for a pebble of mass M due to abrasion becomes $dM/dt = -kMu_s^2$, where u_s is the velocity of the pebble, and k is a coefficient related to strength of the rock and additional transport parameters not explicitly considered. For bed load transport in a typical alluvial river, u_s is proportional to the stream fluid velocity (u_f) (see *Lajeunesse et al.* (2010); *Martin et al.* (2012), which is only a slowly-varying function of discharge ($u_f \propto Q^{1/6}$) (*Leopold et al.*, 1964; *Parker et al.*, 2007). To first order, one can thus consider pebble velocity constant, with two consequences: (1) the rate of mass loss of a pebble is proportional to its mass; and (2) downstream distance in a river is proportional (but not equivalent) to time ($ds \propto u_s dt$). Thus, one expects that downstream changes in pebble mass due to abrasion will take the form of an exponential, $dM/M \propto -kdx \rightarrow M \propto M_0 e^{-kx}$. Cast in terms of pebble volume (assuming constant density) and neglecting coefficients of proportionality, the downstream diminution of pebble size due to abrasion takes the form:

$$V = V_0 e^{-kx}. \tag{3.2}$$

It should be apparent that eq. (3.2) is related to Sternberg's Law (eq. (3.1)). Indeed, laboratory experiments that measure mass loss demonstrate the validity of eq. (3.2), but then convert it into Sternberg's Law by assuming that $D \propto V^{1/3}$ (and hence $\alpha = k/3$) to predict the anticipated effect of abrasion on downstream fining (*Kodama*, 1994a; *Lewin and Brewer*, 2002). Although the heuristic derivation above is rather simplistic, it demonstrates that one can rationalize Sternberg's Law (eq. (3.1)) from either size-selective sorting (*Fedele*

and Paola, 2007) or abrasion. The assumed proportionality between pebble diameter and volume results from an assumption that pebbles abrade in a self-similar fashion. This is certainly not true for river rocks which evolve from blocky fragments to smooth ellipsoidal shapes (*Krumbein*, 1941; *Kuenen*, 1956; *Lewin and Brewer*, 2002; *Durian et al.*, 2006; *Domokos et al.*, 2014). For initially polyhedral particles, abrasion may remove up to half of pebble mass without any reduction in D (*Lewin and Brewer*, 2002; *Domokos et al.*, 2014). Proper accounting for this geometric effect will paint a more accurate picture of the significance of abrasion.

3.2.2. Two-Phase Abrasion

The geometric modeling of pebble abrasion dates back to *Bloore* (1977), who described the shape evolution of a single pebble under collisional abrasion. The 2D equivalent of Bloores equation can be formulated as

$$v = 1 + c\kappa \tag{3.3}$$

where v is the attrition speed in the inward normal direction, c is the (average) perimeter of the abrading particles in the environment (*Varkonyi and Domokos*, 2011) and κ is the local curvature of the evolving 2D curve. In this description of abrasion there are two competing terms. If the abrading particles are small then c is also small and the first (so-called Eikonal) term ($v = 1$) dominates the process. This causes shapes to develop sharp edges and flat areas (Fig. 3.1a) such as in case of sandblasting (*Knight*, 2008; *Domokos et al.*, 2009). The second curvature term ($v = c\kappa$) dominates if the abrading particles are much larger, i.e. c is also large (Fig. 3.1b). We will call this second case curvature-driven abrasion. In 3 dimensions, κ is replaced by the linear combination of the so-called Mean and Gaussian curvatures; however, in case of very large abraders the Gaussian term dominates. In the field, curvature-driven abrasion can be interpreted as a saltating pebble undergoing abrasion by collision with a substrate composed of very large particles (boulders or bedrock). Curvature-driven abrasion depicts surface abrasion of a pebble as a diffusion process – akin to hillslope diffusion (*Culling*, 1960; *Hirano*, 1968; *Roering et al.*, 1999) – and it predicts

that arbitrary initial shapes converge asymptotically to a sphere (in 2D, a circle, Fig. 3.1b) (*Firey*, 1974; *Andrews*, 1999). (For a more elaborate description of geometrical abrasion theory, see *Varkonyi and Domokos* (2011); *Szabo et al.* (2013)).

Recently, *Domokos et al.* (2014) performed laboratory experiments simulating curvature-driven abrasion in which a single cuboid was abraded in a rotating drum that can be thought of as a very large abrader. They demonstrated that curvature-driven abrasion occurs in two phases, both in numerical simulation and in experiments: in phase I, sharp edges with high curvatures rapidly round off without major changes in the global axis dimensions until the original angular particle evolves to an ellipsoid-like shape; subsequently, in phase II, axis dimensions start to decrease slowly and the pebble becomes more spherical in shape (Fig. 3.2). While shape evolution occurred in two phases, they found that the rate of mass loss was continuous through both phases, and depended only on pebble mass; in other words, the volumetric diminution described by eq. (3.2) applies to abrasion in all phases, regardless of shape. However, the diameter diminution described by eq. (3.1) (Sternberg's Law) does not apply to Phase I abrasion, where diameter is almost constant. These authors thus suggested that eq. (3.2) is a more applicable "Generalized Sternberg's Law", relevant for abrasion. Although theory and experiment were for the idealized case of a single particle colliding with an infinitely large abrader, *Domokos et al.* (2014) suggested that this assumption might be relaxed such that the theory could apply to like-sized colliders in bed load transport. There are qualitative indications from a re-examination of classic experiments by *Krumbein* (1941) and *Kuenen* (1956) that this is indeed the case. This idea is explicitly tested in this study with field data.

Domokos et al. (2014)tracked several shape descriptors in both laboratory experiments and the corresponding numerical models. The simplest shape descriptors are the axis ratios S/L and I/L, where $L > I > S$ denote the three axis lengths of the bounding box of the pebble (Fig. 3.3). Axis ratios S/L and I/L remained approximately constant during phase I, and increased in phase II as the particle evolved towards a spherical shape. Another shape

descriptor tracked in their work was the convexity defined as $Conv_{3D} = S_C/S_H$, where S_C is the surface area of the convex regions and S_H is the total surface area of the convex hull of the particle. As the area of the intact surfaces of the abraded particle decreased during phase I, convexity increased in their experiments and numerical simulation until reaching $Conv_{3D} = 1$, and this value stayed constant in the subsequent phase II.

Numerous other shape parameters have been proposed in the literature to quantify the morphology of pebbles (*Blott and Pye*, 2007). Many of these parameters are defined on 2D projections of pebbles. The advantage of the latter is that one may take photographs of pebbles in the field and compute the shape descriptors automatically using standard image processing software. However, the evolution of most of these shape descriptors under curvature-driven abrasion is unknown. Nevertheless, we are aware of two 2D-shape descriptors, which are known to change monotonically under curvature-driven abrasion – and hence may be used to test the geometric theory. The first one is the isoperimetric ratio defined as $IR = 4\pi A/P^2$, where A is the area enclosed by the evolving 2D curve and P is the perimeter of the curve (Fig. 3.3). IR is often referred to as circularity (*Blott and Pye*, 2007) or roundness (*Cox*, 1927) in the literature. For a perfect circle $IR = 1$, and for any other curve $IR < 1$. It was proven by *Gage* (1983) that IR increases monotonically under curvature-driven abrasion. Although the shape evolution of a 2D curve differs from the shape evolution of the 2D projection of a 3D particle, we expect similar behavior for the projections.

The second shape descriptor is the entropy defined by the curvature distribution along the perimeter of the 2D curve, which we will refer to as the curvature entropy. Curvature entropy was originally defined for smooth, convex curves by *Chow* (1991), who showed that if the perimeter of the curve is normalized to unity ($P = 1$) then the curvature entropy increases under curvature-driven abrasion. However, a pebbles surface is naturally non-smooth (*Domokos et al.*, 2012) and, moreover, a photo taken of the 2D projection of a pebble has a finite resolution, so in our approximation pebble contours are represented by

convex polygons. By suitable interpolation we replace the original polygon by a polygon with equal sides. In this case, instead of using the curvature entropy as described in *Chow* (1991), we apply its discrete analogue, the so-called Shannon information entropy (*Shannon*, 1948), $H_S = -\sum_{i=1}^{m} \frac{\alpha_i}{2\pi} \log\left(\frac{\alpha_i}{2\pi}\right)$. Here, α_i is the external angle at the ith vertex of the m-sided convex hull of the pixel contour resulting from the image processing (Fig. 3.4). Based on the results of *Chow* (1991), it can be shown that for fixed value of m, the Shannon curvature entropy H_S also increases under curvature-driven abrasion. The physical interpretation is as follows. As the 2D contour of a pebble evolves toward a circle under abrasion, the curvature along the pebbles perimeter becomes more uniform (and curvature entropy increases); for a perfect circle, curvature is equal at all points on the curve (and entropy is maximized).

The last shape descriptor applied in our study is the number of static equilibrium points, which was recently proposed to classify pebble shape (*Domokos et al.*, 2010). Equilibrium points are points on an objects surface where the object may rest stationary on a horizontal surface. Stable and unstable equilibrium points correspond to local minima and maxima of the objects radius from its center of gravity. One advantage of measuring equilibrium points is that they are integers that may be objectively counted in the field by simple balancing (as long as grains can be manually lifted). Figure 3.2 illustrates that the numbers of stable (S) and unstable (U) equilibria are expected to decrease during phase I abrasion, as corners round and the initially angular shape with many equilibrium points approaches an ellipse-like shape with only two stable and two unstable equilibrium points. In phase II, this decreasing trend stops and the number of equilibrium points is expected to remain $S = U = 2$. Table 3.1 summarizes the above discussed shape descriptors and their expected evolution under curvature-driven abrasion; these will be used to test for the presence of two-phase abrasion in field data.

3.2.3. Box Equations for Modeling Phase II Abrasion

While eq. (3.3) can capture the shape evolution in both phase I and phase II, this equation and especially its 3D equivalent (*Bloore*, 1977) are difficult to analyze both analytically

and numerically. They also assume an invariable environment; i.e. that there is only one abraded particle and that impacting particles are all identical and unchanging in shape and size. Another drawback is that they only treat collisional abrasion, although frictional abrasion (rolling, sliding) is likely to be important in Phase II of curvature-driven abrasion. Thus, while eq. (3.3) and its 3D equivalent offer an adequate tool to understand the abrasion of a single particle, and also offer a good approximation to the abrasion in Phase I, they are, in their original form, inappropriate to numerically simulate the shape evolution of large particle populations in the second phase where the shape evolution is dominated by collective (particles abrade each other) and frictional abrasion.

A suitable solution for these problems is the use of box equations recently published by *Domokos et al.* (2012). box equations were derived from the 3D equivalent of eq. (3.3) by assuming that pebble shape is always a tri-axial ellipsoid. Thus, the box equations are limited in that shape evolution may only be tracked in phase II, where the assumption of ellipsoidal pebbles is valid. However, the main advantage of box equations is that they are based on the concept of mutual abrasion and therefore they offer a model for the collective evolution of a large number of pebbles through binary collisions. Additionally, frictional abrasion can be easily included as an additive term. The original concept of box equations was developed further in *Domokos and Gibbons* (2013), incorporating an independent physical model for volume diminution. The general form of box equations is:

$$\dot{\mathbf{y}} = f^c(\mathbf{y},\mathbf{z})\mathbf{F}^c(\mathbf{y},\mathbf{z}) + f^f(\mathbf{y})\mathbf{F}^f(\mathbf{y},v_s,v_r) \tag{3.4}$$

$$\dot{\mathbf{z}} = f^c(\mathbf{z},\mathbf{y})\mathbf{F}^c(\mathbf{z},\mathbf{y}) + f^f(\mathbf{z})\mathbf{F}^f(\mathbf{z},v_s,v_r) \tag{3.5}$$

(cf. *Domokos and Gibbons* (2013) where the exact formulation of functions $\mathbf{F}^c$ and $\mathbf{F}^f$ can be found). In this system of equations, $\mathbf{y}$ and $\mathbf{z}$ are two interacting particles where $\mathbf{y}$ represents the abrading environment for $\mathbf{z}$ and vice versa and (.) denotes differentiation with respect to time. Both $\mathbf{y}$ and $\mathbf{z}$ are three-component vectors with components S_y/L_y, I_y/L_y, $L_y/2$ and S_y/L_z, I_y/L_z, $L_z/2$, respectively, so box equations aim to track the evolution of the axis

ratios and the size (the semi-major axis length) of the pebbles. The first additive term on the right-hand sides of eqs. (3.4)-(3.5), with superscripts c, describes collisional abrasion; i.e. the result of many binary collisions between $\mathbf{y}$ and $\mathbf{z}$. (Accordingly the arguments include both $\mathbf{y}$ and $\mathbf{z}$.) The second additive term, with superscripts f, describes frictional abrasion, i.e. the rolling or sliding of a pebble on a substrate. (The arguments here include only the particle in question, i.e. either $\mathbf{y}$ or $\mathbf{z}$). The separate effects of frictional and collisional abrasion in eqs. (3.4)-(3.5) are illustrated in Fig. 3.5. Coefficients C_y^c, C_z^c and C_y^f, C_z^f represent the intensity of collisional and frictional abrasion, respectively. These coefficients may depend on the size of the particle, since it is well known that the mode of transport (sliding, rolling, saltation, suspension) and thus the intensity of frictional versus collisional abrasion depends on the size of the particle (*Abbott and Francis*, 1977; *Drake et al.*, 1988). Below, the box equations are developed into a numerical model that, when applied to field data, allows us to quantify the contribution of abrasion to downstream fining in a natural river.

3.3. Field Setting and Measuring Methods

3.3.1. Field Setting

We seek a demonstration that two-phase abrasion – predicted by the idealized geometric model of a single abrader colliding with an infinite plane – occurs in the downstream evolution of pebbles undergoing collision due to bed load transport in a natural river. In addition, we aim to quantify the contributions of abrasion and size-selective sorting to downstream diminution of pebble mass and diameter in a river, by employing the box equations. We expect, in general, that the dominant process governing pebble evolution in rivers changes from abrasion in the energetic headwaters to size-selective sorting in the depositional alluvial plain (*Shaw and Kellerhals*, 1982; *Dawson*, 1988; *Paola and Seal*, 1995; *Gasparini et al.*, 1999; *Jerolmack and Brzinski*, 2010). Accordingly, an ideal field setting would be a wadeable river that may be traversed from source to sink, with a point source of sediment input at its headwaters. The river should be of very steep slope in the upper portions, with a

bedrock channel bottom and no floodplain, to facilitate abrasion and suppress size-selective sorting. The lower reaches of the stream should be characterized by a low-gradient alluvial channel with well-developed floodplains, to allow the effect of size-selective transport to manifest through deposition.

Our river of study is the Rio Mameyes and its steep tributary Bisley 3, located in the Luquillo Critical Zone Observatory in northeastern Puerto Rico. Sediments in the channel are composed almost exclusively of volcaniclastic lithology, which are fine-grained sedimentary rocks (*Seiders and Pease*, 1971; *Briggs and Aguilar-Cortes*, 1980). The section of river under study is $\sim$ 10 km long and its profile exhibits a concave shape, but with a clear break in slope at the junction of Bisley 3 with the Mameyes (Fig. 3.6a). This tributary was selected because of its continuous accessibility from the headwaters to the gravel-sand transition in the mainstem. Bisley 3 contains a $\sim$ 10 m high knickpoint in its upper reaches. The knick point appears to be a significant source of sediment to the channel downstream, as piles of rocks up to $\sim$ 1 m in diameter may be seen just below it. Beyond 100 m downstream of the knickpoint, rocks within the stream exhibit no visible weathering rinds, and are angular and irregular in shape (Fig. 3.6c). We performed Schmidt hammer tests on $\sim$ 10 particles larger than 1 m (the minimum size required for reliable measurements) at each pebble count site to assess material strength. With the exception of the weathered boulders in the vicinity of the knickpoint, sampled particles had consistent strength values (mean of 95 N/mm^2) with little variability and no downstream trend (Fig. 3.6b). Results suggest that bed load sediments should have approximately uniform susceptibility to abrasion downstream. The lack of weathering rinds also indicates that abrasion is rapid compared to in-stream weathering. We take the knickpoint as the beginning of bed load transport in the river, and the limiting source location for sediment in the stream; it is thus the origin of our profile ($x = 0$ km). Unfortunately it is not the only source of sediment; landslides are prevalent along the steep valley walls of Bisley 3, and are capable of delivering very coarse and angular particles to the stream. Thus, sediment input is spatially distributed rather than from a point source. Numerical models and field studies have shown

that spatial variations in sediment supply can produce either downstream fining (*Pizzuto*, 1995; *Sklar et al.*, 2006) or coarsening (*Attal et al.*, 2006) grain-size trends. The potential effects of spatially-varying sediment supply could obscure expected patterns from abrasion, and must be carefully considered when interpreting observed trends and model results.

Along the ~ 2 km distance from the knickpoint to its junction with the Mameyes, Bisley 3 exhibits sporadic bedrock exposure, slopes generally greater than 0.1, and no floodplain; it is a partially alluviated bedrock river (*Howard*, 1980; *Whipple*, 2004). We expect abrasion to be dominant in this tributary with little to no size-selective transport, due to the general preference for deposition in fully alluviated reaches and the lack of sediment storage in bedrock reaches (*Hodge et al.*, 2011). At the junction of the Bisley 3 tributary with the mainstem Mameyes, the Mameyes is an alluviated bedrock channel confined in a valley. It transitions at $x = 5$ km to a fully alluvial stream with a well-developed floodplain on its exit from the mountains (Fig. 3.6a). River rocks in the Mameyes are rounded and nearly ellipsoidal in shape (Fig. 3.6d). Our study region ends at the upstream boundary of the gravel-sand transition on the Mameyes – i.e., we only examine the gravel portion of the river where bed load predominates. We expect size-selective transport to dominate over abrasion in the lower alluvial portion of the Mameyes.

The drainage area of the Mameyes watershed is 44 km^2, with a mean annual rainfall of $>$ 4500 mm/yr at the headwaters and 1500 mm/yr at the mouth (*Garcia-Martino et al.*, 1996). Orographic effects and hurricanes produce intense rainfall events and frequent bed load transport (*Scatena et al.*, 2004; *Heartsill-Scalley et al.*, 2007; *Pike et al.*, 2010). A recent study of tagged cobbles in Bisley 3 and the Mameyes showed that pebbles up to 0.3 m in diameter are mobilized approximately 20 times per year, and that some traveled up to 1.2 km over a two-year study period (*Phillips et al.*, 2013). Based on the description above, we expect that rapid Phase I abrasion occurs in the steep and energetic Bisley 3 tributary, and then transitions to Phase II in the Mameyes. Because mass loss from abrasion reduces the collision energy of a pebble (eq. (3.2)) (*Jerolmack and Brzinski*, 2010), we expect a

downstream gradient of decreasing abrasion rate along the study profile, while fining due to size-selective deposition should begin in the Mameyes on its exit from the mountains. A key assumption in our approach is that abrasion occurs by chipping and planing, i.e., that fragmentation due to crushing is not significant. Rock fragmentation would partially reset particle shape evolution by creating sharp edges. If this process were dominant, none of the observed downstream trends in particle shape would be consistent with the geometric theory. It is likely that some degree of fragmentation occurs, which would slow the observed rate of downstream rounding of grains, but the trends we present below indicate that it cannot be dominant. Indeed, visual inspection of bed sediments showed very few fresh fracture faces at each site, indicating that fragmentation was not significant in this river. However, no attempt was made to quantify the occurrence of fragmentation as the required judgment was deemed too subjective.

3.3.2. Measuring Methods

We selected 9 sites along Bisley 3 and 8 sites along the Rio Mameyes for detailed study (Fig. 3.7). At each site, we performed measurements on two grain populations. For grain population A, we collected 100-150 grains randomly, from the size range 20-200 mm (in terms of axis length L). The lower limit in size was based on our desire to sample only particles transported primarily in bed load; the upper limit represents the maximum reasonable size of a rock that could be lifted. We measured the three axis lengths ($L > I > S$) of each pebble and counted the number of stable (S) and unstable (U) equilibrium points by hand (*Domokos et al.*, 2010). These grains were also placed on a rigid board, with axis S perpendicular to the board, and photographed from above to obtain images of the maximum 2D projection of the grain. Axis ratios S/L and I/L were computed from the measured axis lengths, while the images were used to compute the isoperimetric ratio (IR), the curvature entropy (H_S) and a 2D version of convexity defined as $Conv_{2D} = A_P/A_H$, where A_P is the area of the grains projection and A_H is the area of the convex hull of the projection (Fig. 3.3c). This convexity index is sometimes referred to as solidity (*Rashband*,

1997). Measurements at each site were averaged in stratified grain size ranges – 20-64 mm, 65-128 mm, and larger than 128 mm – to compensate for noise while allowing some assessment of relations between size and shape that may arise, for example, by differing modes or frequency of transport. For grain population B, Wolman pebble counts (*Wolman*, 1954) were performed by randomly selecting 100 particles from the surface of the bed and measuring L, I, and S for each of them. There was no size restriction for measurement B. The manual measurements provide rich data but are time intensive. To complement and extend the spatial range of these data, we selected an additional 58 sites along the Rio Mameyes and Bisley 3, where only image-based data were collected by taking photographs of 40 randomly selected grains; we denote this as grain population C. Shape parameters estimated from all grains at each site were averaged together to produce a single value per site.

3.4. Results

3.4.1. Field Data and Two-Phase Abrasion

We first examine the downstream trend in axis dimensions measured from pebble counts, in particular the I-axis length since this is the most commonly reported parameter in other field studies. Throughout the length of Bisley 3 and the upper 3.5 km of the Mameyes, there is no discernible trend in axis dimension for the entire grain population, as well as within grain size groups (Fig. 3.8c). At approximately $x = 5$ km in the profile, roughly coincident with the transition to the alluvial plain on the Mameyes, I begins to systematically decline with distance downstream (Fig. 3.8c). The data permit but do not confirm – an exponential fit to this downstream trend (eq. (3.1)). The axis ratios S/L and I/L fluctuate but show no trend over the first $\sim$ 2 km studied, and then begin to slowly increase. These two patterns are compatible with the constant and increasing trends expected from Phase I and II, respectively, of the geometric abrasion theory, but are not conclusive (Table 3.1).

Convexity ($Conv_{2D}$) shows a more robust and smooth pattern with distance downstream

(Fig. 3.8h); it first rapidly increases over a distance of 1.5 km, and then appears to saturate at a value of approximately 0.981 indicating almost completely convex shapes. Values for IR increase rapidly over the same distance as convexity, and then continue to increase but at a lower rate over the remaining distance downstream (Fig. 3.8g). Similarly, the trend for entropy tracks convexity and IR (Fig. 3.8i). Finally, the number of equilibrium points declines rapidly over the same distance as other rapid shape changes, and then fluctuates widely in the lower 8.5 km of the river. All of the observed shape parameter trends are in agreement with qualitative predictions of curvature-driven abrasion (Table 3.1). Although the exact location of the transition from Phase I to Phase II is uncertain, the shape data together indicate that it begins around $x = 1.5$ km (around the mouth of Bisley 3) and is complete by $x = 3$ km.

Average values for equilibrium points indicate that pebbles in Phase II are not ellipsoids ($S = 3.1$ and $U = 2.9$), which may be a consequence of natural heterogeneity or effects such as friction that are not accounted for in eq. (3.3) (*Szabo et al.*, 2013). Nonetheless they are almost entirely convex and smooth, indicating that describing pebbles in Phase II as tri-axial ellipsoids – a prerequisite for applying the box equations – is a reasonable approximation. Although pebble volume was not measured, it may be estimated for pebbles in Phase II from measured axis dimensions (grain population B) by using the assumption of tri-axial ellipsoidal shape: $V = \frac{\pi}{6} SIL$. Results show that pebble volume decreases downstream in Phase II (Fig. 3.8d), in a manner consistent with an exponential form, i.e., eq. (3.2). However, this volume decline may combine effects from both abrasion and size-selective transport.

3.4.2. Numerical Model

Here we develop and implement a simple numerical model based on eqs. (3.4)-(3.5) presented above. The box equations are capable of modeling the collective evolution of a large population of particles through binary collisions, assuming Phase II abrasion. Additional terms may be added to account for deposition and frictional effects; by adjusting the mag-

nitude of these terms in the model in order to match field observations, we may assess the relative contribution of different processes to downstream changes in pebble size and shape. Downstream pebble evolution is modeled below for the portion of the Mameyes over which we infer that Phase II abrasion is operative. Therefore, the model is only run to simulate grain evolution down the mainstem Mameyes, not Bisley 3. Initial size and shape parameters for the model are taken from measured field values along the headwaters channel Bisley 3, as this channel and other similar tributaries are the primary sediment sources for the Rio Mameyes.

Abrasion

In the numerical simulation of the eqs (3.4)-(3.5), following (*Domokos et al.*, 2012) we consider n particles and in each iterative step we choose the two particles $\mathbf{y}$ and $\mathbf{z}$ randomly from the population and run the discretization of eqs. (3.4)-(3.5) for a short time period Δt:

$$\mathbf{y}^{i+1} = \mathbf{y}^i + \Delta t[f^c(\mathbf{y},\mathbf{z})\mathbf{F}^c(\mathbf{y},\mathbf{z}) + f^f)\mathbf{y})\mathbf{F}^f(\mathbf{y}, v_s, v_r)] \quad (3.6)$$

$$\mathbf{z}^{i+1} = \mathbf{z}^i + \Delta t[f^c(\mathbf{z},\mathbf{y})\mathbf{F}^c(\mathbf{z},\mathbf{y}) + f^f)\mathbf{z})\mathbf{F}^f(\mathbf{z}, v_s, v_r)]. \quad (3.7)$$

Following the argument laid out in Section 3.2.1, we assume that the pebble travel distance and model time are linearly related (also see *Szabo et al.* (2013)). This assumption presumes a constant transport velocity as a first-order approximation, recognizing that the actual virtual velocity of particles may vary downstream (*Hassan et al.*, 1992; *Ferguson et al.*, 1996). We begin the simulation with an initial pebble population obtained from the field measurements, and apply eqs. (3.6)-(3.7) iteratively for randomly chosen pebble-pairs; the model result generates a time evolution for the axis dimensions of each pebble that is equivalent to a downstream evolution (Fig. 3.5).

The mode of sediment transport depends on the size of the particle; small pebbles are mainly saltating, while larger particles experience rolling and sliding (*Abbott and Francis*,

1977; *Drake et al.*, 1988). To take this effect into account, we assume that the intensity of frictional abrasion grows linearly with the size of the particle, that is $C_y^f(L_y) = c_1 L_y$ and $C_z^f(L_z) = c_1 L_z$, where c_1 is a constant and L is measured in mm. For the coefficient of collisional abrasion, we assume constants $C_y^c = C_z^c = 1$. Since C_y^c and C_z^c do not depend on the size of the particles, our assumption allows that even large boulders can collide with each other sometimes. While this is probably not physically realistic, due to its rarity it has little effect on the results. Also, by assuming a constant value for C_y^c and C_z^c we can allow the physically relevant situation of a large particle (cobble, boulder) impacted by a mobile pebble.

Selective Deposition

We use the numerical box model to analyze the role of abrasion and selective transport simultaneously in the Rio Mameyes. Although several physical models of selective transport have been proposed in the literature (*Fedele and Paola*, 2007; *Ferguson et al.*, 1996; *Paola and Seal*, 1995), and these models could, in principle, be integrated into the box equations, this is beyond the scope of this paper. Instead, we couple the box equations with a simplistic, phenomenological selective-deposition rule. Each pebble has an expected value for the final distance traveled to deposition, X. Tracer measurements from the Rio Mameyes showed that normalized step lengths are exponentially distributed in the river (*Phillips et al.*, 2013), thus we assumed that the final distance X is a random variable with exponential distribution, where the parameter of the distribution is $1/E[X]$. We assumed that the expected value of X depends on the maximal size L_y of the particle: $E[X] = c_2 e^{-c_3 L_y}$, where c_2 and c_3 are constants. We implemented this simple deposition rule into the numerical box model eqs. (3.6)-(3.7) in the following way: in each iterative step, both for particles $\mathbf{y}$ and $\mathbf{z}$, we randomly draw a value for the final travel distance X using the above exponential distribution. Then, if the actual distance from the source is larger than X, the particle is deposited out of the flow, i.e. we remove it from the particle population.

Abrasion and Selective Deposition

The three parameters (c_1, c_2, and c_3) of the numerical model were fitted to obtain the best agreement with the measured field data for the Rio Mameyes. The numerical simulation began with approximately 3000 particles in the system, whose size ranged from $L = 20$ mm to 4 m. The time step was $\Delta t = 1/1000$, and the total number of iterative steps was 500,000. We found that the optimal value for c_1 (the coefficient in the assumed linear size-dependence of friction intensity) is around 0.005. For the selective deposition law we used $c_2 = 10^8$ and $c_3 = 0.006$. This produces an expected travel distance $E[X] = 3.8$ mm for the upper limit (4 m grain), practically meaning that such a large boulder does not move. For the lower size limit (20 mm grain) we have $E[X] = 89000$ km, i.e. such a small pebble will never be deposited in the model. Figure 3.9 shows that the site-averages of the measured field data and the corresponding model results match well using the above parameters. The first row shows the averages from grain population A, where corresponding model results were computed only from the particles which fell into the size range of measured field data, i.e., 20-200 mm. The second row shows the shape and size evolution of the whole size range (grain population B).

To better understand the role of competing physical processes in the numerical model, Figure 3.10 shows the main limiting cases. Model results with no selective deposition (solid line) are not in agreement with the data for the entire size range, indicating that abrasion significantly underpredicts the degree of downstream fining. However, the predicted size and shape evolution in the 20-200 mm size range is reasonable, suggesting that size-selective deposition is ineffective in this restricted size range. For the second limiting case of no abrasion (dotted line), we see that selective deposition alone cannot reproduce the observed increase in the axis ratios of particles in the 20-200 mm size range. However, the results for the whole particle population are reasonably good. We conclude that the strong downstream fining observed in the whole size range is essentially due to selective deposition, however, the role of abrasion is significant for particles in the size range of 20-200 mm. The

third limiting case includes both selective deposition and collisional abrasion, but neglects frictional abrasion (dashed line). Here we see that the predicted evolution of the axis ratios in the whole size range is incorrect; simulated axis ratios increase, indicating movement towards the sphere. This is because frictional and collisional abrasion work against each other (Fig. 3.5); while particles get flatter and thinner under frictional abrasion (axis ratios decrease), particles colliding with similar-size particles converge towards the sphere (axis ratios increase) (*Domokos et al.*, 2012). Thus the constant axis ratios measured for the whole grain population in the field indicate that collisional abrasion of pebbles is balanced by frictional abrasion of larger particles such as boulders.

3.5. Discussion

Data strongly indicate that two-phase abrasion occurs in the downstream evolution of pebbles along the Mameyes-Bisley 3 river system. Although downstream trends of individual shape parameters are scattered, the collection of independent parameters all behave as predicted from the geometric theory (Table 3.1). Phase I abrasion occurs mostly in the energetic and steep Bisley 3 stream, where pebble shapes evolve rapidly toward smooth ellipsoids but axis dimensions remain constant. This result is consistent with anecdotal reports that rapid rounding occurs "in the first few kilometers" of a river (*Krumbein*, 1941; *Kuenen*, 1956; *Adams*, 1979; *Parker*, 1991). Phase II abrasion plays out in the lower Mameyes river, where axis ratios slowly increase while all other shape parameters remain approximately constant. At the tributary junction between Bisley 3 and the mainstem Mameyes, shape descriptors all show a smooth transition; this suggests that phase I abrasion is completed within the headwater stream, and that downstream trends are not an artifact of merging these two different rivers into one profile. That predictions from an idealized geometric theory – of a single particle colliding with an infinite plain – are supported by field data from a highly heterogeneous system of mutually-colliding pebbles under bed load transport, provides compelling evidence that two-phase abrasion should be a general phenomenon. A major difference in shape data from the field as compared to the idealized drum experiments

of *Domokos et al.* (2014), however, is that pebbles in the Mameyes never become completely ellipsoidal (Fig. 3.8e-f). It appears that collision-induced abrasion drives initially blocky pebbles toward ellipsoids; but, as pebbles move into lower-gradient reaches of the river, frictional abrasion from sliding and rolling prevents pebbles from further evolution along this trajectory.

If sorting is absent in Bisley 3, as expected, we can observe the isolated effects of abrasion in this steep, bedrock channel. In the alluvial portion of the Mameyes stream, however, sorting exerts a strong influence on downstream trends of particle size. Grain diameter data show significant decreases in pebble size, consistent with observations in other alluvial rivers (*Adams*, 1978; *Lewin and Brewer*, 2002). Grain shape data, in particular the axis ratios, show that abrasion is also occurring in these lower alluvial reaches. One central question is "how much of a pebble's mass is lost due to abrasion?"; this requires separating and removing the effects of sorting. If pebble volume were known along the entire stream profile, one could simply fit the "Generalized Sternberg's Law" (eq. (3.2)) to Phase I data – where we assume that no sorting occurs – to produce a model for mass loss due to abrasion over the entire river length. However, it was not feasible to measure volume for all pebbles in Bisley 3 and the Mameyes (and is likely not feasible for many rivers) due to their large size. Separating the effects of abrasion and sorting from data alone therefore is not possible. Here the box equations with deposition can be applied to interpret field data, in regions where Phase II abrasion is operative. We examine the predicted trend in volume diminution (in m^3) for the box equations with no deposition included; the result, considering the full particle population, is $V = (0.012)e^{-0.053x}$. Because volume diminution by abrasion should primarily be a function of pebble volume (eq. (3.2)) (*Domokos et al.*, 2014), we use this expression to extrapolate upstream to $x = 0$ km. The model result is that 38% of a pebble's mass, on average, is lost over the 10 km distance from the headwaters to the gravel-sand transition.

That pebbles could lose approximately 40% of their mass along a relatively short ($\sim$ 10

km) distance implies that pebble mobility changes significantly due to abrasion. Parameters that assess mobility, such as threshold Shields stress and sediment transport equations, may produce misleading results when applied to steeper rivers where abrasion is significant, because they assume that particles are spherical and may be represented by a single diameter. In addition, the inferred pebble mass loss implies that significant quantities of sand and silt are produced *in situ*. This generation of fine sediment may be a significant part of the sediment budget, but it has never been quantified. Future field studies should aim to determine if and what fraction of fine sediment in a river is the product of abrasion. Whether there are geophysical and geochemical signatures of abrasion that may be used to separate its products from other fine sediment sources is unknown to these authors.

It is encouraging that 2D shape parameters measured from images – in particular the isoperimetric ratio, convexity, and entropy – are in agreement with the more laborious, manual 3D measurements. Results suggest that the two phases of abrasion may be identified from images alone, which should encourage researchers to test the generality of two-phase abrasion in other rivers, and also aeolian environments where abrasion and sorting have been observed (e.g., *Jerolmack et al.* (2011)). While these data serve to delineate the phase transition from collisional abrasion, they are not sufficient to quantify pebble mass loss. A practical guide for this problem, based on our findings here, is as follows: (1) Use 2D image data to identify phases I and II of abrasion; (2) measure all three axis lengths of pebbles contained within the regime of phase II abrasion to determine pebble volume (or, measure the masses of all pebbles if they are small enough to be lifted!; if so, then no further work is needed); (3) fit the box model with deposition to the downstream pattern of axis ratios in Phase II; and (4) use model results to identify the rate of volume diminution that is due to abrasion alone.

A final note of caution is warranted in the interpretation of our observations and modeling results. While it is beyond the scope of this work to explicitly model the effect of spatially varying sediment input on particle size and shape trends, we must acknowledge that

sediment input in our study river (and indeed, in most other rivers) is spatially variable. The effects of spatial variability have been explored in models (*Pizzuto*, 1995; *Attal et al.*, 2006; *Sklar et al.*, 2006; *Chatanantavet et al.*, 2010), which have demonstrated that the combination of lithologic changes and tributary inputs may cause downstream trends in grain size that are independent of either abrasion or size-selective sorting. It is possible that spatially varying sediment inputs, and spatial trends in input shape, could conspire to produce the observed downstream patterns of size and shape in the Mameyes watershed. This is unlikely, however, and strength measurements (Fig. 3.6b) indicate at least that the observed trends are not related to variation in material properties. The most likely influence of spatially varying sediment input would be to obscure the trends of two-phase abrasion, rather than to introduce new trends. The primary contribution of the work presented here is the demonstration of the significance of two-phase abrasion in a natural stream, which we believe to be qualitatively robust. The quantitative results and modeling efforts illustrate the potential magnitudes of abrasion versus sorting, but spatially varying sediment input likely exerts an influence on the reported numerical values of each.

3.6. Conclusions

To summarize, this field investigation has demonstrated two-phase abrasion in a natural setting using a set of shape descriptors determined from simple hand measurements and image analysis techniques. Phase I abrasion takes place over the first few kilometers in the steep headwater channel, while phase II plays out over a larger distance in the lower-gradient alluvial mainstem. This work provides a way to determine the relative importance of abrasion versus selective transport for a given river system; the results of the box model simulations give evidence that abrasion and selective deposition are both important to reproduce observed size and shape patterns in the Mameyes watershed. Although the relative importance of abrasion versus sorting can vary due to sediment supply, lithology and transport conditions, application of the geometric theory suggests that abrasion controls the downstream reduction in pebble mass while sorting determines the downstream trend in

diameter. Incorporating explicit measures of pebble shape into future studies should allow researchers to assess the contribution of abrasion in other river systems. To truly test the generality of the two-phase abrasion model, future studies should replicate and expand on this analysis, in other river systems and also in aeolian dune fields.

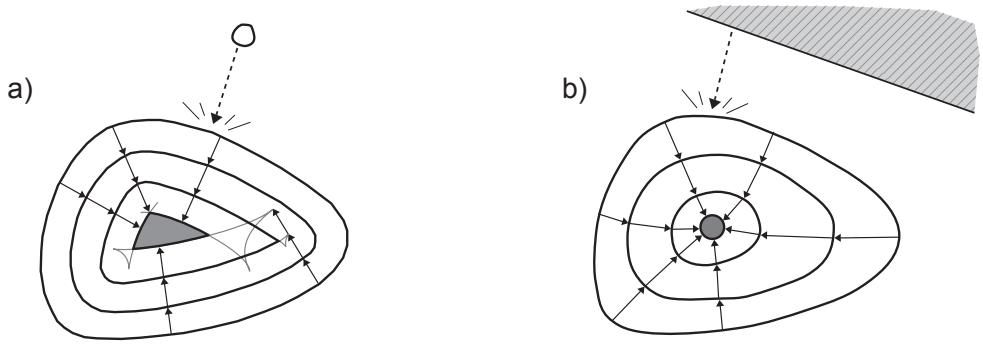

Figure 3.1: Sketch of shape evolution under the two terms of eq. (3.3). (a) The Eikonal term; and (b) the curvature term. Figures are adapted from *Szabo et al.* (2013).

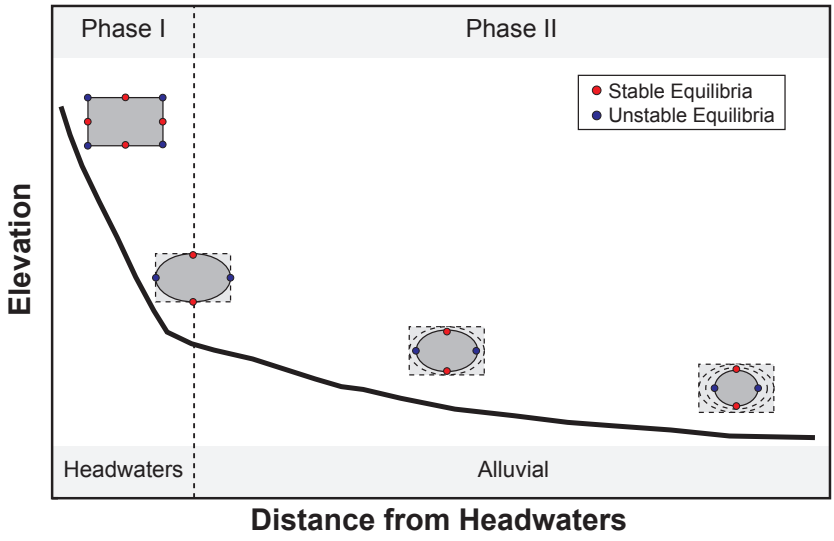

Figure 3.2: Conceptual figure of two-phase abrasion on a rectangle, and its expected behavior along a river profile. In the energetic upper reaches of a river phase I occurs where corners are abraded without any change in axis lengths while the numbers of both stable and unstable equilibrium points decrease. In lower-gradient reaches phase II occurs, where the axis ratio S/L (in 3D, S/L and I/L) increases, indicating that the pebble approaches a circle (in 3D, a sphere), while the number of equilibrium points remains constant.

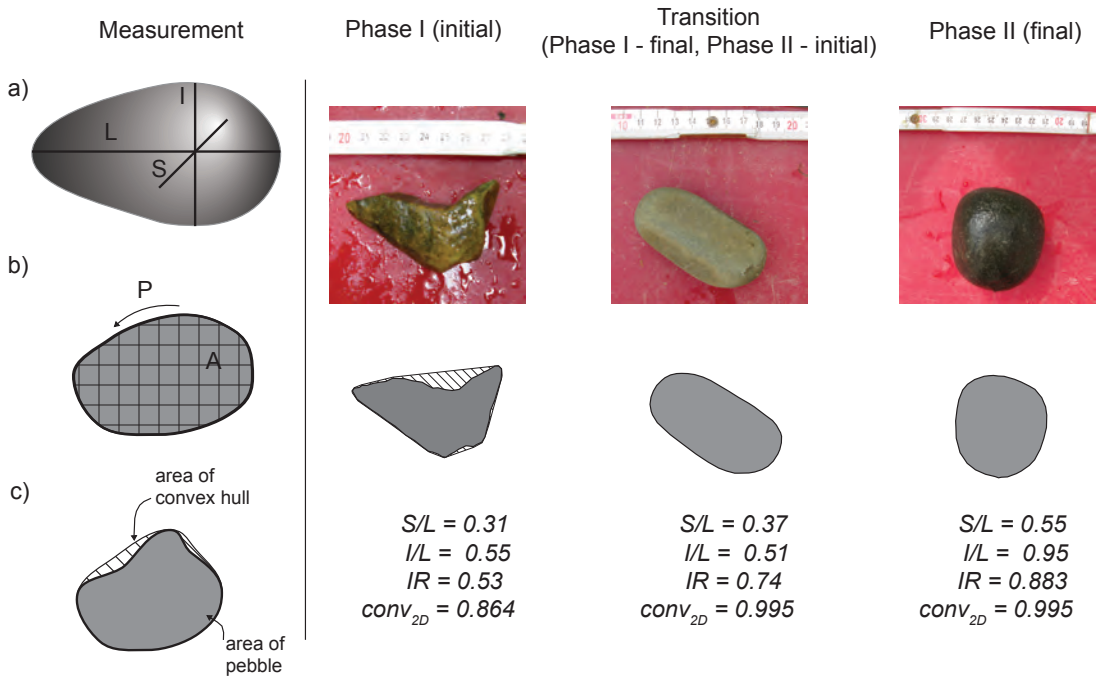

Figure 3.3: Shape descriptors. (a) Axis dimensions $L > I > S$, as they are measured for pebbles in the field. (b) Isoperimetric ratio IR measured from 2D projections of pebbles. (c) Convexity $Conv_{2D}$ measured from 2D projections of pebbles.

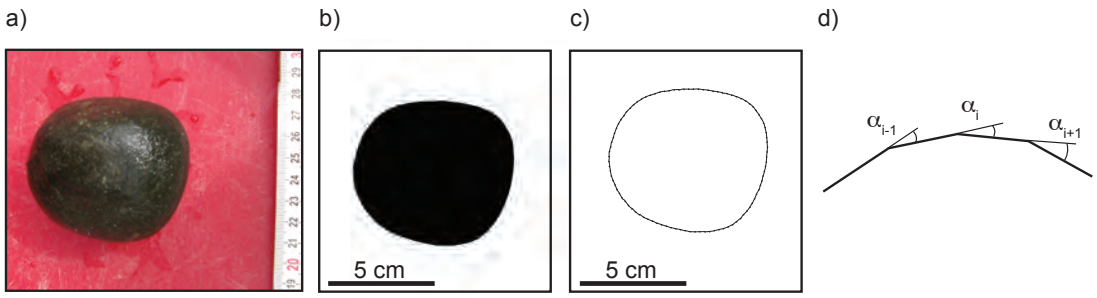

Figure 3.4: Image processing and curvature entropy (a) Raw image of pebble taken in the field. (b) Image prepared for bulk-shape data analysis by converting to binary image. (c) Interpolated polygon with equal sides. (d) External angles used to calculate curvature entropy.

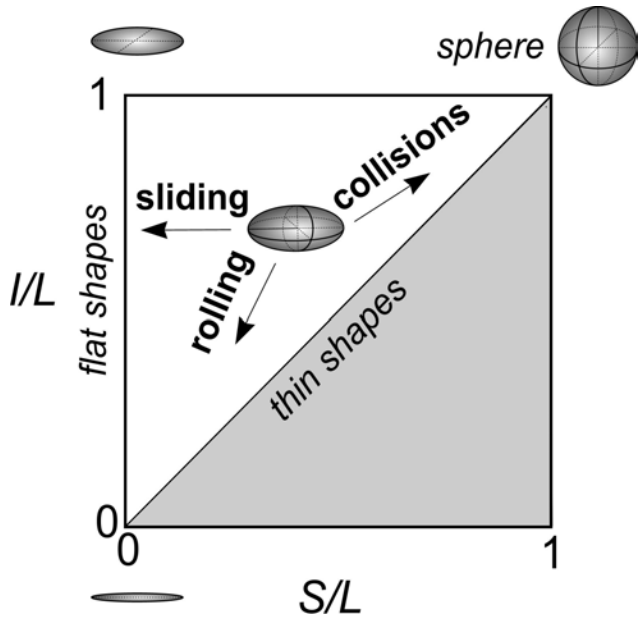

Figure 3.5: Conceptual illustration of the effects of frictional and collisional abrasion in eqs. (3.4)-(3.5) on the plane S/L - I/L. Sliding drives particles towards infinitely flat shapes ($S/L = 0$), rolling results in an infinitely thin needle-like shape ($S/L = I/L = 0$), while collisions between like-size particles produce spheres ($S/L = I/L = 1$). Figure adapted from *Domokos et al.* (2012).

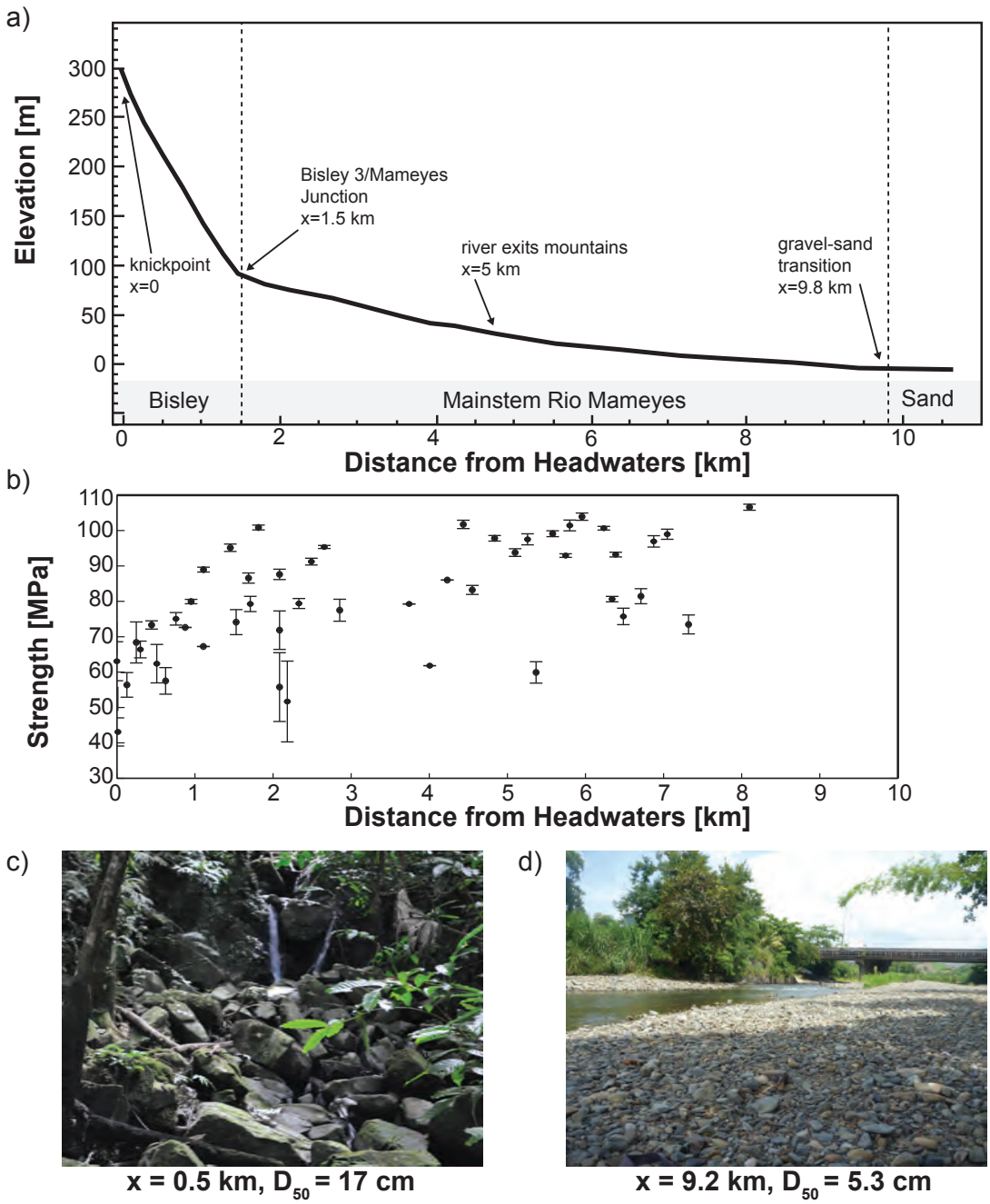

Figure 3.6: Photographs of the field site. (a) River elevation profile with important transitions labeled. (b) Plot of uniaxial compressive strength (UCS) measured by Schmidt hammer (converted from hammer rebound to UCS using relation in *Kahraman* (2001)) versus distance from headwaters. (c) Headwater tributary Bisley 3 is steep and contains large angular pebbles. (d) Lower alluvial mainstem Rio Mameyes has shallow slope and contains smaller rounded rocks.

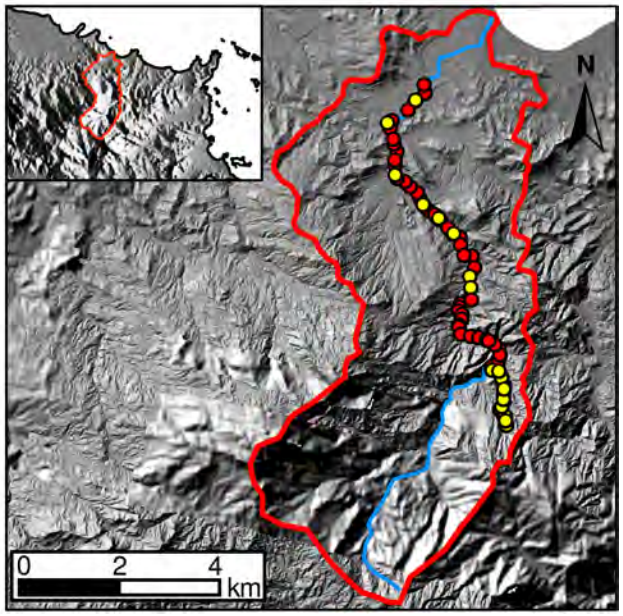

Figure 3.7: Map of field site, located within the Luquillo Critical Zone Observatory in northeastern Puerto Rico. The red line outlines the Rio Mameyes watershed and the blue line denotes the channel. Circles mark sampling sites. Yellow circles represent detailed sampling sites where equilibrium points and axis dimensions were measured in addition to images of pebbles (grain populations A and B). Red circles represent sampling sites where only images of pebbles were taken (grain population C).

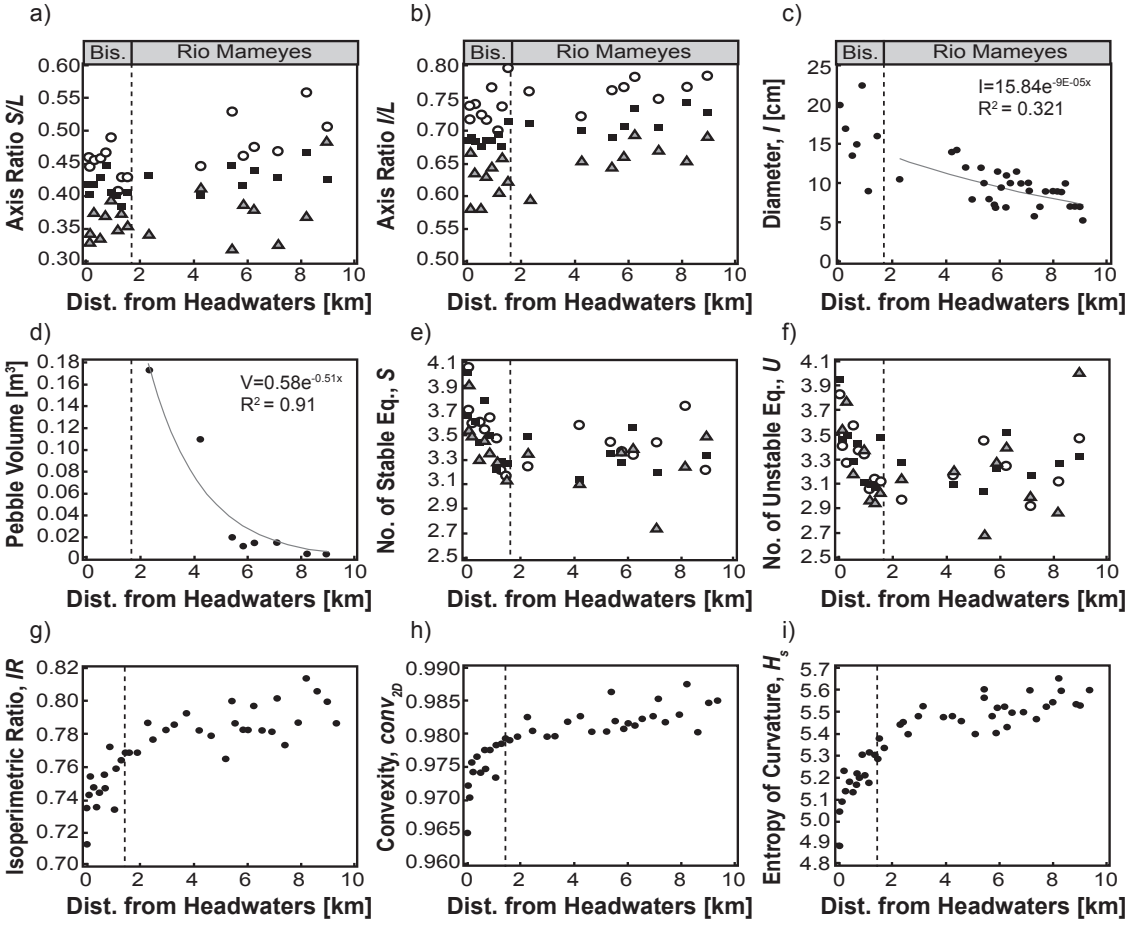

Figure 3.8: Field results – Plots of site-averaged shape descriptors as a function of distance downstream of the origin. Data in plots (a)-(b) and (e)-(f) are averaged at a site by the following size classes: 20 to 64 mm (open circles), 65 to 128 mm (black squares), and greater than 128 mm (grey triangles). Plots show: (a) average axis ratio S/L by different size class; (b) average axis ratio I/L by different size class; (c) grain size measured as the intermediate pebble diameter I; (d) estimated total pebble volume; (e) average stable equilibrium points by different size class; (f) average unstable equilibrium points by different size class; (g) average 2D convexity; (h) average isoperimetric ratio; and (i) average curvature entropy of 2D image contours.

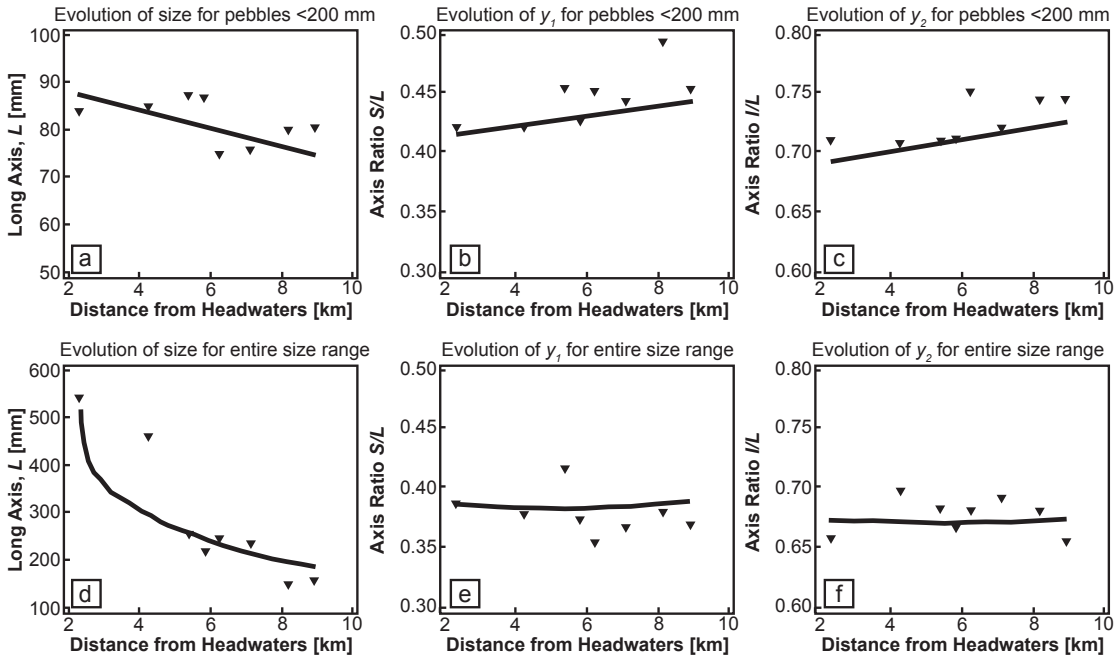

Figure 3.9: Plots of field data (black triangles) overlaid with results from full box model simulations, showing trends for downstream distance for Phase II abrasion (only mainstem Mameyes). (a) Average long axis for pebbles under 200 mm in length of L. (b) Axis ratio S/L for pebbles under 200 mm in length of L. (c) Axis ratio I/L for pebbles under 200 mm in length of L. (d)-(f) Same as (a)-(c), but for the entire size range of pebbles.

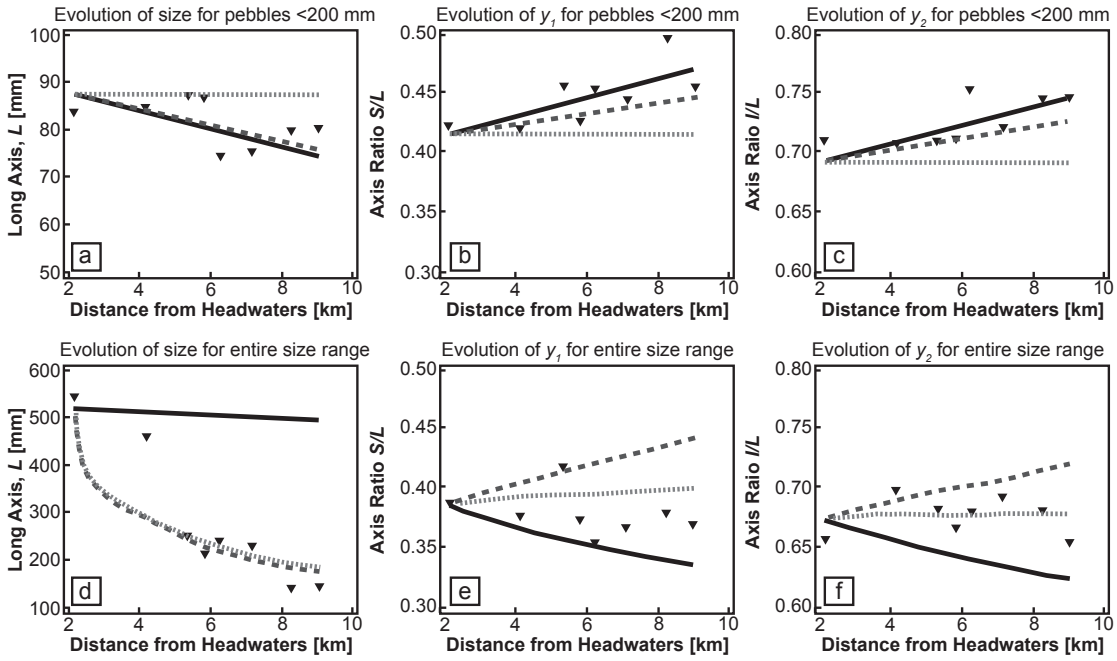

Figure 3.10: Plots of field data (black triangles) overlaid with results from box model simulations in mainstem Mameyes with limiting conditions. Solid line is for model run with no selective deposition, dotted line for no abrasion at all, and dashed line for no frictional abrasion. (a)-(f) are the same as for Fig. 3.9.

Shape Descriptor	Measurement Method	Expected Behavior	
		Phase I	Phase II
Axis Ratios (y_1 and y_2)	Hand Measure	Constant	Increase $\rightarrow y_1 = y_2 = 1$
Convexity ($Conv_{3D}$)	Image Technique ($Conv_{2D}$)	Increase $\rightarrow Conv_{3D} = 1$	Constant ($Conv_{3D} = 1$)
Equilibrium Points (S and U)	Hand Measure	Decrease $\rightarrow S = U = 2$	Constants ($S = U = 2$)
Isoperimetric Ratio (IR)	Image Technique	Increase $\rightarrow IR = 1$	
Curvature Entropy (H_S)	Image Technique	Increase	

Table 3.1: Table 3.1. Expected evolution of various 3D and 2D shape descriptors under curvature-dependent abrasion.

CHAPTER 4 : Universal Scaling Relations for Pebble Abrasion

Abstract:

River rocks round through the process of abrasion, where energetic collisions during bedload transport chip and wear away the surface of the grain. Although previous work has shown that impact energy and lithology are controlling factors determining abrasion rates, the functional dependence between these quantities is unknown. Furthermore, most abrasion studies only focus on the evolution of the initial grain, neglecting the fine particles produced in the process. In this laboratory investigation, we examine the control of impact energy on abrasion rates using a double-pendulum apparatus to look at the abrasion between two-grains, and using a high-speed camera to quantify impact energy. We run experiments on a range of lithologies and measure material properties to determine their dependence on abrasion rates. Finally we collect and characterize the daughter products of abrasion. Results from experiments verify that mass loss is proportional to kinetic energy. We define a material parameter that incorporates material density, Young's modulus, and tensile stress and show that this parameter is directly related to the proportionality between mass loss and energy. We identify an initial region of the mass loss curves in which abrasion is independent of energy and material properties; results suggest this region is determined by shape. We show that grain size distributions of daughter products are universal and independent of material; they follow a Weibull distribution, which is expected distribution from brittle fracture theory. Finally, scanning electron microscope (SEM) images show a thin damage zone near the surface, the length of which correlates with the maximum grain size of the daughter products. The apparent universality of both mass loss curves and particle size distributions is in need of theoretical investigation to better understand the underlying mechanics. However, the results are already proving useful for interpreting the role of in-stream abrasion in downstream fining and the production of sand in the field.

4.1. Introduction

Traveling downstream in a typical river, one observes river sediments becoming rounder in shape (*Sneed and Folk*, 1958; *Adams*, 1978) and smaller in size (*Sternberg*, 1875; *Ferguson et al.*, 1996). While there is a debate over whether mechanical breakdown by abrasion or hydraulic sorting caused by relative transport rates is responsible for fining patterns (*Kodama*, 1991; *Ferguson et al.*, 1996; *Gasparini et al.*, 1999; *Lewin and Brewer*, 2002), it is generally agreed that abrasion is the chief mechanism producing the rounding of sediments (*Kuenen*, 1956; *Sneed and Folk*, 1958; *Schumm and Stevens*, 1973). Abrasion is the process where river sediments are worn away due to energetic collisions with other grains and the channel bed during transport (*Kuenen*, 1956; *Kodama*, 1994a). While there have been a great deal of previous work investigating the process (*Kodama*, 1994a; *Lewin and Brewer*, 2002; *Attal and Lave*, 2009), there is a lack of understanding of the fundamental physics involved in sediment abrasion.

Sternberg (1875) attributed the downstream fining of grains to abrasion and quantitatively described it by the exponential function:

$$D(x) = D_0 e^{-\alpha x} \tag{4.1}$$

where $D(x)$ is the grain size at downstream distance x, D_0 is the initial grain size at $x = 0$, and α is the empirically determined diminution coefficient, which describes the rate of grain size fining. Despite the fact that this expression lacks a mechanistic framework, α values remain the most common way to describe abrasion rates. Most previous work on abrasion has been through laboratory experiments (*Krumbein*, 1941; *Kuenen*, 1956; *Kodama*, 1994a; *Lewin and Brewer*, 2002; *Attal and Lave*, 2009) because of the difficulty in directly observing abrasion in the field (*Sneed and Folk*, 1958; *Kodama*, 1994b). These experiments utilize tumbling mills or circular flumes to simulate abrasion and extrapolate results to the field by using duration of experiment as a proxy for downstream distance

(*Wentworth*, 1919; *Krumbein*, 1941; *Kuenen*, 1956; *Kodama*, 1994a; *Lewin and Brewer*, 2002; *Attal and Lave*, 2009). However, laboratory measured α values (*Wentworth*, 1919; *Krumbein*, 1941; *Kuenen*, 1956; *Kodama*, 1994a; *Lewin and Brewer*, 2002; *Attal and Lave*, 2009) tend to be lower than those measured in the field (*Ferguson et al.*, 1996; *Hoey and Bluck*, 1999; *Morris and Williams*, 1999) either because impact energies in experiments are not as high as in the field (*Kodama*, 1994a), the assumption that experimental duration is a proxy for travel distance does not account for abrasion in place (*Schumm and Stevens*, 1973), or added effects of hydraulic sorting on fining rates in the field (*Ferguson et al.*, 1996; *Paola et al.*, 1992). These reasons highlight the need for a more mechanistic approach to abrasion.

There has been some previous work relating impact energy to abrasion, however, none of it has focused on fluvial sediments. *Bitter* (1963) proposed that deformation caused by damage from repeated collisions between two bodies at low energies leads to material wear. He suggested that the amount of volume detached from a material depends on impact energy and material properties and confirmed this idea with measurements of wear of glass spheres. Furthermore, field and laboratory investigations of windblown sand on stationary targets, such as yardangs, have verified that the amount of abrasion is proportional to the kinetic energy from collisions and that the proportionality factor depends on the material properties of the target (*Anderson*, 1986; *Wang et al.*, 2011). Finally, numerical simulations of agglomerate breakage from direct impacts have shown that the amount of damage depends on the ratio of incoming kinetic energy from collision to the internal bond energy, determined by material properties (*Kafui and Thornton*, 1993; *Le Bouteiller and Naaim*, 2011). Experiments simulating fluvial abrasion have observed an increase in diminution rates associated with increasing sediment transport velocities, but the exact functional relationship between energy and abrasion has not been determined.

As mentioned above, research has shown that material properties determine the amount of mass detached from an object after an impact of specific energy. Different lithologies

can lead up to two orders of magnitude difference in abrasion rates (*Attal and Lave*, 2009). Experiments by *Attal and Lave* (2009), conclude that lithologies with low tensile strength, like sandstone, abrade faster than those with higher values, like limestone and quartzite. Besides tensile strength, the field work on yardangs (*Wang et al.*, 2011) and numerical work on agglomerates (*Le Bouteiller and Naaim*, 2011) have demonstrated that material density and Young's modulus are also important quantities for abrasion. Although material properties are known to have an effect on abrasion rates, the explicit dependence between lithology and magnitude of mass loss is unknown.

Finally, most research on abrasion neglects the fine particles produced from the process, even though it has been hypothesized that these products heavily contribute to sand and silt populations found in rivers (*Jerolmack and Brzinski*, 2010). Recent work on the geometric evolution of pebbles during abrasion predict that sediment can lose up to 48% of its original mass just from rounding the edges of an initially angular pebble (*Domokos et al.*, 2014). With the large quantity of fines produced from abrasion, it is necessary to understand the size distribution of these particles to understand their role in the river system. Recently, *Kok* (2011) found that the grain size distribution resulting from dust aggregates follow a Weibull distribution, which is in agreement with brittle fracture theory. However, the daughter products of abrasion have never been examined in this manner.

Although previous work has shown that lithology (*Attal and Lave*, 2009; *Wang et al.*, 2011) and energy of collision (*Bitter*, 1963; *Anderson*, 1986; *Le Bouteiller and Naaim*, 2011; *Wang et al.*, 2011) are contributing factors that control abrasion rates of riverbed material, little is known regarding the relationship between these factors and diminution rates. This research explicitly isolates and investigates how these factors influence rates of abrasion. First we determine how abrasion rates scale with energy by performing well-controlled abrasion experiments. We run experiments over a range of different lithologies to see if measured material properties determine the magnitude of abrasion rates. Finally, we characterize the grain size distribution of the daughter products created during the abrasion process to

see if it follows the expected distribution from brittle fracture theory (*Kok*, 2011). Unlike previous abrasion studies, this work will rigorously consider the mechanics of fracture and damage in solid materials to provide a better understanding of the underlying physics of the abrasion process.

4.2. Methods

4.2.1. Hypothesis and Experimental Approach

We have two hypotheses that guide our experimental design. First, we hypothesize that kinetic energy and lithology control abrasion rates of river sediments. From previous research (*Sklar and Dietrich*, 2004; *Attal and Lave*, 2009; *Le Bouteiller and Naaim*, 2011; *Wang et al.*, 2011) and mechanical considerations we can state that

$$M = f(E, \rho, Y, \sigma) \tag{4.2}$$

where M is the mass removed from an object after impact of energy E, and ρ, Y, and σ are the material properties density, Young's modulus, and tensile strength, respectively. Dimensional analysis yields two dimensionless groups, $\Pi_1 = \frac{\sigma M}{\rho E}$ and $\Pi_2 = \frac{Y}{\sigma}$. Rewriting to solve for mass loss per impact energy, we obtain:

$$\frac{M}{E} = f(A) \tag{4.3}$$

where

$$A \equiv \frac{\rho Y}{\sigma^2} \tag{4.4}$$

This analysis suggests that abrasion rate should be an explicit function of the material property grouping A, which we refer to as the Abrasion number. The utility of A will be tested experimentally in this study.

The second hypothesis that guides this work is regarding the daughter products of abrasion. By the assumption from Griffith's fracture theory that pre-existing flaws are distributed in-

dependently within a material and activate randomly during a fracture event, it is expected that fragments produced follow a Weibull distribution (*Gilvarry*, 1961). Research by *Kok* (2011) recently found that the particle size distribution from dust aerosols eroded from soils are described by a Weibull distribution:

$$\frac{dN_f}{d\ln D_f} \propto D_f^{-2} \tag{4.5}$$

where N_f is the number of fragments of size D_f. *Kok* (2011) discusses how this power-law relation follow from brittle fracture theory and is a consequence of the way in which cracks nucleate and propagate within the material as stress is applied. These principles describe the full fragmentation of materials, meaning that the aggregate breaks into many small pieces with the largest piece being significantly smaller than the parent particle. We will test whether the products of these abrasion experiments follow the same power-law scaling for surface abrasion. Although collision energies for abrasion are well below values that lead to complete fragmentation of the parent grain, we hypothesize that brittle fragmentation may still occur over a small penetration depth near the impact site.

4.2.2. Experimental Design and Methods

To simulate abrasion between grains during saltation, while isolating the effects of impact energy on mass attrition, we examine the amount of mass lost due to abrasion during a single collision event between two grains. Although collisions in water can be viscously damped, a laboratory investigation showed that bedload impacts, similar to those we are modeling in these experiments on abrasion are partially elastic and alike to collisions in air (*Schmeeckle et al.*, 2001). Therefore, since our main goal is to determine the energy scaling of abrasion, we conduct the experiments in air instead of water for simplicity, looking at impact energies that are comparable to those observed in nature. Experiments are conducted using a "Newtons-cradle" style double pendulum designed within a clear tank to allow for the collection of the products of abrasion (Fig. 4.1). Rock samples are attached to threaded rods within the tank by gluing flat-faced nuts to the top of each sample. The rod with

the impacting grain is lifted by a motor and then released once it reaches a desired height, colliding with the stationary target grain. After the collision, a braking system steadies the target grain while the motor lifts the impacting grain again for the next collision. Both rods containing impacting and target grains are able to rotate freely around in any direction, allowing abrasion to occur evenly around the entire rock sample. To test the randomness of the grain rotation, we filmed approximately 450 collisions between two test grains, recording the location of impact on both the impacting and target grains. The distribution of impact locations indicates that the collisions occur uniformly around each grain, with preferentially impacting the high curvature regions of the protruding corners, as expected from geometric abrasion theory (*Firey*, 1974) (Fig. 4.2). Grains are collided for set interval of collisions, which increases throughout the experiment from 50 to 10,000 impacts. After each set of collisions, the mass of both the impacting and target grains is measured using a microbalance to determine the amount of mass lost due to abrasion.

In order to measure the impact energy, we recorded videos at the beginning of every set of collisions with a high-speed camera mounted below the clear bottom of the abrasion tank. We captured 5-10 collisions per set at 1000 frames per second. From the videos, we measure the velocity of the impacting grain at the time of collision by tracking the location of the grain as it approaches the target grain over approximately 40 frames, which equals 0.04 seconds. The impact velocity is measured as the slope of a linear fit to plots of travel distance versus time. The average velocity for all experiments was approximately 1 m/s. The kinetic energy at impact (E) is then calculated using the expression, $E = \frac{1}{2} m_i v^2$, where m_i is the mass of the impacting grain at the beginning of the set and v is the average velocity measured from all videos in that particular set. Energies for experimental runs ranged from 0.035-0.220 j.

We run the binary collision experiment on the following 5 different materials to determine the effect of lithology on abrasion rates: brick, quartz diorite, sandstone, schist, and volcaniclastic (Fig. 4.3). The brick was selected as a test material for its homogenous structure.

We used standard red clay builders bricks. Both the quartz diorite and volcaniclastic rocks were collected in the Luquillo Mountains in northeastern Puerto Rico. The quartz diorite is tertiary in age and originates from a batholith on the southern side of the mountain (*Pike et al.*, 2010). The volcaniclastic comprises most of the mountain and was formed in the late cretaceous by marine deposited volcanic sediments (*Pike et al.*, 2010). The sandstone is a triassic reddish arkose sandstone of the Stockton formation in southeast Pennsylvania (*Olsen*, 1980). The schist is Wissahickon schist from southeast Pennsylvania and is highly deformed due to regional metamorphism during the lower Paleozoic (*Weiss*, 1949). The brick was run multiple times with different size samples to see the effect of increased impact energy on abrasion rate. Table 4.1 lists the different rock types and corresponding size for each experimental run.

To control for shape effects on abrasion rates, we initially cut all grains into cubes. Then throughout the experiment, we track changes in the shape of both impacting and target grains by using a laser displacement sensor to scan a single surface contour around the grain. Scans are made at the beginning of each set of collisions by holding the sensor in a fixed position, while the grain rotates at a constant rate of 3 rpm on a turning platform. A single contour for each grain is made by averaging 1 kHz laser data from approximately 7 full rotations. The distance data is then smoothed using a high pass filter at the noise floor, which was determined from the time series of the entire dataset. The peak local curvature at each corner was calculated from the second derivative of the contour. The peak from all four corners was averaged together to give a mean curvature value. We also use a second method to characterize the shape evolution of the abraded grains. *Litwin Miller et al.* (in review) demonstrated that the curvature entropy is a monotonically increasing quantity indicating the rounding of grains from collisional abrasion. We measure this quantity from the laser scanned contours using the methods outlined in *Litwin Miller et al.* (in review). Shape data were only collected for two sets of bricks, and a single set of quartz diorite and sandstone specimens.

Strength and material properties, including density, tensile strength, and elastic modulus, were measured for each lithology used in the experiment. All measurements were made on 50 mm cores cut from $\sim$ 0.5 m rocks collected in the field (except for brick specimens). The density of each core was calculated by dividing measured mass by volume determined from triplicate caliper measurements of the diameter and length of the cores. The average density of each lithology is comprised of individual values from 10-15 cores. Tensile strength, a material property which describes the amount of stress applied in tension a material can withstand before failing, was measured using an indirect method called the Brazilian tensile strength test. This test measures the peak load for each sample to fail in tension. A stress was applied to each sample by placing it in a specially fabricated metal fixture with a thin stick of bamboo between the sample and the fixture on each side of the loading plane. The bamboo sticks ensured that the load was only applied to the parallel radial axes at the top and bottom of each sample. The fixture was then placed between two metal plates of a Versa-Loader, an apparatus that raises its bottom plate, thereby applying a load at a constant strain rate to the sample. After the sample fails breaking parallel to the loading, the peak load at failure is recorded. The tensile strength of each sample is computed using this value of peak load in addition to the dimensions of the sample, through the following expression: $\sigma_t = \frac{2F_p}{\pi l d}$, where F_p is the peak force applied to the sample at failure, l is the length and d is the diameter of the cylindrical sample (*Vutukuri*, 1974). In order to reduce the uncertainty of the value of the tensile strength, 10-15 measurements of each lithology were measured and averaged together to get a mean value. Finally, we measured the elastic modulus, also known as the Young's modulus which describes the stiffness of the material by relating the amount of deformation of the material to an applied stress. We measure this quantity for each lithology using an Olsen Resonance Tester (RT-1) and the methods prescribed by the ASTM C215 standard. With this method, an accelerometer is attached to the flat face of one end of the core, while a force is applied to the other end by hitting it with a small hammer. The applied force sends a vibrational wave through the core where the accelerometer records the longitudinal fundamental frequency. The elastic modulus

(Y) is then calculated using the expression: $Y = Dmf^2$, where D is the shape correction factor equal to $5.093\frac{l}{d^2}$ for cylindrical cores, m is the sample mass, and f is the recorded fundamental frequency. As with the other material properties, 10-15 measurements were taken and averaged together to get a mean value for each lithology. This method produced reliable values of elastic modulus for brick, schist, and sandstone, but because the sample specimens were not long enough, we were not able to preform this test on the quartz diorite or volcaniclastic rocks. Instead ranges of elastic modulus values from the literature were compiled indicating that quartz diorite span a range from 20 to 70 GPa (*Hughes and Jones*, 1950; *Merriam et al.*, 1970; *Pratt et al.*, 1972; *Fletcher et al.*, 2006) and volcaniclastic span values from 5 to 50 GPa (*Carlson and Wilkens*, 1983; *Apuani et al.*, 2005; *Frolova*, 2008; *Rotonda et al.*, 2010). Table 4.1 lists all the material properties values used in this study.

To better understand the modes of mechanical failure in the abraded particles, we prepare polished thin sections and examine them using an scanning electron microscope (SEM). The thin sections made from the plane perpendicular to the impact surface (Fig. 4.4a) and are imaged between 200 to 6000 times magnification using a FEI 600 Quanta FEG environmental scanning electron microscope. Images were taken moving along the edge of the grains (Fig. 4.4b/c) and compared to images of the interior of the grain. We then quantify the length scale over which damage occurs by taking between 600 to 1000 measurements from different locations around each grain of the distance of the most interior crack that can be continuously tracked to the surface.

Finally, following each set of collisions, the daughter products of the abrasion process were collected from the bottom of the tank. Although we attempted to collect all of the products from the abrasion experiments, small dust particles (< 1 μm) were observed to settle outside the tank, so we only reliably collected grains larger than that size. Fines produced throughout the entire experimental run for each pair of rocks were combined into one population for grain size analysis. Because the daughter products span a wide range of sizes, to fully characterize the grain size distribution, we employ two methods. First, to describe

the coarse grains, we wet sieve the daughter products into three size fractions: < 0.5 mm, 0.5 mm to 1.0 mm, and > 1.0 mm. The coarser two fractions are dried in an oven and subsequently weighed to determine their contribution to the entire size distribution. The grain size of the daughter products finer than 0.5 mm is measured using the Beckman Coulter laser diffraction particle analyzer, which determines the volumetric grain size distribution by deconstructing the diffraction pattern produced by shining a laser through a liquid solution containing the fine-grained sample. Because of the large quantity of fines produced from the abrasion experiments, we perform repeated subsampled measurements of grain size using the Coulter counter. We select five subsamples from a mixture of fine particles and deionized water. To ensure consistent subsampling of a homogenous mixture, we use a magnetic stirrer while selecting samples. We compare measured distributions from all five subsamples to ensure that each were uniform and representative of the entire population. We then merge the grain size date for the coarse grains from sieving with the fine grains from the particle analyzer by normalizing the volume fraction for each by the total volume lost during the experiment, calculated from measured mass and density values. Following the method used by the particle analyzer, the distribution is converted from volume fraction to number fraction by assuming the grains are spheres.

4.3. Results

We ran the binary collisions experiment on a total of 5 sets of bricks, 2 sets of quartz diorite, and a single set of sandstone, schist, and volcaniclastic. Throughout the course of each experimental run, the initially cuboid rocks would quickly lose their sharp corners and then slowly become rounder without any major fragmentation. There were two exceptions to this case. First with the sandstone around 20,000 collisions, a large piece, roughly 2 cm long and 1 cm wide, broke off one of the corners exposing a reddish-orange oxidized surface. Then with the schist on three occasions, an entire block of the cube grain fell off, fracturing at weathering planes. In both cases, fracturing occurred at a pre-existing weak region of the rock that appeared to be associated with chemically-weathered surfaces. Furthermore, we

observed in both the instance of the sandstone and the schist, that immediately following the large fracture events, the mass loss of the finer fragments from the parent grain would increase as the freshly exposed rough surface of the grain smoothed.

Plots of mass loss against cumulative impact energy for all rock types show two distinct patterns: an initial rapid phase of mass loss that is similar for all lithologies and impact energies, and then a transition to a slower, linear mass loss curve whose slope varies with rock type (Fig. 4.5a). To test the functional relationship between mass loss and energy, we performed experiments with three different masses of brick, spanning a range of collision energies of 0.04-0.22 j. Mass loss curves for all experiments are in good agreement with each other, and with a single linear trend (Fig. 4.6). Linear fits were then made to all mass loss curves, resulting in the relation:

$$M = kE + b. \tag{4.6}$$

To test the robustness of the linear fit, we generated a plot of $M - b$ versus kE; the collapse of data for all experiments shows that a linear relation is reasonable, but as anticipated fails to fit the initially-steep portion of the mass loss curve (Fig. 4.5b). We want to relate the two parameters in the linear fit (eq. (4.6)) to physically-meaningful quantities. The slope k, which controls the longterm abrasion rate for a given energy, should be controlled by material properties and hence be related to A. Data indicate that indeed the fitting parameter k is proportional to A (Fig. 4.7a). The intercept of this plot ($k = 0$) indicates that abrasion rates approach zero at a finite value of A; in other words, for the (low) energies explored in this experiment, very strong rocks should experience little to no abrasion. The volcaniclastic rock appears to be close to this value, and indeed this is the one rock type that never reaches the asymptotic linear regime of abrasion. From a plot of b versus initial mass (M_0), we find that the value b in relation (4.6) is related to the quantity of pebble mass that is lost before abrasion reaches the slower, linear portion of the mass loss curve (Fig. 4.7b). In other words, it is the amount of abrasion that occurs in the rapid, first

portion. The parameter b shows a linear relation with the initial mass of each particle, indicating that the ratio $b/M_0 = 0.0018$ is approximately constant for all experiments (Fig. 4.7b). This result suggests that all particles transition to the slower, linear portion of the mass loss curve when they have lost a certain fraction of mass. Since collision energies and rock strengths are different, the only factor common to all experiments was particle shape; all particles were initially cuboids. To test whether b is related to shape, we plot the evolution of corner curvature and mass against cumulative energy (Fig. 4.7c); results show that the former tracks the latter, and becomes approximately constant when rock mass $M/M_0 = 0.0018$. This is the same value as b/M_0, meaning that curvature of corners becomes constant when the fraction of mass lost is equal to b/M_0. This result is additionally verified by the curvature entropy characterization of grain shape. For the two brick sets and the sandstone, the change in curvature entropy mirrors the change in mass loss (Fig. 4.8). It appears that the intercept b is indeed related to shape.

By putting together the abrasion number and initial mass corresponding to k and b, the abrasion relation for mass loss versus impact energy is:

$$M = C_1 \frac{\rho Y}{\sigma^2} E + C_2 M_0 = C_1 A E + C_2 M_0 \tag{4.7}$$

where

$$C_1 = 8 \times 10^{-6} \quad C_2 = 0.0018 \tag{4.8}$$

For the case when $M \gg 0.0018 M_0$, the abrasion relation reduces to

$$M = C_1 A E \rightarrow \frac{M}{E} = C_1 A \tag{4.9}$$

This abrasion relation suggests that when the sharp edges are worn away, the abrasion rate is directly proportional to the abrasion number multiplied by the constant C_1.

The SEM images show a considerable amount of damage in the region near the edge of the grains (Fig. 4.5b/c). This damage is characterized by large cracks that span parallel to the

abrasion surface with smaller cracks branching perpendicular to them. In some instances, these cracks produced from impact intersect with inherent cracks or grain boundaries of the material, extending the damage zone further into the interior of the grain. The results of the damage zone length measurements are plotted in Fig. 4.9. The tail of the distribution of lengths shows power-law scaling with exponents that range in value from -1 to -2.3. We observe convergence of all distributions for each lithology in the large length limit, where the cracks are easiest to discern and measure. However, in the lower length limit, the distributions diverge as the length measurements become less reliable due to the resolution of the images.

The results from the daughter product grain size characterization are shown in Fig. 4.10. The plot combines the full measurements from the laser particle analyzer and sieving methods. Distributions from all lithologies and experimental runs show the same functional form. However, the full distributions displays artifacts of the measuring techniques in both the fine and coarse tails of the distributions. For the fine tail, the distributions drops off rapidly presumably due to the combined effects of the low end measuring limit of the particle analyzer and the loss of material during the collection of daughter products. For the coarse end of the Coulter counter data, sieving produces artifacts in the grain size distributions as the particle size approaches the sieve diameter, as evident by the erratic fluctuations in the grain size distributions on approach to $d = 0.5$ mm. Ignoring Coulter counter data over the range 0.2-1.0 mm, we observe a consistent and smooth grain size distributions from 1 μm to the maximum observed size from sieve analysis, for all rock types.

To determine the functional form of the grain size data, we remove the unreliable data points that are biased by the measurement method; for the fine tail, this includes grain sizes less than 1 μm, and for the coarse tail includes particle analyzer data greater than 200 μm. We normalize each curve by its mean value causing all curves to collapse on each other so we may fit one function to the entire data set for all lithologies. We then solve for the best fit power law to all data points. The fit shows an exponent of 2.5, which is slightly

higher than the expectation for full fragmentation, but still follows a Weibull distribution with very good agreement (Fig. 4.10).

4.4. Discussion

While a linear relation has been shown to reasonably model aeolian erosion (*Anderson*, 1986), our experiments definitively demonstrate that this linear relation is applicable for energies associated with fluvial bed load transport, over a wide range of rock strengths. There is an intriguing shape dependence on the initial abrasion rate. Indeed, data seem to indicate that these initially very angular cubes all abrade at the same rate regardless of energy or strength, until the corners are suitably rounded such that energy and rock strength become important. We speculate that in this region the corners are so sharp that virtually any impact can remove mass, because the required crack is infinitesimal in the limit of infinite curvature. However, rocks achieve the secondary linear mass loss curve quickly while the rocks are still very close to cuboids. Thus, for natural streams it is likely a reasonable assumption that b may be neglected; therefore, the relation $M/E = C_1 A$ is the applicable one to examine abrasion in natural streams.

The demonstration that A indeed controls mass loss is a very important one. Previous work on bedrock erosion has shown that the amount of mass removed depends on the inverse square of the tensile strength (*Sklar and Dietrich*, 2004). However, these experiments elucidate clearly and simply which rock material properties need to be taken into account through the development and verification of the Abrasion number A. A similar dimensionless number was proposed by *Wang et al.* (2011) for the abrasion of yardangs by windblown sand, but here we verify the concept for energies relevant to fluvial transport. However, we find that mass loss and impact energy are not directly proportional by A, but instead $C_1 A$. The physical meaning of C_1 likely combines a few factors, of which we hypothesize the proportion of impact energy that goes into damage may be most important. This amount of energy is not only related to material properties, but also to the details of the collision itself; the impact angle, rotation speed of the impacter, etc. (*Wang et al.*, 2011). The value

of C_1 may also be related to particle shape, although experiments by *Domokos et al.* (2014) show that M/E is constant for a given particle over nearly the entire evolution from cuboid to sphere, suggesting perhaps the C_1 is independent of shape. Regardless, the Abrasion number, A, is a useful similarity criterion for comparing laboratory and field abrasion rates, however rates determined from our experiments may not yet be directly scalable to the field due to uncertainty in the controls on C_1.

Although results from these experiments display a steady linear mass loss with impact energy, as we saw with the large fracture events with the sandstone and schist, chemical weathering can play an important role in the breakdown of river sediment. *Howard* (1998) observed higher rates of bedrock erosion in regions with more chemical weathering and thereby showed that chemical weathering weakens rocks and reduces material strength. While we find that material properties control abrasion rates, chemical weathering can cause a weakening of these material properties. We observe fragmentation events along weathering planes, similar to those observed in experiments of *Kodama* (1994a). In these instances, new angular and rough surfaces produced from the fragmentation process have high abrasion rates. On the one hand, chemical weathering appeared to create internal planes of weakness that facilitated failure of large chunks under low-energy abrasion. Indeed, these events caused fluctuations in the mass loss curves that were not observed in more structurally sound (stronger) materials. However, when observed over thousands of collisions (i.e., many fracture/failure events), the sandstone and schist rocks collapsed onto the same linear curve as other lithologies after accounting for material strength. It appears that mechanical weakening from chemical weathering may be reasonably described with the measured material properties that constitute A, so long as tested rock cores are representative of the particles in question. In a natural setting, we expect that the effects of chemical weathering will be more dominant in transport-limited environments where chemical weathering rates outpace mechanical abrasion. On the contrary, where sediment is transported frequently, abrasion is actively maintaining fresh unweathered surfaces on rocks, and therefore weathering features are not able to persist.

In the limit where $k = 0$, the Abrasion number, A, does not likewise approach zero, but instead is associated with $A = 0.25$. This non-vanishing value of A implies that for the range of energies examined in this experiment, there is a limiting rock strength at which little or no abrasion occurs. This result would suggest that some materials should not abrade significantly under impact energies representative of bed load transport. For our experiments, the volcaniclastic rocks are close to this limit. Observations of downstream evolution of pebble shape for volcaniclastic rocks in the River Mameyes in Puerto Rico have shown that significant abrasion occurs (*Litwin Miller et al.*, in review). However, the pebbles from the field were all at least 4 times larger than those used in the laboratory, while estimated collision velocities were comparable. The combined observations of volcaniclastic rocks from experiments and the field suggest that possibility that, as particles lose mass downstream due to abrasion, there is a potential lower limit in size that is controlled by rock strength. This idea needs to be explored in more detail.

The results from the SEM images display a region of damage near the impact surface of the rocks. However, because the distributions of crack lengths from the SEM images are unreliable in the small length limit, the only sound conclusions we can make from these results are for the large crack sizes. It should be noted that the large length limit is an order of magnitude larger than the smallest resolvable length, so these measurements are dependable. Furthermore, with the thin sections imaged, we were only examining a 2-dimensional slice of a 3-dimensional object. Therefore, the measured distribution of crack lengths is a result of both the actual crack length and its orientation, as the length of the cracks running obliquely to the thin section plane will be underestimated. With these considerations, we find that the maximum damage length measured from the SEM images is on the order of 1 mm, which corresponds to the maximum size of daughter products (Fig. 4.9). If the maximum crack length was governed by the attenuation of impact energy, as we hypothesized, the length scale would vary with material properties. Surprisingly however, the maximum crack size and the maximum daughter product are comparable in size across all lithologies, suggesting that for the low energies of abrasion explored in this experiment,

material properties do not control the scale of these features. We speculate that for the range of energies explored here, the maximum length of the damage zone is dominantly controlled by the geometry of crack growth and merger. In this geometric argument, cracks initiate at the surface and propagate inward until they intersect with another crack. The maximum size would then relate to the maximum length a crack can propagate before merging with another crack to liberate material. However, application of fracture theory to 3-dimensional reconstructions of the damage zone is necessary to fully understand the fracture mechanics of the abrasion of these rocks.

A classic model for understanding the grain size distribution resulting from wear is brittle fracture theory developed by *Griffith* (1921), who hypothesized that all materials contain pre-existing flaws or cracks. The theory also states that when an applied stress exceeds a critical value, the concentrated stress at the tips of these cracks is released as the crack propagates. Growth and intersection of these cracks cause ultimate failure of the material. In the large energy limit of crushing, where complete disintegration of the parent particle occurs, *Gilvarry and Bergstrom* (1961) showed that the Griffith fracture model implies that the daughter products should have a grain size distribution that follows the form of eq. (4.5). More recent numerical simulations and laboratory experiments have shown that the value of the exponent depends on the mechanism of fracture (i.e. grinding, collision, or expansive explosion) and the impact energy (*Kun and Herrmann*, 1999; *Astrom et al.*, 2004; *Kok*, 2011). However, none of these studies examined the low-energy limit of chipping and abrasion that is relevant for bed load transport. The scaling exponent of 2.5 for the daughter products of these binary collision experiments is surprisingly robust across a range of rock types, indicating a commonality in the failure modes of these different materials under the energies examined. The exponent is also within the range of values reported from studies of brittle fracture fragmentation. We tentatively suggest that brittle fracture is the mechanism that creates the daughter products of abrasion in our experiments. However, it appears that fragmentation is confined to a skin depth on the order of a few hundred microns. Examination of SEM images reveals an apparent damage zone for each examined

particle, which we have attempted to quantify crudely by tracing identified cracks. Data are insufficient to attribute the maximum observed particle size of daughter products to this identified damage zone, but the agreement in terms of order of magnitude is encouraging. Whether this damage zone is mechanically related to an attenuation depth of impact energy, or arises simply as a geometric consequence of crack growth inward from the surface, cannot be determined. As for the lower size limit in the daughter products, an obvious candidate would be the size of constituent particles in each rock type; i.e., sand grains for the sandstone or clay particles for the brick. Although we could not resolve the finest particles owing to loss, it is clear that fragmentation through constituent particles occurs. The determinant of the lower size limit remains unknown.

4.5. Conclusion

The results of this laboratory investigation suggest that the main consequences of fluvial abrasion are encapsulated in two "universal" relations. First, we verified the linear abrasion law for energies and particle sizes associated with fluvial transport. In doing so, we have shown which material properties control the amount of mass loss per unit energy, providing a mechanistic underpinning to abrasion "Susceptibility" (*Anderson*, 1986) and helping guide researchers regarding how to characterize lithology. Second, the grain size distributions for daughter products appear to suggest that brittle fracture creates fragmentation over a restricted skin depth, which has been correlated to maximum particle size. However, more theoretical work is necessary to understand the underlying mechanics of fracture and damage. In addition, we have identified a possible shape control on abrasion rate in the initial stage where particles are very angular, which is intriguing from a mechanics point of view, but is likely irrelevant in nature as the effect is only manifest when corners are exceedingly sharp.

Our experiments have shown that material properties can be accounted for reasonably simply, however results cannot be scaled directly to the field until constant C_1 is understood. We hypothesize that this coefficient is primarily controlled by the details of the collision

process, which determine how much impact energy contributes to damage as opposed to friction or rebound of the target. Once C_1 is resolved, one may use a mechanistic model of bed load collision energy and frequency to estimate abrasion rates in natural rivers. If the grain size distributions of daughter products are indeed universal, they could also be used to estimate the quantities of sand, silt and dust that result from abrasion by bed load transport. If the results of *Domokos et al.* (2014) and (*Litwin Miller et al.*, in review) are correct that up to 50% of a pebble's mass is lost during transport downstream, significant quantities of these fine grains are produced in natural rivers.

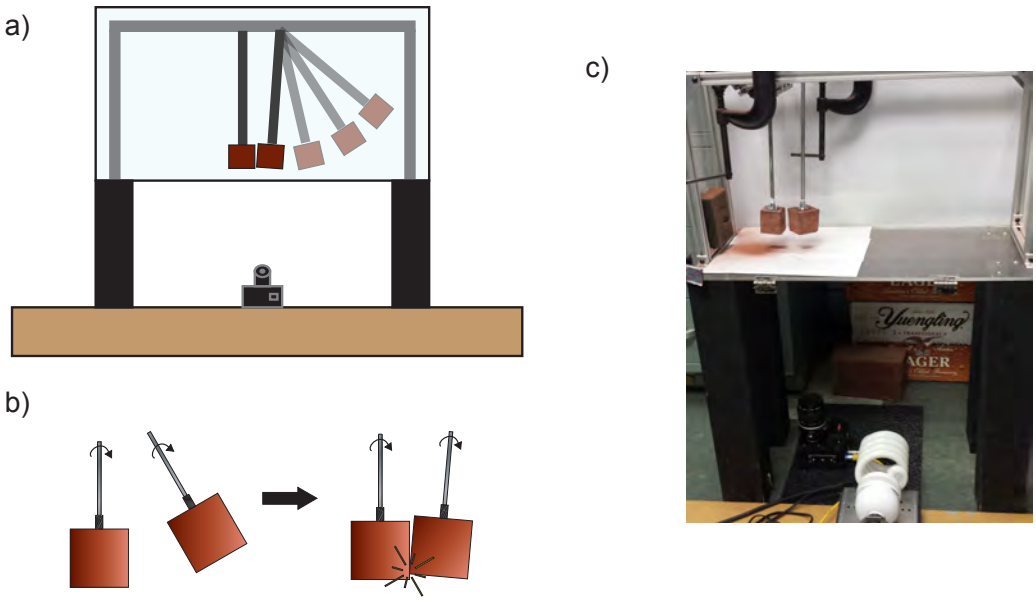

Figure 4.1: Schematic of experimental set-up. (a) Front view drawing depicting binary collisions double-pendulum apparatus. (b) Close-up drawing illustrating how grains impact during collision. The impacting grain is raised then released, colliding with the stationary target grain. Both grains are able to rotate freely. (c) Picture of set-up with brick clasts.

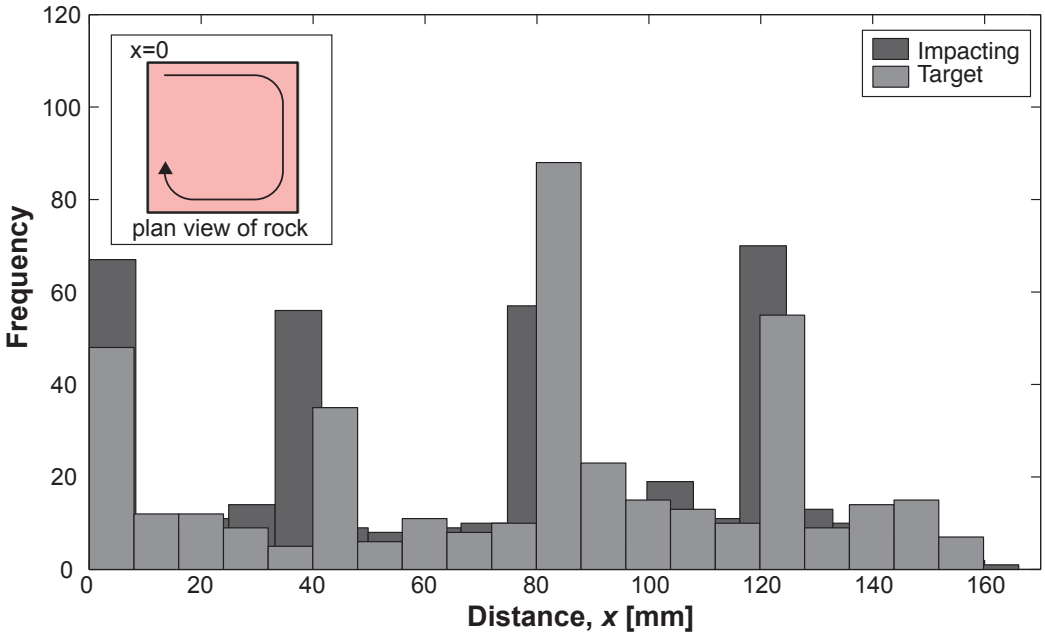

Figure 4.2: Randomness test for collision rotation. Plot showing the histogram of impact locations for impacting and target grains. Peaks correspond to corners of the grains. Inset shows plane view of rock with labeled location of $x = 0$ at one of the corners.

Figure 4.3: Images of samples. Images of all lithologies used in the experiment. Images taken at the end of the experiment so there is noticeable rounding of the edges at the impact zone.

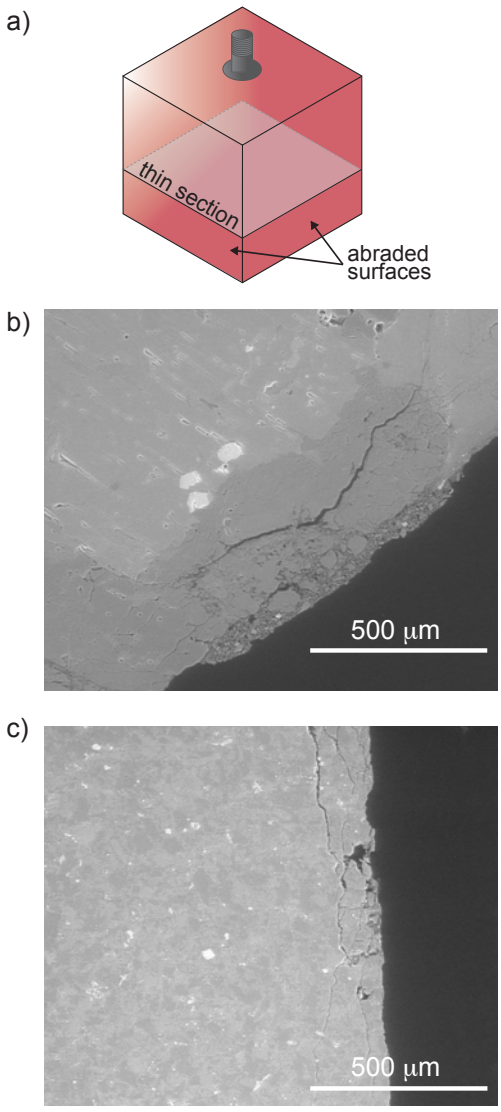

Figure 4.4: Thin section preparation and SEM images. (a) Schematic drawing showing location in grain where thin sections were made. (b) SEM image of quartz diorite. (c) SEM image of volcaniclastic rock.

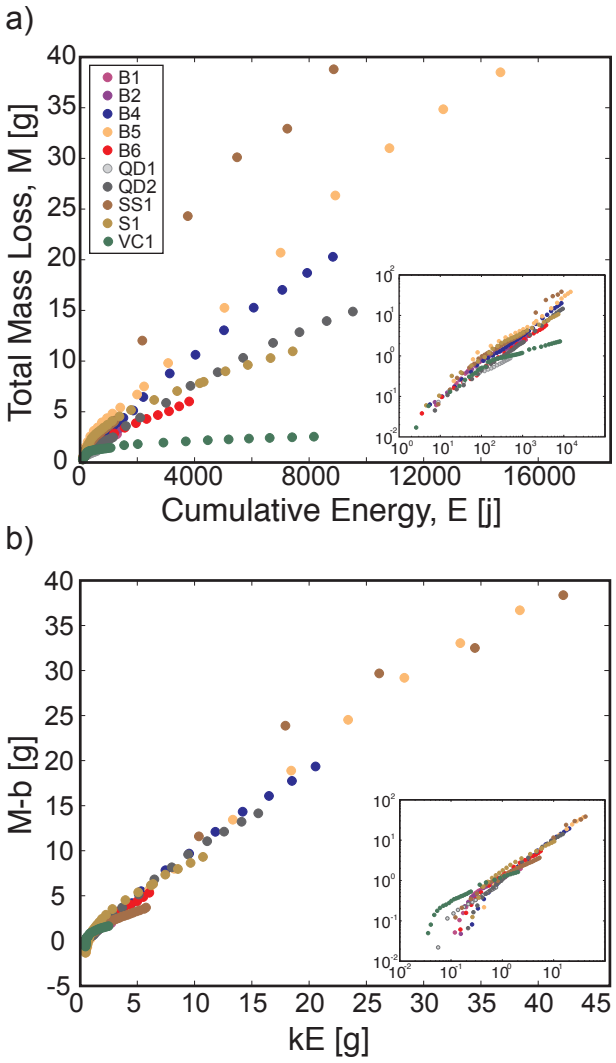

Figure 4.5: Abrasion mass loss curves. (a) Plot of total cumulative mass loss versus cumulative impact energy for each set of rocks. (b) Plot of total cumulative mass loss minus y-intercept, b, from linear fits to raw data in (a) versus cumulative impact energy multiplied by value of fit slope. Inset for both (a) and (b) displays plots with log-log axes.

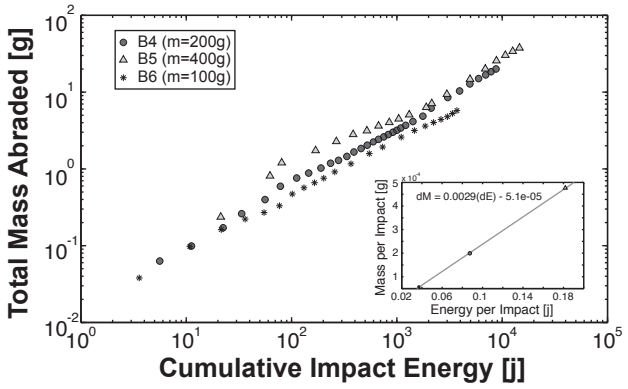

Figure 4.6: Abrasion rate for bricks with different collision energies. Plot of total cumulative mass abraded versus cumulative impact energy for three sets of brick with different masses. Inset displays plot of average mass abraded per impact versus average energy per impact. Each data point corresponds to a separate set of bricks.

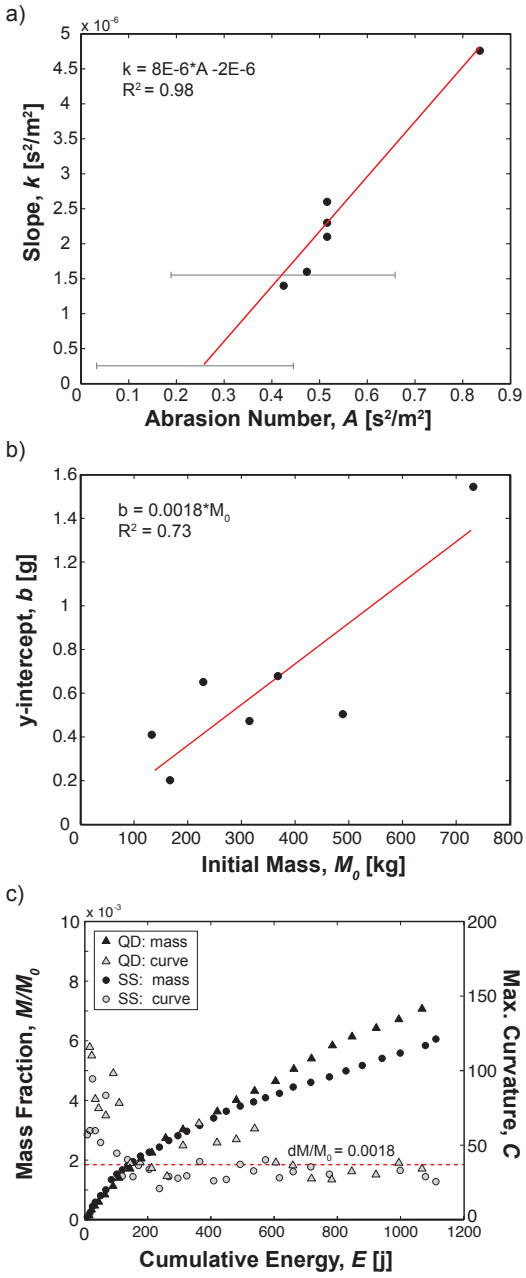

Figure 4.7: Normalization of slope and intercept. (a) Plot of slope (k) from linear fits to raw mass curves versus Abrasion Number. All data points based on measured values of material properties, while grey brackets (for quartz diorite and volcaniclastic) use range of values for Youngs modulus from the literature. (b) Plot of y-intercept from linear fits to raw mass curves versus initial mass of both impacting and target grains. This plot excludes sandstone and schist because of fragmentation events. (c) Plot showing change in mass fraction (left axis) and maximum curvature (right axis) versus cumulative impact energy. They both transition from a high rate of change to a slower one at $M/M_0 = 0.0018$.

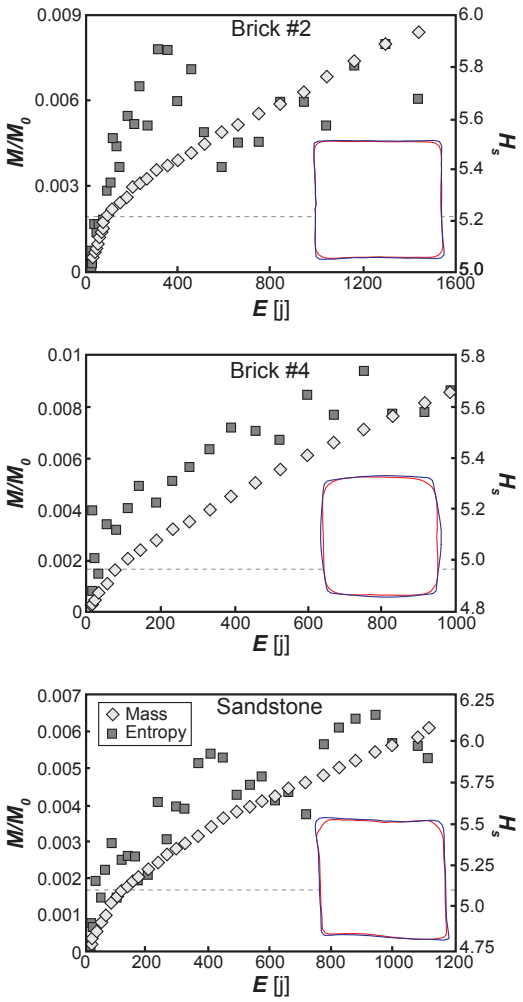

Figure 4.8: Shape evolution with curvature entropy. Plot of curvature entropy (right axis) versus cumulative impact energy overlaid on plot of mass loss normalized by initial mass (left axis) versus cumulative impact energy. Inset shows the scanned contours with blue contour from the initial scan and red contour from the final scan. (a) Brick set #2 (b) Brick set #4 (c) Sandstone.

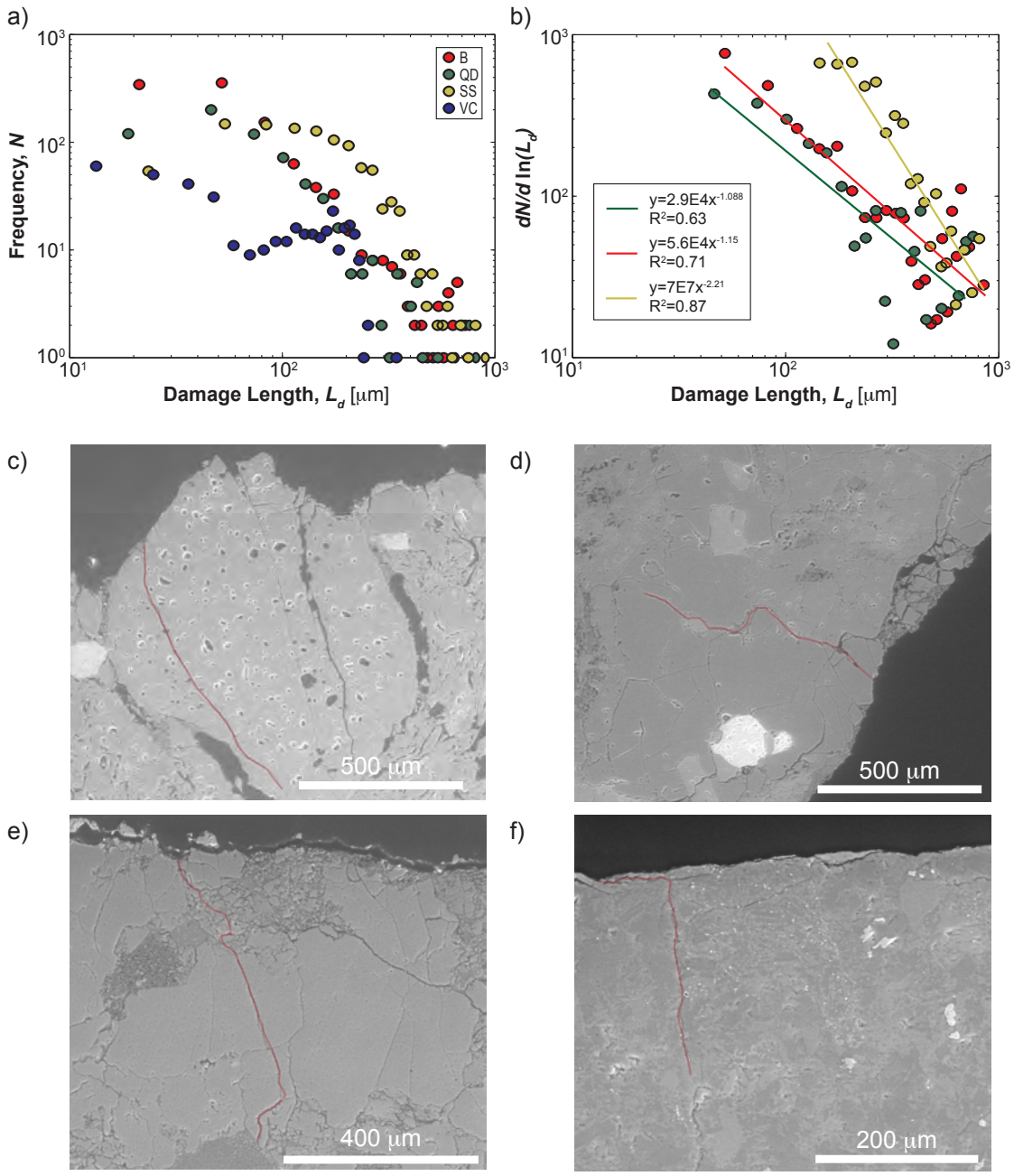

Figure 4.9: SEM results. (a) Plot of the distribution of length of damage within abraded rocks from SEM images of thin sections. (b) Damage lengths plotted in the form of the eq. (4.5) with corresponding power-law fits. (c)-(f) SEM images of the largest crack length for each rock type outlined in red. (c) Brick (d) Quartz diorite (e) Sandstone (f) Volcaniclastic

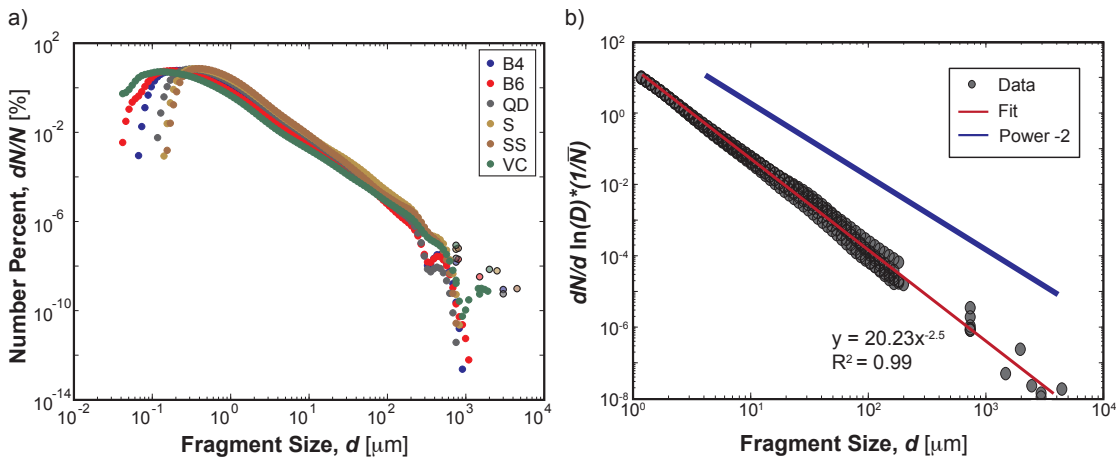

Figure 4.10: Grain size distributions of products of abrasion. (a) Plot of number distribution of grain size from particle analyzer (solid circles) and sieving (circles with black outlines) methods. (b) Number distribution of grain size plotted in the form of eq. (4.3) and normalized by the mean value. Data are combined for all lithologies. Data believed to be affected by measuring technique are excluded from plot (< 1 μm and > 200 μm from particle analyzer). Data fit with power law function with exponent of -2.5. Solid blue line denotes expectation from brittle fragmentation of power law with exponent -2.

Sample	Lithology	Density ρ [kg/m^3]	Tensile Str. σ_t [MPa]	Youngs Mod. Y [GPa]	Int. Mass M_0 [g]	Impact Energy E_i [j]
B1	brick	2072	7.5	14	490	0.159
B2	brick	2072	7.5	14	394	0.148
B4	brick	2072	7.5	14	369	0.112
B5	brick	2072	7.5	14	734	0.213
B6	brick	2072	7.5	14	133	0.036
QD1	quartz diortie	2704	16.9	20-70	167	0.090
QD2	quartz diorite	2704	16.9	20-70	315	0.148
SS1	sandstone	2330	5.28	10	636	0.179
S1	schist	2667	20.5	7	381	0.091
VC1	volcaniclastic	2672	6.63	5-50	229	0.052

Table 4.1: Table listing measured material properties and experimental conditions for each set of samples

CHAPTER 5 : Summary and Conclusions

5.1. Summary

This dissertation reports on the mechanisms that produce downstream grain size patterns in fluvial systems and discusses its consequences on channel morphology. Whether abrasion or sorting, both of these processes illustrate how the physics of sediment transport play an important role in shaping the natural environment. The chapters of this dissertation aim to provide links between the underlying physics, active processes, and observable quantities in order to create a complete description of grain size trends in rivers.

Chapter 2 investigated sorting patterns on an alluvial fan. In the upper gravel portion of the fan, we found that mean grain size and standard deviation of grain size do not decline downstream at the same rate, as expected from the self-similar profiles of *Fedele and Paola* (2007). Instead gravel sorting converges to a limit of equal mobility where a range of the grain size distribution can be transported under the same flow conditions (*Parker and Klingeman*, 1982; *Wiberg and Smith*, 1987). Further downfan, we found that sand sorting from gravel to produce the well-known feature of the gravel-sand transition (*Smith and Ferguson*, 1995; *Cui and Parker*, 1998; *Knighton*, 1999; *Ferguson*, 2003) is self-similar in form. Downstream surface sand fraction profiles from two field sites and a laboratory experiment collapse to a single curve when downstream distance is normalized by the length of the upstream gravel reach, suggesting that the transition stretches as the size of the river increases. A two-fraction transport model can explain the segregation of sand from gravel (*Wilcock and Kenworthy*, 2002), however, the self-similarity of these profiles suggest that a universal transport mechanism controls the overall channel length of this sorting feature. More generally, this work demonstrated that threshold transport and equal mobility control sorting patterns on alluvial fans.

Chapter 3 examined the effects of both abrasion and sorting throughout an entire length of a river by tracking the evolution of pebble size and shape, which provided the first

field verification of 2-phase abrasion theory (*Domokos et al.*, 2014). We found phase I, marked by rapid mass loss and shape change as the edges of the pebbles got worn away until it was completely convex, occurred quickly in the headwater stream over a distance of a few kilometers from the sediment supply. Slower phase II happened over the longer distances of the mainstem of the river as the pebble gradually reduced in axes dimensions while approaching a more spherical shape. Numerical model results showed that abrasion alone could not account for the total observed decrease in grain size while selective sorting could not account for observed changes in pebble shape, suggesting that both processes are responsible for observed downstream pebble trends. Finally, we found that as a pebble travels through this watershed, it will lose approximately 38% of its total volume due to abrasion, which has implications for fine sediment production (*Jerolmack and Brzinski*, 2010).

In Chapter 4, we conducted laboratory experiments to determine the energy scaling of abrasion rates of different lithologies of rocks by looking at single collision events between two pebbles. We found that the amount of mass removed during abrasion scales linearly with impact energy. Through a dimensional analysis (*Buckingham*, 1914), we normalized impact energy by material properties specific to each rock-type and found that this normalization produced a collapse of the abrasion data, indicating that material properties determine the magnitude of the abrasion rate. Scanning electron microscope images of the abraded pebbles used in the experiments, showed a zone of damage at the rocks surface, suggesting that impact energy is attenuated over this length. From the grain size characterization of the products of abrasion collected from these binary collision experiments, we found that they exhibit a Weibull distribution, as expected from brittle fracture theory (*Brown and Wohletz*, 1995; *Kok*, 2011), implying that the same mechanics responsible for high energy fragmentation (*Gilvarry*, 1961; *Oddershede et al.*, 1993; *Astrom et al.*, 2004; *Astrom*, 2006) may be applied to low energy abrasion.

The results of this dissertation demonstrate that sediment interactions during transport

drive grain size trends. For sorting, hiding and protruding effects caused by the relative sizes of grains will either limit grain sorting, as is the case of equal mobility, or enhance segregation, as is the case for sand and gravel producing an abrupt transition. For abrasion, collisions between saltating grains during bedload transport provide the required energy to remove mass. The research in these chapters develop the links between sediment transport and the processes that produce grain size patterns, which have widespread implications on channel morphology.

5.2. Implications and Future Prospects

5.2.1. Specific Implications and Future Work

This section describes the implications of the work described in this dissertation, as well as its limitations and future work that arises from the results. Because of its ease of field measurement, the grain size of particles in a river is one of the most common quantifiable variables in fluvial systems (*Leopold et al.*, 1957), so an understanding of what controls its value and in turn how it controls the surrounding landscape is necessary for describing the natural environment.

On Dog Canyon alluvial fan (Chapter 2) we observed that the river has a finite length over which gravel sorting approaches a limit based on a state of equal mobility where the effects of local and system-wide grain size variance are balanced (*Fedele and Paola*, 2007). However, this work was completed in the highly out-of-equilibrium channel of an alluvial fan with large amounts of sand deposition not permitting the gravel sorting to reach its steady state. In order to generalize this result to other systems, additional fieldwork and experiments tracking changes in grain size distributions near their sediment source are needed to describe the manner to which gravel sorts. Furthermore, the self-similarity of the surface sand fraction profiles implies that transport conditions control the length over which sand sorts from gravel. This result prompts the development of an analytical framework to describe the gravel-sand transition.

The research in Puerto Rico not only provides the first field evidence of 2-phase abrasion, but also offers new methods and measuring techniques, through the use of simple hand and image-based shape descriptors, to observe the effects of abrasion in the field (Chapter 3). Also, through numerical modeling using the Puerto Rico data, we learn that selective sorting is likely the dominant contributing process to downstream changes in measured median pebble axis. Although the Mameyes river does not have a single point source of sediment, we were still able to see strong trends in shape and size. To make the results more robust, future work can incorporate the effects of a spatially varying sediment supply so that it may be applied to more widespread river systems.

Finally, the work on the abrasion due to binary collisions of grains implies that energy and material properties are also controlling factors determining abrasion rates of river (Chapter 4). Most importantly from this work is the development of the "Abrasion Number" (A), which describes how abrasion rates vary by lithology. The next step in this work is to see if the results for the single collision of two grains hold for multiple collisions of many grains by conducting tumbling mill experiments. We designed a tumbling mill one single grain diameter in width so that the experiment will be essentially 2-dimensional. With a high-speed camera mounted in front of a clear faceplate, we can characterize all of the collision energies between the grains. From this experiment we can extend the work from the binary collision experiments. Once we have a complete understanding of the roles of impact energy and lithology have on abrasion rates, we can apply the concept to the field to make estimates of abrasion rates.

5.2.2. Broad Prospects

One thing that is required for both size selective sorting and abrasion to be effective is sediment transport. In selective sorting, it is the differential transport of sediment that causes large grains to deposit while smaller grains move further downstream, thus segregating them by size (*Paola et al.*, 1992; *Ferguson et al.*, 1996; *Gasparini et al.*, 1999). In abrasion, bedload transport provides the collisions that drive mass loss (*Wentworth*, 1919; *Kuenen*, 1956;

Sneed and Folk, 1958; *Parker*, 1991; *Kodama*, 1994a; *Lewin and Brewer*, 2002). Therefore, to make the results of this dissertation applicable to natural settings, we need a complete understanding of sediment transport. Although there is a whole field of study devoted to sediment transport, there are still high levels of uncertainty in quantifying transport rates (*Wilcock*, 2001). For example, in determining bedload transport rates, effects of channel slope (*Mueller et al.*, 2005; *Lamb et al.*, 2008) and bed roughness (*Wiberg and Smith*, 1987; *Wilcock and Crowe*, 2003; *Yager et al.*, 2012) can lead to discrepancies between calculated and measured values. These inconsistencies usually stem from the difficulty in determining the critical Shield's stress for the threshold of motion (*Carling*, 1983; *Ferguson*, 1994). However, recent work using tracer particles has shown that quasi-steady flow approximations are acceptable for modeling long timescale river processes (*Phillips et al.*, 2013). Future studies need to determine the level of detail in modeling sediment transport necessary for linking the processes of size selective sorting and abrasion to field settings.

Another important concept in fluvial systems is the idea of scale, both spatial and temporal (*Paola et al.*, 2009). Some features in the landscape may be scale invariant, meaning their form does not change as the system size changes, and others are scale dependent, meaning they are controlled by system size (*Hallet*, 1990). We observe scale invariance in many of the results of this dissertation. The self-similar sand fraction profiles suggest that the length of the gravel-sand transition merely stretches as the size of the river increases (Chapter 2). That is to say, the ratio of the length of the gravel-sand transition to the length of the entire river is constant and therefore scale invariant. From the binary collision experiments, we find that mass loss from abrasion scales linearly with impact energy producing a constant rate of abrasion (Chapter 4). The scaling parameter, (A), based on material properties, collapses mass loss curves across different lithologies, signifying that abrasion is a universal process. Additionally, the grain size distributions of the daughter products exhibit power law scaling, indicating scale invariance (Chapter 4). Recently *Paola et al.* (2009) advocated for research to focus on understanding the scale independence of natural processes and features, like the ones in this dissertation, to make extrapolating results from the laboratory to the field more

straightforward. In my future work, I will be examining the effects of scaling on laboratory experiments that reproduce features in the landscape at a fraction of the size and in a fraction of the time than their natural counterparts.

Ultimately, the combined results of all the research in this dissertation have implications on channel structure and evolution. Grain size exerts a strong control on channel gradient and cross-stream geometry (*Gasparini et al.*, 2004). As in the case of the gravel-sand transition, sorting segregates the two-grain population while the river becomes shallower in slope and wider and deeper in cross-section, transitioning its geometry from a gravel-bedded river adjusted to transport bedload (*Parker*, 1978) to a sandy river adjusted to transport suspended load (*Parker*, 1978). However, it is not known whether grain size produces the change in channel slope and geometry or vice-versa; or perhaps some more complicated feedback between them. Previous work using numerical models have shown that grain size changes drive channel concavity and slope (*Snow and Slingerland*, 1987; *Sinha and Parker*, 1996; *Morris and Williams*, 1997). On the other hand, equilibrium channel theory suggests a feedback between grain size, threshold entrainment stress, and bankfull channel depth (*Parker*, 1978). More work is needed to compare the adjustment timescales between grain size, channel geometry, and channel gradient to elucidate the connections between the evolution of these properties.

BIBLIOGRAPHY

Abbott, J. E., and J. R. D. Francis (1977), Saltation and Suspension Trajectories of Solid Grains in a Water Stream, *Philosophical Transactions of the Royal Society A: Mathematical, Physical and Engineering Sciences*, *284*(1321), 225–254, doi:10.1098/rsta.1977.0009.

Adams, J. (1978), Data for New Zealand pebble abrasion studies, *New Zealand Journal of Science*, *21*, 607610.

Adams, J. (1979), Wear of unsound pebbles in river headwaters., *Science (New York, N.Y.)*, *203*(4376), 171–2, doi:10.1126/science.203.4376.171.

Anderson, R. S. (1986), Erosion profiles due to particles entrained by wind: Application of an eolian sediment-transport model, *Geological Society of America Bulletin*, *97*(10), 1270, doi:10.1130/0016-7606(1986)97⟨1270:EPDTPE⟩2.0.CO;2.

Andrews, B. (1999), Gauss curvature flow: the fate of the rolling stones, *Inventiones Mathematicae*, *138*(1), 151–161, doi:10.1007/s002220050344.

Apuani, T., C. Corazzato, A. Cancelli, and A. Tibaldi (2005), Physical and mechanical properties of rock masses at Stromboli: a dataset for volcano instability evaluation, *Bull Eng Geol Environ*, *64*(4), 419–431, doi:10.1007/s10064-005-0007-0.

Astrom, J. A. (2006), Statistical models of brittle fragmentation, *Advances in Physics*, *55*(3-4), 247–278, doi:10.1080/00018730600731907.

Astrom, J. A., F. Ouchterlony, R. P. Linna, and J. Timonen (2004), Universal Dynamic Fragmentation in D Dimensions, *Phys. Rev. Lett.*, *92*(24), 245506, doi:10.1103/PhysRevLett.92.245506.

Attal, M., and J. Lave (2009), Pebble abrasion during fluvial transport: Experimental results and implications for the evolution of the sediment load along rivers, *J. Geophys. Res.*, *114*(F4), F04023, doi:10.1029/2009JF001328.

Attal, M., J. Lave, and J.-P. Masson (2006), New Facility to Study River Abrasion Processes, *Journal of Hydraulic Engineering*, *132*(6), 624–628, doi:10.1061/(ASCE)0733-9429(2006)132:6(624).

Bitter, J. (1963), A study of erosion phenomena part I, *Wear*, *6*(1), 5–21, doi:10.1016/0043-1648(63)90003-6.

Blair, T. C., and J. G. McPherson (1994), Alluvial fans and their natural distinction from rivers based on morphology, hydraulic processes, sedimentary processes, and facies assemblages, *Journal of Sedimentary Research*, *64*(3a), 450–489, doi:10.1306/D4267DDE-2B26-11D7-8648000102C1865D.

Bloore, F. J. (1977), The shape of pebbles, *Journal of the International Association for Mathematical Geology*, *9*(2), 113–122, doi:10.1007/BF02312507.

Blott, S. J., and K. Pye (2007), Particle shape: a review and new methods of characterization and classification, *Sedimentology*, *0*(0), 070921092734002–???, doi:10.1111/j.1365-3091.2007.00892.x.

Bradley, W. C., R. K. Fahnestock, and E. T. Rowekamp (1972), Coarse Sediment Transport by Flood Flows on Knik River, Alaska, *Geological Society of America Bulletin*, *83*(5), 1261–1284, doi:10.1130/0016-7606(1972)83[1261:CSTBFF]2.0.CO;2.

Brewer, P., G. Leeks, and J. Lewin (1992), Direct measurement of in-channel abrasion processes, in *Erosion and sediment transport monitoring programmes in river basins (Proceedings of the Oslo Symposium, August 1992)*, p. 2129.

Briggs, R. P., and E. Aguilar-Cortes (1980), Geologic map of the Fajardo and Icacos: quadrangles, Puerto Rico, *US Geological Survey, Map I-1153, scale*, *1*(20,000).

Brown, W. K., and K. H. Wohletz (1995), Derivation of the Weibull distribution based on physical principles and its connection to the RosinRammler and lognormal distributions, *Journal of Applied Physics*, *78*(4), 2758–2763, doi:10.1063/1.360073.

Buckingham, E. (1914), On Physically Similar Systems; Illustrations of the Use of Dimensional Equations, *Phys. Rev.*, *4*(4), 345–376, doi:10.1103/PhysRev.4.345.

Carling, P. A. (1983), Threshold of coarse sediment transport in broad and narrow natural streams, *Earth Surf. Process. Landforms*, *8*(1), 1–18, doi:10.1002/esp.3290080102.

Carlson, R., and R. Wilkens (1983), Seismic Crustal Structure and the Elastic Properties of Rocks Recovered by Drilling in the Philippine Sea, in *Geodynamics of the Western Pacific-Indonesian Region*, edited by T. W. C. Hilde and S. Uyeda, pp. 127–136, American Geophysical Union.

Chatanantavet, P., E. Lajeunesse, G. Parker, L. Malverti, and P. Meunier (2010), Physically based model of downstream fining in bedrock streams with lateral input, *Water Resour. Res.*, *46*(2), W02518, doi:10.1029/2008WR007208.

Chow, B. (1991), On Harnack's inequality and entropy for the gaussian curvature flow, *Communications on Pure and Applied Mathematics*, *44*(4), 469–483, doi:10.1002/cpa.3160440405.

Colombini, M., G. Seminara, and M. Tubino (1987), Finite-amplitude alternate bars, *Journal of Fluid Mechanics*, *181*, 213–232, doi:10.1017/S0022112087002064.

Cox, E. P. (1927), A method of assigning numerical and percentage values to the degree of roundness of sand grains, *Journal of Paleontology*, *1*(3), 179183.

Cui, Y., and G. Parker (1998), The arrested gravel front: stable gravel-sand transitions in rivers Part 2: General numerical solution, *Journal of Hydraulic Research*, *36*(2), 159–182, doi:10.1080/00221689809498631.

Culling, W. E. H. (1960), Analytical theory of erosion, *The Journal of Geology*, p. 336344.

Dade, W. B., and P. F. Friend (1998), Grain-Size, Sediment-Transport Regime, and Channel Slope in Alluvial Rivers, *Journal of Geology*, *106*, 661–676, doi:10.1086/516052.

Dawson, M. (1988), Sediment size variation in a braided reach of the Sunwapta River, Alberta, Canada, *Earth Surf. Process. Landforms*, *13*(7), 599–618, doi:10.1002/esp.3290130705.

Domokos, G., and G. W. Gibbons (2013), Geometrical and physical models of abrasion, *arXiv preprint arXiv:1307.5633*.

Domokos, G., A. A. Sipos, and P. L. Varkonyi (2009), Countinuous and discrete models for abrasion processes, *Architecture*, *40*(1), 3–8, doi:10.3311/pp.ar.2009-1.01.

Domokos, G., A. Sipos, T. Szabo, and P. Varkonyi (2010), Pebbles, Shapes, and Equilibria, *Math Geosci*, *42*(1), 29–47, doi:10.1007/s11004-009-9250-4.

Domokos, G., A. . Sipos, and T. Szab (2012), The Mechanics of Rocking Stones: Equilibria on Separated Scales, *Math Geosci*, *44*(1), 71–89, doi:10.1007/s11004-011-9378-x.

Domokos, G., D. J. Jerolmack, A. Sipos, and A. Torok (2014), How River Rocks Round: Resolving the Shape-Size Paradox, *PLoS ONE*, *9*(2), e88657, doi:10.1371/journal.pone.0088657.

Drake, T. G., R. L. Shreve, W. E. Dietrich, P. J. Whiting, and L. B. Leopold (1988), Bedload transport of fine gravel observed by motion-picture photography, *Journal of Fluid Mechanics*, *192*, 193–217, doi:10.1017/S0022112088001831.

Durian, D. J., H. Bideaud, P. Duringer, A. Schroder, F. Thalmann, and C. M. Marques (2006), What Is in a Pebble Shape?, *Phys. Rev. Lett.*, *97*(2), 028001, doi:10.1103/PhysRevLett.97.028001.

Fedele, J. J., and C. Paola (2007), Similarity solutions for fluvial sediment fining by selective deposition, *J. Geophys. Res.*, *112*(F2), F02038, doi:10.1029/2005JF000409.

Ferguson, R., T. Hoey, S. Wathen, and A. Werritty (1996), Field evidence for rapid downstream fining of river gravels through selective transport, *Geology*, *24*(2), 179–182, doi:10.1130/0091-7613(1996)024⟨0179:FEFRDF⟩2.3.CO;2.

Ferguson, R. I. (1994), Critical discharge for entrainment of poorly sorted gravel, *Earth Surf. Process. Landforms*, *19*(2), 179–186, doi:10.1002/esp.3290190208.

Ferguson, R. I. (2003), Emergence of abrupt gravel to sand transitions along rivers through sorting processes, *Geology*, *31*(2), 159, doi:10.1130/0091-7613(2003)031⟨0159:EOAGTS⟩2.0.CO;2.

Firey, W. J. (1974), Shapes of worn stones, *Mathematika*, *21*(01), 1, doi:10.1112/S0025579300005714.

Fletcher, R. C., H. L. Buss, and S. L. Brantley (2006), A spheroidal weathering model coupling porewater chemistry to soil thicknesses during steady-state denudation, *Earth and Planetary Science Letters*, *244*(12), 444–457, doi:10.1016/j.epsl.2006.01.055.

Frings, R. M. (2011), Sedimentary Characteristics of the Gravel-Sand Transition in the River Rhine, *Journal of Sedimentary Research*, *81*(1), 52–63, doi:10.2110/jsr.2011.2.

Frolova, Y. V. (2008), Specific features in the composition, structure, and properties of volcaniclastic rocks, *Moscow Univ. Geol. Bull.*, *63*(1), 28–37, doi:10.1007/s11969-008-1004-z.

Gage, M. E. (1983), An isoperimetric inequality with applications to curve shortening, *Duke Math. J.*, *50*(4), 1225–1229, doi:10.1215/S0012-7094-83-05052-4.

Garcia-Martino, A. R., G. S. Warner, F. N. Scatena, and D. L. Civco (1996), Rainfall, runoff and elevation relationships in the Luquillo Mountains of Puerto Rico, *Caribbean Journal of Science*, *32*, 413424.

Gasparini, N. M., G. E. Tucker, and R. L. Bras (1999), Downstream fining through selective particle sorting in an equilibrium drainage network, *Geology*, *27*(12), 1079, doi:10.1130/0091-7613(1999)027⟨1079:DFTSPS⟩2.3.CO;2.

Gasparini, N. M., G. E. Tucker, and R. L. Bras (2004), Network-scale dynamics of grain-size sorting: implications for downstream fining, stream-profile concavity, and drainage basin morphology, *Earth Surf. Process. Landforms*, *29*(4), 401–421, doi:10.1002/esp.1031.

Gilvarry, J. J. (1961), Fracture of Brittle Solids. I. Distribution Function for Fragment Size in Single Fracture (Theoretical), *Journal of Applied Physics*, *32*(3), 391 –399, doi:10.1063/1.1736016.

Gilvarry, J. J., and B. H. Bergstrom (1961), Fracture of Brittle Solids. II. Distribution Function for Fragment Size in Single Fracture (Experimental), *Journal of Applied Physics*, *32*(3), 400–410, doi:10.1063/1.1736017.

Griffith, A. A. (1921), The phenomena of rupture and flow in solids, *Philosophical transactions of the royal society of london. Series A, containing papers of a mathematical or physical character*, *221*, 163198.

Hallet, B. (1990), Spatial self-organization in geomorphology: from periodic bedforms and patterned ground to scale-invariant topography, *Earth-Science Reviews*, *29*(14), 57–75, doi:10.1016/0012-8252(0)90028-T.

Hassan, M. A., M. Church, and P. J. Ashworth (1992), Virtual rate and mean distance of travel of individual clasts in gravel-bed channels, *Earth Surf. Process. Landforms*, *17*(6), 617–627, doi:10.1002/esp.3290170607.

Heartsill-Scalley, T., F. N. Scatena, C. Estrada, W. H. McDowell, and A. E. Lugo (2007), Disturbance and long-term patterns of rainfall and throughfall nutrient fluxes in a subtropical wet forest in Puerto Rico, *Journal of Hydrology*, *333*(24), 472–485, doi: 10.1016/j.jhydrol.2006.09.019.

Herrick, C. L. (1900), The geology of the white sands of New Mexico, *The Journal of Geology*, *8*(2), 112128.

Hirano, M. (1968), A mathematical model of slope development, *Journal of Geosciences, Osaka City University*, *11*, 1352.

Hodge, R. A., T. B. Hoey, and L. S. Sklar (2011), Bed load transport in bedrock rivers: The role of sediment cover in grain entrainment, translation, and deposition, *J. Geophys. Res.*, *116*(F4), F04028, doi:10.1029/2011JF002032.

Hoey, T. B., and B. J. Bluck (1999), Identifying the controls over downstream fining of river gravels, *Journal of Sedimentary Research*, *69*(1), 40–50, doi:10.2110/jsr.69.40.

Hooke, R. L. (1967), Processes on arid-region alluvial fans, *The Journal of Geology*, p. 438460.

Howard, A. D. (1980), Thresholds in river regimes, *Thresholds in geomorphology*, p. 227258.

Howard, A. D. (1998), Long Profile Development of Bedrock Channels: Interaction of Weathering, Mass Wasting, Bed Erosion, and Sediment Transport, in *Rivers Over Rock: Fluvial Processes in Bedrock Channels*, edited by K. J. Tinkler and E. E. Wohl, pp. 297–319, American Geophysical Union.

Hughes, D. S., and H. J. Jones (1950), Variation of Elastic Moduli of Igneous Rocks with Pressure and Temperature, *Geological Society of America Bulletin*, *61*(8), 843–856, doi: 10.1130/0016-7606(1950)61[843:VOEMOI]2.0.CO;2.

Jerolmack, D. J., and T. A. Brzinski (2010), Equivalence of abrupt grain-size transitions in alluvial rivers and eolian sand seas: A hypothesis, *Geology*, *38*(8), 719–722, doi:10.1130/ G30922.1.

Jerolmack, D. J., M. D. Reitz, and R. L. Martin (2011), Sorting out abrasion in a gypsum dune field, *Journal of Geophysical Research*, *116*(F2), doi:10.1029/2010JF001821.

Kafui, K. D., and C. Thornton (1993), Computer simulated impact of agglomerates, *Powders and Grains*, *93*, 401406.

Kahraman, S. (2001), Evaluation of simple methods for assessing the uniaxial compressive

strength of rock, *International Journal of Rock Mechanics and Mining Sciences*, *38*(7), 981–994, doi:10.1016/S1365-1609(01)00039-9.

Kennedy, J. F. (1969), The Formation of Sediment Ripples, Dunes, and Antidunes, *Annual Review of Fluid Mechanics*, *1*(1), 147–168, doi:10.1146/annurev.fl.01.010169.001051.

Knight, J. (2008), The environmental significance of ventifacts: A critical review, *Earth-Science Reviews*, *86*(14), 89–105, doi:10.1016/j.earscirev.2007.08.003.

Knighton, A. (1999), The gravelsand transition in a disturbed catchment, *Geomorphology*, *27*(3-4), 325–341, doi:10.1016/S0169-555X(98)00078-6.

Kodama, Y. (1991), Effect of abrasion on downstream gravel-size reduction in the Watarase river, Japan : field work and laboratory experiment.

Kodama, Y. (1994a), Experimental study of abrasion and its role in producing downstream fining in gravel-bed rivers, *Journal of Sedimentary Research*, *64*(1a), 76.

Kodama, Y. (1994b), Downstream Changes in the Lithology and Grain Size of Fluvial Gravels, the Watarase River, Japan: Evidence of the Role of Abrasion in Downstream Fining, *SEPM Journal of Sedimentary Research*, *Vol. 64A*, doi:10.1306/D4267D0C-2B26-11D7-8648000102C1865D.

Kok, J. F. (2011), A Scaling Theory for the Size Distribution of Emitted Dust Aerosols Suggests Climate Models Underestimate the Size of the Global Dust Cycle, *PNAS*, *108*(3), 1016–1021, doi:10.1073/pnas.1014798108.

Kondolf, G. M., and M. G. Wolman (1993), The sizes of salmonid spawning gravels, *Water Resources Research*, *29*(7), 22752285.

Krumbein, W. C. (1941), Measurement and geological significance of shape and roundness of sedimentary particles, *Journal of Sedimentary Research*, *11*(2), 6472.

Kuenen, P. H. (1956), Experimental abrasion of pebbles: 2. Rolling by current, *The Journal of Geology*, *64*(4), 336368.

Kun, F., and H. J. Herrmann (1999), Transition from damage to fragmentation in collision of solids, *Phys. Rev. E*, *59*(3), 2623–2632, doi:10.1103/PhysRevE.59.2623.

Lajeunesse, E., L. Malverti, and F. Charru (2010), Bed load transport in turbulent flow at the grain scale: Experiments and modeling, *J. Geophys. Res.*, *115*(F4), F04001, doi:10.1029/2009JF001628.

Lamb, M. P., W. E. Dietrich, and J. G. Venditti (2008), Is the critical Shields stress for incipient sediment motion dependent on channel-bed slope?, *Journal of Geophysical Research: Earth Surface (20032012)*, *113*(F2).

Le Bouteiller, C., and M. Naaim (2011), Aggregate breakage under dynamic loading, *Granular Matter*, *13*(4), 385–393, doi:10.1007/s10035-010-0235-2.

Leopold, L. B. (1992), Sediment size that determines channel morphology, *Dynamics of gravel-bed rivers*, p. 297311.

Leopold, L. B., M. G. Wolman, M. G. Wolman, and M. G. Wolman (1957), *River channel patterns: braided, meandering, and straight*, US Government Printing Office Washington, DC.

Leopold, L. B., M. G. Wolman, and J. P. Miller (1964), Fluvial process in geomorphology, *WH Freeman and Company*.

Lewin, J., and P. A. Brewer (2002), Laboratory simulation of clast abrasion, *Earth Surface Processes and Landforms*, *27*(2), 145–164, doi:10.1002/esp.306.

Lisle, T. E. (1989), Sediment transport and resulting deposition in spawning gravels, north coastal California, *Water resources research*, *25*(6), 13031319.

Litwin Miller, K., T. Szabó, D. J. Jerolmack, and G. Domokos (in review), Quantifying the significance of abrasion and selective transport on downstream pebble evolution (in review), *Journal of Geophysical Research: Earth Surface*.

Martin, R. L., D. J. Jerolmack, and R. Schumer (2012), The physical basis for anomalous diffusion in bed load transport, *Journal of Geophysical Research: Earth Surface (20032012)*, *117*(F1).

Merriam, R., H. H. Rieke III, and Y. C. Kim (1970), Tensile strength related to mineralogy and texture of some granitic rocks, *Engineering Geology*, *4*(2), 155–160, doi:10.1016/0013-7952(70)90010-4.

Mikos, M. (1995), Fluvial Abrasion: Converting Size Reduction Coefficients into Weight Reduction Rates, *Journal of Sedimentary Research*, *65*(3).

Morris, P. H., and D. J. Williams (1997), Exponential Longitudinal Profiles of Streams, *Earth Surf. Process. Landforms*, *22*(2), 143–163, doi:10.1002/(SICI)1096-9837(199702)22:2⟨143::AID-ESP681⟩3.0.CO;2-Z.

Morris, P. H., and D. J. Williams (1999), A worldwide correlation for exponential bed particle size variation in subaerial aqueous flows, *Earth Surface Processes and Landforms*, *24*(9), 835–847, doi:10.1002/(SICI)1096-9837(199908)24:9⟨835::AID-ESP15⟩3.0.CO;2-G.

Mueller, E. R., J. Pitlick, and J. M. Nelson (2005), Variation in the reference Shields stress for bed load transport in gravel-bed streams and rivers, *Water Resour. Res.*, *41*(4), W04006, doi:10.1029/2004WR003692.

Oddershede, L., P. Dimon, and J. Bohr (1993), Self-organized criticality in fragmenting, *Phys. Rev. Lett.*, *71*(19), 3107–3110, doi:10.1103/PhysRevLett.71.3107.

Olsen, P. (1980), Triassic and Jurassic formations of the Newark Basin, in *Field studies of New Jersey geology and guide to field trips: 52nd annual meeting of the New York State Geological Association, ed. W. Manspeizer*, p. 241.

Paola, C., and R. Seal (1995), Grain Size Patchiness as a Cause of Selective Deposition and Downstream Fining, *Water Resources Research*, *31*(5), 1395–1407, doi: 10.1029/94WR02975.

Paola, C., G. Parker, R. Seal, S. K. Sinha, J. B. Southard, and P. R. Wilcock (1992), Downstream fining by selective deposition in a laboratory flume, *Science*, *258*(5089), 17571760.

Paola, C., K. Straub, D. Mohrig, and L. Reinhardt (2009), The "unreasonable effectiveness" of stratigraphic and geomorphic experiments, *Earth-Science Reviews*, *97*(1 4), 1–43, doi: 10.1016/j.earscirev.2009.05.003.

Parker, G. (1976), On the cause and characteristic scales of meandering and braiding in rivers, *Journal of Fluid Mechanics*, *76*(03), 457–480, doi:10.1017/S0022112076000748.

Parker, G. (1978), Self-formed straight rivers with equilibrium banks and mobile bed. Part 2. The gravel river, *Journal of Fluid Mechanics*, *89*(01), 127, doi:10.1017/S0022112078002505.

Parker, G. (1990), Surface-based bedload transport relation for gravel rivers, *Journal of Hydraulic Research*, *28*(4), 417–436, doi:10.1080/00221689009499058.

Parker, G. (1991), Selective sorting and abrasion of river gravel. I: Theory, *Journal of Hydraulic Engineering*, *117*(2), 131149.

Parker, G., and Y. Cui (1998), The arrested gravel front: Stable gravel-sand transitions in Rivers Part 1: Simplified analytical solution, *Journal of hydraulic research*, *36*(1), 75100.

Parker, G., and P. C. Klingeman (1982), On why gravel bed streams are paved, *Water Resources Research*, *18*(5), 1409–1423, doi:10.1029/WR018i005p01409.

Parker, G., C. Paola, K. X. Whipple, and D. Mohrig (1998), Alluvial fans formed by channelized fluvial and sheet flow. I: Theory, *Journal of Hydraulic Engineering*, *124*(10), 985995.

Parker, G., P. R. Wilcock, C. Paola, W. E. Dietrich, and J. Pitlick (2007), Physical basis for quasi-universal relations describing bankfull hydraulic geometry of single-thread gravel bed rivers, *Journal of Geophysical Research*, *112*(F4), doi:10.1029/2006JF000549.

Phillips, C. B., R. L. Martin, and D. J. Jerolmack (2013), Impulse framework for unsteady flows reveals superdiffusive bed load transport: Impulse framework for unsteady flows, *Geophysical Research Letters*, *40*(7), 1328–1333, doi:10.1002/grl.50323.

Pike, A. S., F. N. Scatena, and E. E. Wohl (2010), Lithological and fluvial controls on the geomorphology of tropical montane stream channels in Puerto Rico, *Earth Surface Processes and Landforms*, *35*(12), 14021417, doi:10.1002/esp.1978.

Pizzuto, J. E. (1995), Downstream Fining in a Network of Gravel-Bedded Rivers, *Water Resour. Res.*, *31*(3), 753–759, doi:10.1029/94WR02532.

Pratt, H. R., A. D. Black, W. S. Brown, and W. F. Brace (1972), The effect of speciment size on the mechanical properties of unjointed diorite, *International Journal of Rock Mechanics and Mining Sciences & Geomechanics Abstracts*, *9*(4), 513–516, doi:10.1016/0148-9062(72)90042-3.

Rashband, W. S. (1997), ImageJ, *Bethesda, MD: US National Institutes of Health*, *2008*.

Reitz, M. D., and D. J. Jerolmack (2012), Experimental alluvial fan evolution: Channel dynamics, slope controls, and shoreline growth, *Journal of Geophysical Research: Earth Surface (20032012)*, *117*(F2).

Rice, S. (1999), The Nature and Controls on Downstream Fining Within Sedimentary Links, *Journal of Sedimentary Research*, *69*(1).

Roering, J. J., J. W. Kirchner, and W. E. Dietrich (1999), Evidence for nonlinear, diffusive sediment transport on hillslopes and implications for landscape morphology, *Water Resources Research*, *35*(3), 853870.

Rotonda, T., P. Tommasi, and D. Boldini (2010), Geomechanical Characterization of the Volcaniclastic Material Involved in the 2002 Landslides at Stromboli, *Journal of Geotechnical and Geoenvironmental Engineering*, *136*(2), 389–401, doi:10.1061/(ASCE)GT.1943-5606.0000218.

Rubin, D. M. (2004), A Simple Autocorrelation Algorithm for Determining Grain Size from Digital Images of Sediment, *Journal of Sedimentary Research*, *74*(1), 160–165, doi:⟨p⟩10.1306/052203740160⟨/p⟩.

Scatena, F. N., E. O. Planos-Gutierrez, J. Schellekens, M. Bonell, and L. A. Bruijnzeel (2004), Natural disturbances and the hydrology of humid tropical forests., in *The joint UNESCO International Hydrological Programme (IHP)-International Union of Forestry Research Organizations (IUFRO) symposium and workshop, Forest-water-people in the humid tropics: past, present and future hydrological research for integrated land and water management, Universiti Kebangsaan Malaysia, 30 July-4 August 2000.*, p. 489512, Cambridge University Press.

Schmeeckle, M. W., J. M. Nelson, J. Pitlick, and J. P. Bennett (2001), Interparticle collision of natural sediment grains in water, *Water Resour. Res.*, *37*(9), 2377–2391, doi:10.1029/2001WR000531.

Schumm, S. A. (1985), Patterns of alluvial rivers, *Annual Review of Earth and Planetary Sciences*, *13*, 5.

Schumm, S. A., and M. A. Stevens (1973), Abrasion in Place: A Mechanism for Rounding and Size Reduction of Coarse Sediments in Rivers, *Geology*, *1*(1), 37–40, doi:10.1130/0091-7613(1973)1⟨37:AIPAMF⟩2.0.CO;2.

Seal, R., and C. Paola (1995), Observations of Downstream Fining on the North Fork Toutle River Near Mount St. Helens, Washington, *Water Resources Research*, *31*(5), 14091419, doi:10.1029/94WR02976.

Seiders, V. M., and M. H. Pease (1971), *Geologic map of the El Yunque quadrangle, Puerto Rico*, US Geological Survey.

Shannon, C. E. (1948), A mathematical theory of communication, *ACM SIGMOBILE Mobile Computing and Communications Review*, *5*(1), 355.

Shaw, J., and R. Kellerhals (1982), *The composition of recent alluvial gravels in Alberta river beds*, Alberta Research Council.

Sinha, S. K., and G. Parker (1996), Causes of Concavity in Longitudinal Profiles of Rivers, *Water Resour. Res.*, *32*(5), 1417–1428, doi:10.1029/95WR03819.

Sklar, L., and W. E. Dietrich (1998), River Longitudinal Profiles and Bedrock Incision Models: Stream Power and the Influence of Sediment Supply, in *Rivers Over Rock: Fluvial Processes in Bedrock Channels*, edited by K. J. Tinkler and E. E. Wohl, pp. 237–260, American Geophysical Union.

Sklar, L. S., and W. E. Dietrich (2004), A mechanistic model for river incision into bedrock by saltating bed load, *Water Resources Research*, *40*(6).

Sklar, L. S., W. E. Dietrich, E. Foufoula-Georgiou, B. Lashermes, and D. Bellugi (2006), Do gravel bed river size distributions record channel network structure?, *Water Resour. Res.*, *42*(6), W06D18, doi:10.1029/2006WR005035.

Smith, G. H. S., and R. I. Ferguson (1995), The gravel-sand transition along river channels, *Journal of Sedimentary Research*, *65*(2).

Sneed, E. D., and R. L. Folk (1958), Pebbles in the lower Colorado River, Texas a study in particle morphogenesis, *The Journal of Geology*, p. 114150.

Snow, R. S., and R. L. Slingerland (1987), Mathematical Modeling of Graded River Profiles, *Journal of Geology*, *95*, 15–33, doi:10.1086/629104.

Sternberg, H. (1875), *Untersuchungen Uber Ungen-und Querprofil geschiebefuhrender Flusse*.

Stock, J. D., K. M. Schmidt, and D. M. Miller (2008), Controls on alluvial fan long-profiles, *Geological Society of America Bulletin*, *120*(5-6), 619–640, doi:10.1130/B26208.1.

Szabo, T., S. Fityus, and G. Domokos (2013), Abrasion model of downstream changes in grain shape and size along the Williams River, Australia, *Journal of Geophysical Research: Earth Surface*, *118*(4), 2059–2071, doi:10.1002/jgrf.20142.

Turowski, J. M., A. Badoux, J. Leuzinger, and R. Hegglin (2013), Large floods, alluvial overprint, and bedrock erosion, *Earth Surface Processes and Landforms*, *38*(9), 947–958, doi:10.1002/esp.3341.

van Rijn, L. (1984a), Sediment Transport, Part I: Bed Load Transport, *Journal of Hydraulic Engineering*, *110*(10), 1431–1456, doi:10.1061/(ASCE)0733-9429(1984)110:10(1431).

van Rijn, L. (1984b), Sediment Transport, Part II: Suspended Load Transport, *Journal of Hydraulic Engineering*, *110*(11), 1613–1641, doi:10.1061/(ASCE)0733-9429(1984)110:11(1613).

Varkonyi, P. L., and G. Domokos (2011), A general model for collision-based abrasion processes, *IMA journal of applied mathematics*, *76*(1), 4756.

Vutukuri, V. S. (1974), *Handbook on mechanical properties of rocks: Testing techniques and results*, 1st ed., distributed by Trans Tech Publications.

Wang, Z.-T., H.-T. Wang, Q.-H. Niu, Z.-B. Dong, and T. Wang (2011), Abrasion of yardangs, *Phys. Rev. E*, *84*(3), 031304, doi:10.1103/PhysRevE.84.031304.

Warrick, J. A., D. M. Rubin, P. Ruggiero, J. N. Harney, A. E. Draut, and D. Buscombe (2009), Cobble cam: grainsize measurements of sand to boulder from digital photographs and autocorrelation analyses, *Earth Surface Processes and Landforms*, *34*(13), 1811–1821, doi:10.1002/esp.1877.

Weiss, J. (1949), Wissahickon Schist at Philadelphia, Pennsylvania, *Geological Society of America Bulletin*, *60*(10), 1689–1726, doi:10.1130/0016-7606(1949)60[1689:WSAPP]2.0.CO;2.

Wentworth, C. K. (1919), A Laboratory and Field Study of Cobble Abrasion, *The Journal of Geology*, *27*(7), 507–521, ArticleType: research-article / Full publication date: Oct. - Nov., 1919 /.

Whipple, K. X. (2004), Bedrock rivers and the geomorphology of active orogens, *Annu. Rev. Earth Planet. Sci.*, *32*, 151185.

Wiberg, P. L., and J. D. Smith (1987), A Theoretical Model for Saltating Grains in Water, *J. Geophys. Res.*, *90*(C4), PP. 7341–7354, doi:198510.1029/JC090iC04p07341.

Wilcock, P., and J. Crowe (2003), Surface-based Transport Model for Mixed-Size Sediment,

Journal of Hydraulic Engineering, *129*(2), 120–128, doi:10.1061/(ASCE)0733-9429(2003)129:2(120).

Wilcock, P. R. (2001), Toward a practical method for estimating sediment-transport rates in gravel-bed rivers, *Earth Surf. Process. Landforms*, *26*(13), 1395–1408, doi:10.1002/esp.301.

Wilcock, P. R., and S. T. Kenworthy (2002), A two-fraction model for the transport of sand/gravel mixtures, *Water Resources Research*, *38*(10), 121.

Wolman, M. G. (1954), A method of sampling coarse river-bed material, *Transactions, American Geophysical Union*, *35*, 951–956, doi:10.1029/TR035i006p00951.

Yager, E. M., J. M. Turowski, D. Rickenmann, and B. W. McArdell (2012), Sediment supply, grain protrusion, and bedload transport in mountain streams, *Geophys. Res. Lett.*, *39*(10), L10402, doi:10.1029/2012GL051654.

Yatsu, E. (1955), On the longitudinal profile of the graded river, *Transactions, American Geophysical Union*, *36*(4), 655, doi:10.1029/TR036i004p00655.

INDEX